PHASE RELATIONS AND MAGNETIC PROPERTIES OF MM-Co-T (T=Fe and Cu) ALLOYS BETWEEN 2 : 7 AND 2 : 17 STOICHIOMETRIES

By

EMUR MANICKAM THANGAVELU

IPMS
1981
D
THA
PHA

TH
IPMS/1981/D
T328P

INTERDISCIPLINARY PROGRAMME IN MATERIALS SCIENCE

INDIAN INSTITUTE OF TECHNOLOGY KANPUR

AUGUST, 1981

71126

PHASE RELATIONS AND MAGNETIC PROPERTIES OF MM-Co-T (T=Fe and Cu) ALLOYS BETWEEN 2 : 7 AND 2 : 17 STOICHIOMETRIES

A Thesis Submitted
in Partial Fulfilment of the Requirements
for the Degree of

DOCTOR OF PHILOSOPHY

By
EMUR MANICKAM THANGAVELU

to the

INTERDISCIPLINARY PROGRAMME IN MATERIALS SCIENCE
INDIAN INSTITUTE OF TECHNOLOGY KANPUR
AUGUST, 1981

IPMS-1981-D-THA-PHA

I.I.T. KANPUR
CENTRAL LIBRARY
Acc. No. A 70494

16 APR 1982

TO THOSE WHO
LOVE
SCIENCE OF MATERIALS

CERTIFICATE

Certified that this work on "PHASE RELATIONS AND MAGNETIC PROPERTIES OF MM-Co-T (T = Fe and Cu) ALLOYS BETWEEN 2:7 AND 2:17 STOICHIOMETRIES" by E.M.T. Velu has been carried out under my supervision and that this has not been submitted elsewhere for a degree.

August, 1981.

(E.C. Subbarao)
Professor
Department of Metallurgical Engineering
Indian Institute of Technology
Kanpur.

POST GRADUATE OFFICE
[illegible]
[illegible]
(Ph.D.)
[illegible]
[illegible]
Institute of Technology Kanpur
Dated: 26/3/1982 BR.

ACKNOWLEDGEMENT

It is a great privilege to have worked with my beloved professor Dr. E.C. Subbarao both for my master's and doctoral degrees. His singular devotion to the science of materials and his dynamic approach to solving problems both scientific and technical have always been sources of immense inspiration to me. I hardly had any problems for materials or equipments throughout this work. The great warmth which lay behind his objective, sometimes slightly cynical and detached approach to problems, will always be remembered.

I am very grateful to Prof. K.P. Gupta, a co-investigator of the MM-Co magnet project who rendered immense help in solving problems in the phase relations study. I acknowledge with gratitude the help of Dr. A.K. Majumdar who had spent considerable amount of his energy and time in setting up an excellent facility for magnetic measurements.

Most of the alloy compositions studied in the present work have been checked by thorough and meticulous chemical analysis by Madam Padmavathi Sankar and I am very grateful to her selfless service. The gratitude is due in the order to our kind and cheerful technician, Mr. B.P. Srivastava who was handy in times of urgency to set right many of the electronic instruments used in the present study.

My association with my past project colleagues Dr. S.N. Kaul, Dr. H.O. Gupta, Dr. M.V. Satyanarayana, Mr. R.C. Mittal, Dr. K.S. Prasad, Mr. G. Sarkar, Mr. N.R. Bonda, Mr. J. Subramanyam and my present colleagues Mr. S.N. Laha, Mr. S. Pandian and Mr. U. Ramakrishna, was quite an enriching experience in my learning and their technical assistance in one form or the other throughout the course of my work was extremely helpful.

I express my gratitude with my other project members to Dr. V.S. Ragunathan of Reactor Research Centre, Kalpakkam for his help in electron-probe micro-analysis.

I am thankful to Mr. R.S. Mishra and Mr. R.N. Srivastava for their careful typing of the manuscript and to Mr. Viswanath for his excellent cyclostyling work.

This work was supported by the Department of Electronics, Government of India under the project DOE/ECS/MT/75-81/21. I have been the longest associated member of the project drawing liberal financial assistance almost throughout my study at I.I.T. Kanpur. I place my sincere gratitude to the sponsorers and to the investigators of the Mischmetal-Cobalt magnet project with dutiful thanks.

Generous last-hour helps were provided by Mr. Mangole, Mr. Mukerjee and Mr. Arunachalam, in photography and proof-reading, and I am thankful to all of them.

E.M.T. VELU

TABLE OF CONTENTS

CHAPTER Page

LIST OF TABLES ix

LIST OF FIGURES xii

LIST OF SYMBOLS xvi

SYNOPSIS xvii

1. INTRODUCTION 1

1.1 A Comparison of Different Permanent Magnets 1

1.2 Primary Magnetic Properties of RE-Co Phases 4

1.3 RE- 3d Metal Phase Diagrams and Structures of Their Intermetallic Compounds 7

1.3.1 RE- 3d Metal Phase Diagrams 7

1.3.2 Structure of Intermetallic Phases in RE-Co Systems 12

1.4 Structure Sensitive Magnetic Properties 17

1.5 Technology of RE-Co Magnet Processing and Permanent Magnet Properties of $RECo_5$ Type Magnets 17

1.5.1 Flow Chart of RE-Co Magnet Processing 17

1.5.2 Magnet Processing Parameters 21

1.5.2.1 Alloy Composition 21

1.5.2.2 Comminution 23

1.5.2.3 Compaction 23

1.5.2.4 Sintering 25

1.5.2.5 Post Sintering Heat Treatment 25

1.5.2.6 Magnetising and Characterisation 25

1.5.3 Processes and Properties of Selected $RECo_5$ Type Magnets 26

REFERENCES 30

2. STATEMENT OF THE PROBLEM 32

3. EXPERIMENTAL 38

3.1 Alloy Preparation 38

CHAPTER Page

3.1.1 Raw Materials 38
3.1.2 Melting 38
3.1.3 Annealing 40
3.1.4 Chemical Analysis 40
3.2 Phase Analysis 41
3.2.1 Metallography 41
3.2.2 X-ray Diffraction 41
3.2.3 Thermomagnetic Analysis 42
3.2.4 Electron Probe Microanalysis 43
3.3 Characterisation of Magnetic Properties 43
3.3.1 Primary Magnetic Properties 43
3.3.1.1 Magneto Crystalline Anisotropy 43
3.3.1.2 Saturation Magnetisation 44
3.3.1.3 Curie Temperature 45
3.3.2 Permanent Magnet Properties 47
3.4 Magnet Processing 47
3.4.1 Alloy Preparation 47
3.4.2 Comminution 49
3.4.3 Compaction 49
3.4.4 Sintering 50
3.4.5 Magnetising 50
3.4.6 Characterisation 51
3.4.6.1 Permanent Magnet Properties 51
3.4.6.2 Density 51
3.4.6.3 Phase Composition 51
3.4.6.4 Chemical Composition 52
REFERENCES 53

4. PHASE RELATIONS IN MM-Co-Fe SYSTEM IN Co-RICH REGION 54
4.1 Introduction 54
4.2 Experimental 55
4.3 Results and Discussion 56
4.3.1 Identity and Crystallographic Details of Different Phases in MM-Co-Fe System 56
4.3.1.1 2:7 and 5:19 Phases 56

CHAPTER Page

4.3.1.2 1:5 Phase 67
4.3.1.3 2:17 Phase 72
4.3.1.4 β-Co Phase 72
4.3.1.5 X-Phase 75
4.3.1.6 High Fe Containing MM-Co-Fe Alloys Between 2:7 and 1:5 Stoichiometries 80
4.3.2 Homogeneity Region of 1:5 Phase 80
4.3.3 Phase Stability of 1:5 Phase 83
4.4 Conclusions 92
REFERENCES 94

5. MAGNETIC PROPERTIES OF MM-Co-Fe PHASES 97
5.1 Introduction 97
5.2 Experimental 97
5.3 Results and Discussion 99
5.3.1 Saturation Magnetisation of MM-Co Phases 99
5.3.2 Curie Temperature 100
5.3.2.1 T_c of Stoichiometric Phases in MM-Co System 100
5.3.2.2 T_c of MM-Co-Fe Phases 108
5.4 Conclusion 113
REFERENCES 114

6. PHASE RELATIONS AND MAGNETIC PROPERTIES OF MM(Co_{1-x} Cu_x)$_5$ ALLOYS 115
6.1 Introduction 115
6.2 Experimental 115
6.3 Results and Discussion 116
6.3.1 Phase Relations 116
6.3.2 Magnetic Characteristics 120
6.4 Conclusion 122
REFERENCES 124

7. PERMANENT MAGNET PROPERTIES OF 1:5 TYPE MM-Co ALLOYS 125
7.1 Introduction 125
7.1.1 Previous Work on MMCo$_5$ Magnets 125
7.1.2 Aims of the Present Work 127

CHAPTER Page

7.2 Experimental 127

7.3 Results 127

7.3.1 Resin Bonded MM-Co Magnets 127

7.3.2 Permanent Magnet Properties of Powder Compacts of MM-Co Alloys 130

7.3.3 Permanent Magnet Properties of Sintered MM-Co Magnets and Their Structure 133

7.3.3.1 $MMCo_{4.8}$ Sintered Magnets 133

7.3.3.2 $MMCo_{4.2}$ Sintered Magnets 135

7.3.3.3 $MMCo_{3.5}$ Sintered Magnets 137

7.3.3.4 $MMCo_{3.8}$ Sintered Magnets 138

7.3.3.5 $MMCo_{4.0}$ Sintered Magnets 141

7.3.3.6 $MM_{0.8}Sm_{0.2}Co_{3.8}$ and $MM_{0.8}Sm_{0.2}Co_{4.0}$ Sintered Magnets 141

7.3.4 Demagnetisation Plots of MM-Co Sintered Magnets 146

7.4 Discussion 146

7.4.1 Resin Bonded Magnets 146

7.4.2 Powder Compacts 148

7.4.3 Sintered MM-Co Magnets 149

7.4.3.1 The Occurrence of Oxide in MM-Co Sintered Magnets 149

7.4.3.2 Compositional Shift in MM-Co Sintered Magnets 149

7.4.3.3 Structure and Properties of MM-Co Sintered Magnets 154

7.4.4 Problem Areas in the Preparation of MM-Co Sintered Magnets 155

7.5 Conclusions 155

REFERENCES 157

8. CONCLUSIONS AND SUGGESTIONS FOR FUTURE WORK 158

APPENDIX 1 - SPECIFICATIONS OF RAW MATERIALS: MM, Co, Fe and Cu 162

APPENDIX 2 - COMPUTATIONS OF ALLOY COMPOSITIONS 163

LIST OF TABLES

TABLE Page

1.1 Magnetic properties of $RECo_5$ and RE_2Co_{17} type compounds 5

1.2 Peritectic temperatures of intermetallic phases in RE-Co systems 7

1.3 Theoretically possible Cromer-Larson phases in RE-Co systems 16

1.4 Processes and properties of selected $RECo_5$-type magnets 28

4.1 Chemical and phase composition of the alloys selected for the study of phase relations in MM-Co-Fe system 58

4.2 X-ray diffraction data for the MM_2Co_7 phase 64

4.3 X-ray diffraction data for the MM_5Co_{19} phase 65

4.4 Comparison of lattice parameters of stoichiometric phases of MM-Co system with those of Ce-Co and CeMM-Co systems 67

4.5 X-ray diffraction data for $MMCo_5$ phase 68

4.6 X-ray diffraction data for the MM_2Co_{17} phase 74

4.7 Variation in the position (2θ) of X-ray diffraction lines of 1:5 phase with composition 82

4.8 X-ray diffraction data of as-cast and 700°C, 30 days annealed alloys of E-1 and E-2 90

5.1 Primary magnetic properties of $RECo_5$ phases 98

5.2 Magnetic saturation and anisotropy at 20°C for RE_2Co_7 phases 98

5.3 Saturation magnetisation of MM-Co phases at 20°C 99

TABLE		Page
5.4	Chemical and phase composition of MM-Co-Fe alloys used for TMA	101
5.5	Curie temperature in °C of RE-Co compounds	104
5.6	T_c of the 2:7 and 5:19 phases as a function of Fe concentration in the MM-Co-Fe system	111
5.7	T_c of the 1:5 phase as a function of Fe concentration in the MM-Co-Fe system	113
6.1	Chemical and phase composition of $MM_{1-z}(Co_{1-x-y}Fe_yCu_x)_5$ alloys	117
7.1	Materials used, processes followed and properties developed, for $MMCo_5$ magnets	126
7.2	Composition of MM-Co alloys used for magnet fabrication	128
7.3	Comparative study of ${}_iH_c$ of different resin bonded $MMCo_5$ magnets	132
7.4(a)	Permanent magnet properties of 3 h milled powder compacts and sintered pellets of $MMCo_{4.8}$	134
7.4(b)	Permanent magnet properties of 6 h milled powder compacts and sintered pellets of $MMCo_{4.8}$	134
7.4(c)	Permanent magnet properties of 9 h milled powder compacts and sintered pellets of $MMCo_{4.8}$	135
7.5	Permanent magnet properties of powder compacts and sintered pellets of $MMCo_{4.2}$	137
7.6	Permanent magnet properties of powder compacts and sintered pellets of $MMCo_{3.5}$	138
7.7	Permanent magnet properties of powder compacts and sintered pellets of $MMCo_{3.8}$	139

TABLE		Page
7.8	Permanent magnet properties of powder compacts and sintered pellets of $MMCo_{4.0}$	143
7.9	Permanent magnet properties of powder compacts and sintered pellets of $MM_{0.8}Sm_{0.2}Co_{3.8}$ and $MM_{0.8}Sm_{0.2}Co_{4.0}$	144
7.10	X-ray diffraction data of MM_2O_3 phase	151
7.11	X-ray diffraction data of β-Co phase	151
7.12	Chemical composition of as-cast, powder compact and sintered pellets of $MMCo_{4.2}$	153

LIST OF FIGURES

FIGURE Page

1.1 Progress in permanent magnet quality since 1880 as indicated by the value of the maximum energy product achieved for various material systems 2

1.2 Demagnetisation curve of selected permanent magnet materials 2

1.3 Demonstrating the repelling forces of two identical magnets of alnicos, strontium ferrite and recoma 3

1.4 Phase diagrams of RE-T systems RE = Ce and T = Co, Fe and Cu 8

1.5 Compound formation in (a) RE-Co, (b) RE-Fe and (c) RE-Cu systems 9

1.6 Melting temperature and decomposition temperatures for various members of the $RECo_5$ compound 11

1.7 Isothermal sections of the Sm-Co-Cu phase diagram 13

1.8 Crystal structure of $CaCu_5$ type unit cell 15

1.9 Mode of crystal structure formation in R_xCo_y alloys 15

1.10 Magnetocrystalline anisotropy of RE-Co materials as a function of composition 18

1.11 Dependence of intrinsic as well as induction coercivity and energy product of $SmCo_{5\pm x}$ magnets on cobalt content 19

1.12 Coercivity measured at room temperature as a function of heating temperature for $SmCo_5$ 20

1.13 Process flow diagram for sintered rare earth cobalt permanent magnets 22

1.14 Comparison of optimum particle size distribution with broad particle size distribution 24

FIGURE Page

1.15 Two representations of the hysteresis curve of a permanent magnet 27

3.1 Materials, equipments and methods employed in phase analysis 39

3.2 Experimental set-up for thermomagnetic analysis 46

3.3 Materials, equipments and methods employed in magnet processing 48

4.1 900°C isothermal section of MM-Co-Fe phase diagram 57

4.2 The microstructure of alloy A-1 62

4.3 The low field magnetic moment as a function of temperature for the alloys A-1 and B-5 after annealing at 900°C for 10 days 63

4.4 The microstructure of alloy C-4 69

4.5 The microstructure of alloy 12-5 70

4.6 The microstructure of alloy 6-6 70

4.7 The microstructure of alloy C-11 73

4.8 The microstructure of alloy D-10 73

4.9 An EPMA trace of the alloy D-10 analysed for 3d and c RE elements in β-Co and MM_2Co_{17} 76

4.10 Magnetisation versus temperature at low field for alloys B-5, C-0 and C-3, 900°C annealed 78

4.11 Magnetisation versus temperature at 40 Oe for $MMCo_{4.0}$ (C-0) alloys 79

4.12 Magnetisation versus temperature at 40 Oe for alloys 12-3 and 15-4, 900°C, 7 days annealed 81

4.13 Variation in the lattice parameters with composition of the $MMCo_5$ phase in $MMCo_{5\pm x}$ alloys 84

4.14 The microstructure of alloy C-6 annealed at 700°C for 30 days 86

FIGURE Page

4.15 The microstructure of alloy E-1 annealed at 700° C for 30 days 86

4.16 The microstructure of alloy E-2 annealed at 700° C for 30 days 86

4.17 Low field magnetic moment as a function of temperature for alloy E-1 88

4.18 Low field magnetic moment as a function of temperature for alloy E-2 89

5.1 Low field magnetic moment as a function of temperature for alloys A-1, B-5 and S-1, 900° C annealed 103

5.2 Low field magnetic moment as a function of temperature for C-1 alloy, 900° C, 9 days annealed 105

5.3 Low field magnetic moment as a function of temperature for C-1 alloy 106

5.4 Magnetisation vs. temperature at 40 Oe for $MM_2(Co_{1-x}Fe_x)_{7+y}$ alloys, 900°C, 7 days annealed 109

5.5 Variation of T_c of 2:7, 5:19 and 1:5 phases with Fe concentration in MM-Co-Fe system 110

5.6 Magnetisation vs. temperature at 40 Oe for $MM(Co_{1-x}Fe_x)_{5+y}$ alloys 112

6.1 Lattice parameters vs. composition of 1:5 phase in $MM_{0.93}(Fe_{0.02}Co_{0.98-x}Cu_x)_5$ alloys 119

6.2 $4\pi M_s$ vs. composition of $MM_{0.93}(Fe_{0.02}Co_{0.98-x}Cu_x)_5$ alloys 119

6.3 Low field magnetic moment vs. temperature for $MM_{1-z}(Co_{1-x-y}Fe_yCu_x)_5$ alloys 900° C annealed 121

7.1 $4\pi M_s$ and ${}_iH_c$ for $MMCo_x$ alloys $3.5 \leqslant x \leqslant 5.0$ 129

7.2 Intrinsic and induction demagnetisation curves for (a) $MMCo_{4.2}$ (b) $MMCo_{4.4}$ (c) $MMCo_{4.6}$ and (d) $MMCo_{4.8}$ powder compacts 131

FIGURE Page

7.3 X-ray diffraction patterns of sintered pellets of (a) $MMCo_{4.8}$ (b) $MMCo_{4.2}$ and (c) $MMCo_{3.5}$ alloys 136

7.4 X-ray diffraction patterns of as-cast and sintered pellets of $MMCo_{3.8}$ alloy 140

7.5 X-ray diffraction patterns of (a) as-cast $MMCo_{4.0}$ alloy and sintered pellets of (b) 3 h (c) 6 h and (d) 9 h milled powder compacts of $MMCo_{4.0}$ alloy 142

7.6 X-ray diffraction patterns of sintered pellets of (a) $MM_{0.8}Sm_{0.2}Co_{3.8}$ and (b) $MM_{0.8}Sm_{0.2}Co_{4.0}$ compositions 145

7.7 Intrinsic demagnetisation plots of sintered magnets of $MMCo_x$ alloys $3.5 \leqslant X \leqslant 4.8$ 147

7.8 Intrinsic coercivity vs. composition for sintered $MMCo_x$ alloys $3.8 \leqslant X \leqslant 4.8$ 150

LIST OF SYMBOLS

A, KA : Ampere, Kilo Ampere
a/o : Atom percent
B : Magnetic induction
B_r : Remanent induction
$(BH)_{max}$: Maximum energy product
cc : Cubic centimeters
cps : Counts per second
emu : Electromagnetic unit
g, gms : gram, grams
G, KG : Gauss, Kilo Gauss
H : Magnetic field
H_A : Magnetocrystalline anisotropy field
${}_iH_c$, ${}_bH_c$: Intrinsic coercivity, induction coercivity
J : Joule
k_1 : Magnetocrystalline anisotropy constant
m : Meter
MM : Mischmetal
MGOe : Million Gauss-Oersted
M_s, $4\pi M_s$: Saturation magnetisation
Oe, KOe : Oersted, Kilo Oersted
R, RE : Rare earth
t : Time
T : Tesla (10^4 Gauss)
w/o : Weight percent
μ : Micron

SYNOPSIS

Investigations were undertaken (i) to establish the relation between structure, microstructure and composition of mischmetal (Indian)-cobalt-iron and mischmetal-cobalt-copper systems in the technologically important composition region and (ii) to develop the technology necessary to produce permanent magnets utilising the commercial mischmetal. The work is divided into eight chapters.

Chapter 1 gives a brief review of the existing literature on the phase diagrams and phase relationships of the binary RE-Co, RE-Fe, RE-Cu and the ternary Sm-Co-Cu alloy systems and an up-to-date critical survey of the developmental processes and properties reported for Rare-Earth Cobalt permanent magnets containing mischmetal.

Chapter 2 is the statement of the problem. The objectives of the work were (i) to investigate the phase relationships in the MM-Co-Fe and MM-Co-Cu alloy systems in the composition region of interest for permanent magnets (ii) to characterise the primary magnetic properties of the MM-Co-Fe and MM-Co-Cu phases in order to evaluate their suitability for permanent magnets and (iii) to study and optimise different process parameters to produce MM-Co permanent magnets.

Chapter 3 describes the experimental procedures followed in the phase analysis and the magnet fabrication.

Alloys for the study were prepared by arc melting in a water cooled Cu crucible under Argon atmosphere and subsequently homogenised at 900°C in evacuated quartz ampoules. The phases were studied by metallography, X-ray diffraction, thermomagnetic analysis and electron-probe micro-analysis. Magnets were prepared by powder metallurgy techniques. The as-cast alloy buttons were crushed to-100 mesh and ground to a few micron size powder by rod milling under sodium-gettered toluene. The powder was dried under a vacuum and field pressed in 13 KOe pulse field. The powder compacts were sintered under flowing argon atmosphere. The sintered pellets were magnetised in a pulse field of 60 KOe and their permanent magnet properties were evaluated with a vibrating sample magnetometer.

In Chapter 4 the results of phase relations study of the MM-Co-Fe system at 900°C are discussed. In MM-Co system, six phases, $MMCo_3$, MM_2Co_7, MM_5Co_{19}, $MMCo_5$, MM_2Co_{17} and β-Co were identified between 72 and 92 a/o Co. The $MMCo_3$, MM_2Co_7 and MM_5Co_{19} have very similar X-ray patterns and hence they were identified by thermomagnetic analysis (TMA) based on their distinct Curie temperature. The MM_2Co_7 phase exists both in the hexagonal and rhombohedral modifications. The 2:7, 5:19, 1:5 and 2:17 phases also exist as stable phases at 900°C when Co is partially substituted by Fe. Alloys containing upto 20 a/o Fe were investigated in close composition interval of 1 a/o. The 5:19 phase was found to extend up to about 11 a/o Fe while the 2:7 and 1:5 phases extend to greater than 11 a/o Fe. A new phase with a T_c of 340° C was found to coexist with a number of alloys near the 1:4 composition. A 900° C isothermal section of the ternary MM-Co-Fe system between 2:7 and 2:17 stoichiometry (MM/Co) is given with alloys containing upto 20 a/o Fe. The phase region beyond 12 a/o Fe in the MM-Co-Fe system particularly between 2:7 and 1:5 stoichiometric regions seems to be complicated because the X-ray results alone could not establish the identity of the phases unambiguously. Some of the phases in this region have T_c greater than the safe-limit (700° C) of the TMA apparatus used in this study. Of the various phases only $MMCo_5$ has an observable homogeneity region extending over 2 w/o Co at 900° C. The $MMCo_5$ phase is unstable at temperature below 700° C and the addition of Fe increases its instability.

In Chapter 5 the primary magnetic properties, saturation magnetisation and Curie temperature of the various intermetallic phases identified in the MM-Co-Fe system are reported. The 1:3, 2:7, 5:19, 1:5 and 2:17 phases in the MM-Co system have T_c $<$20° C, 67° C, 280° C, 540° C and $>$700° C respectively. The substitution of Fe for Co increases these values further for all these phases. The $MMCo_5$ has a $4\pi M_s$ of 95 emu/g at 20° C and that of MM_2Co_{17} phase is 114 emu/g. Both the 5:19 and 2:7 phases have a $4\pi M_s$ less than 45 emu/g.

Chapter 6 contains exclusively results on phase relations and magnetic properties of $MM(Co_{1-x}Cu_x)_5$ $0 \leqslant X \leqslant 1$, alloys. Cu can be substituted for Co upto 100% giving rise to stable $CaCu_5$ type phase. At low Cu concentration, 2:17 and a new phase coexist with the matrix 1:5 phase at 900° C. Both the a and c of the hexagonal 1:5 lattice increase with increasing Cu concentration. Cu can be substituted for Co upto 15 w/o in the 1:5 phase with a T_c not less than 500° C and a $4\pi M_s$ of about 70 emu/g. Beyond 15 w/o both the $4\pi M_s$ and the T_c are considerably reduced.

Chapter 7 deals with the permanent magnet properties of MM-Co alloys. Out of the many process parameters for magnet production a selected number of the parameters like, alloy composition, milling time, sintering temperature and time were studied for $MMCo_x$, $3.5 \leqslant X \leqslant 4.8$ alloys. Powder compacts were sintered between 960 and 1030° C for 5 m to 60 m. A maximum ${}_iH_c$ of 5250 Oe was obtained for $MMCo_{4.0}$ alloy sintered at 1000° C for 15 m. A 20% substitution of Sm to $MMCo_{3.8}$ alloy increased the ${}_iH_c$ to greater than 11 KOe. The sintered pellets contained invariably considerable amount of MM_2O_3 as revealed by X-ray and metallography. The chemical analysis of the powder compact and its sintered pellet showed same composition but it was different from the composition of the as-cast alloy indicating that the oxidation should have occurred during the process of powder production.

Chapter 8 is on the conclusions and suggestions for future work. A summary of the results obtained under Chapters 4, 5, 6 and 7 is given. The problem to be solved in the high Fe containing MM-Co-Fe alloys and the steps to be taken to minimise oxidation and improve the permanent magnet properties of the MM-Co alloys are given.

1. INTRODUCTION

1.1 A Comparison of Different Permanent Magnets

A permanent magnet is characterised by its coercivity (H_c), remanent induction (B_r) and maximum energy product ($(BH)_{max}$). High values for H_c and B_r give a magnet with a high $(BH)_{max}$. The $(BH)_{max}$ represents the maximum energy storage per unit volume and is the figure of merit often used for permanent magnet materials. In Figure 1.1 the progress in permanent magnet quality since 1880 as indicated by the value of the maximum energy product achieved for various material systems is illustrated[1]. It could be seen from this figure that the actual development of RE-Co magnet started around the year 1965 and the progress made within a decade following the year 1965 is spectacular over the erstwhile dominating magnets such as alnicos and ferrites. Rare earth cobalt magnets basically of two compositions, $RECo_5$ and $Sm_2(Co,Fe,Cu)_{17}$ have been developed. The demagnetisation curves of selected permanent magnet materials are given in Figure 1.2 where it could be seen again that $RECo_5$ and $RE(Co, Cu, Fe, Zr)_{17-x}$ alloys have superior demagnetisation curves to those of other magnets being used currently[2]. The repelling forces of two identical magnets of alnico, ferrite and a rare earth cobalt magnet (recoma, 1:5 type) is illustrated in Figure 1.3 for a comparison of their strength.[3] The supporting strength of the three materials are in the ratios of 1:6.5:37 respectively.

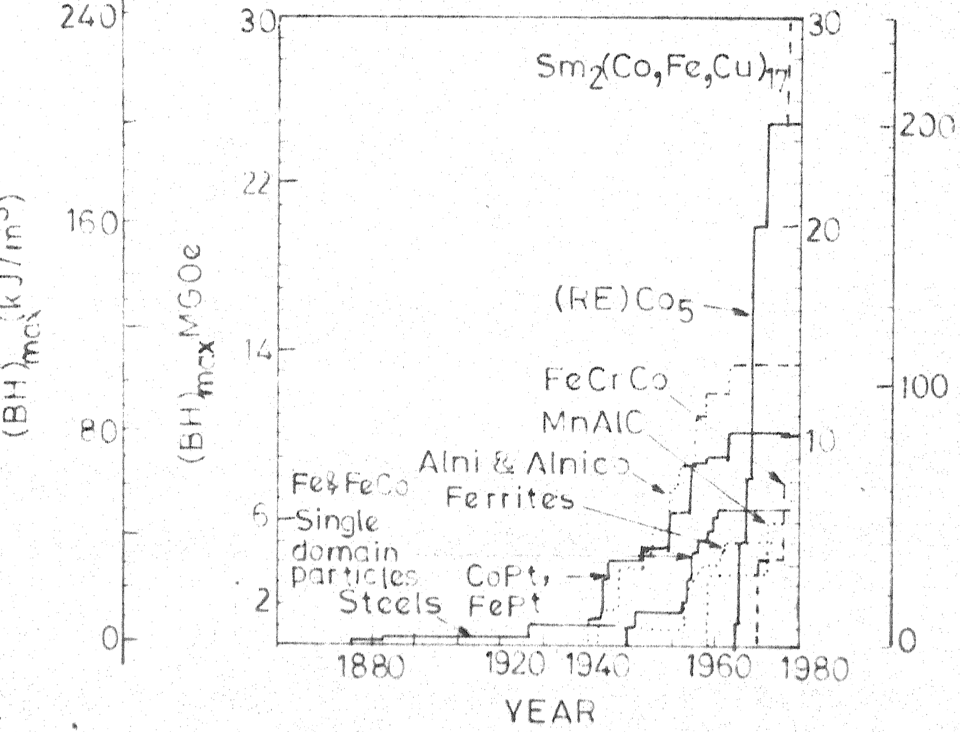

FIG.1.1 PROGRESS IN PERMANENT MAGNET QUALITY SINCE 1880 AS INDICATED BY THE VALUE OF THE MAXIMUM ENERGY PRODUCT ACHIEVED FOR VARIOUS MATERIAL SYSTEMS (Ref. 1)

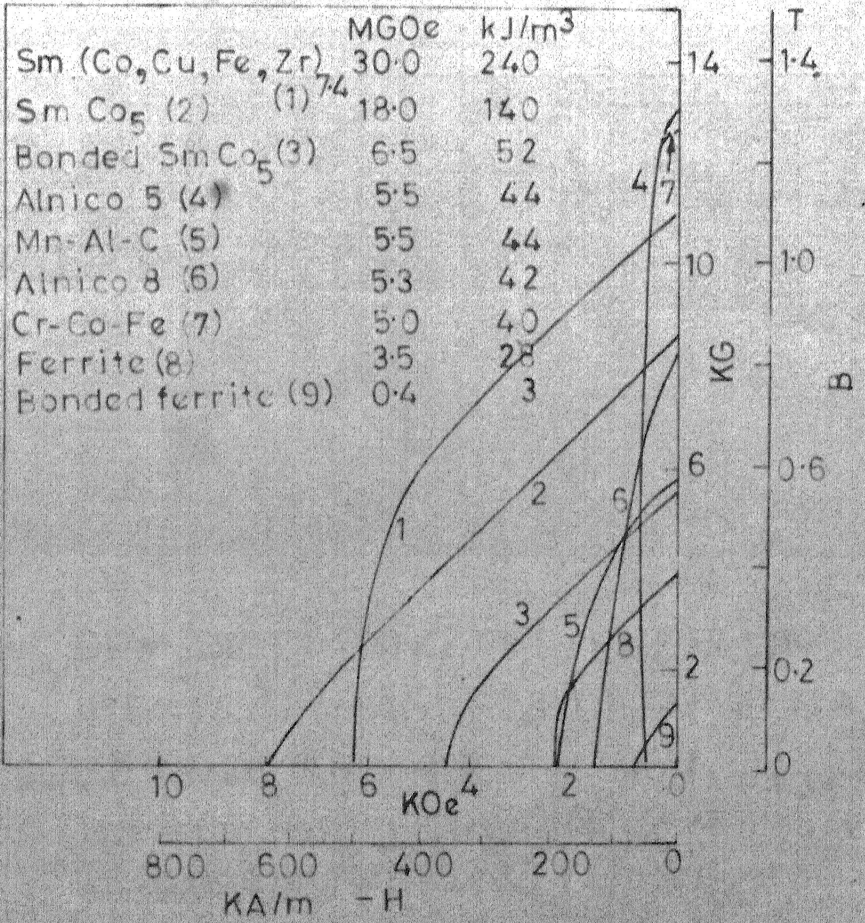

	MGOe	kJ/m^3
$Sm(Co,Cu,Fe,Zr)_{7.4}$ (1)	30·0	240
$SmCo_5$ (2)	18·0	140
Bonded $SmCo_5$ (3)	6·5	52
Alnico 5 (4)	5·5	44
Mn-Al-C (5)	5·5	44
Alnico 8 (6)	5·3	42
Cr-Co-Fe (7)	5·0	40
Ferrite (8)	3·5	28
Bonded ferrite (9)	0·4	3

FIG.1.2 DEMAGNETISATION CURVES OF SELECTED PERMANENT MAGNET MATERIALS (Ref. 2)

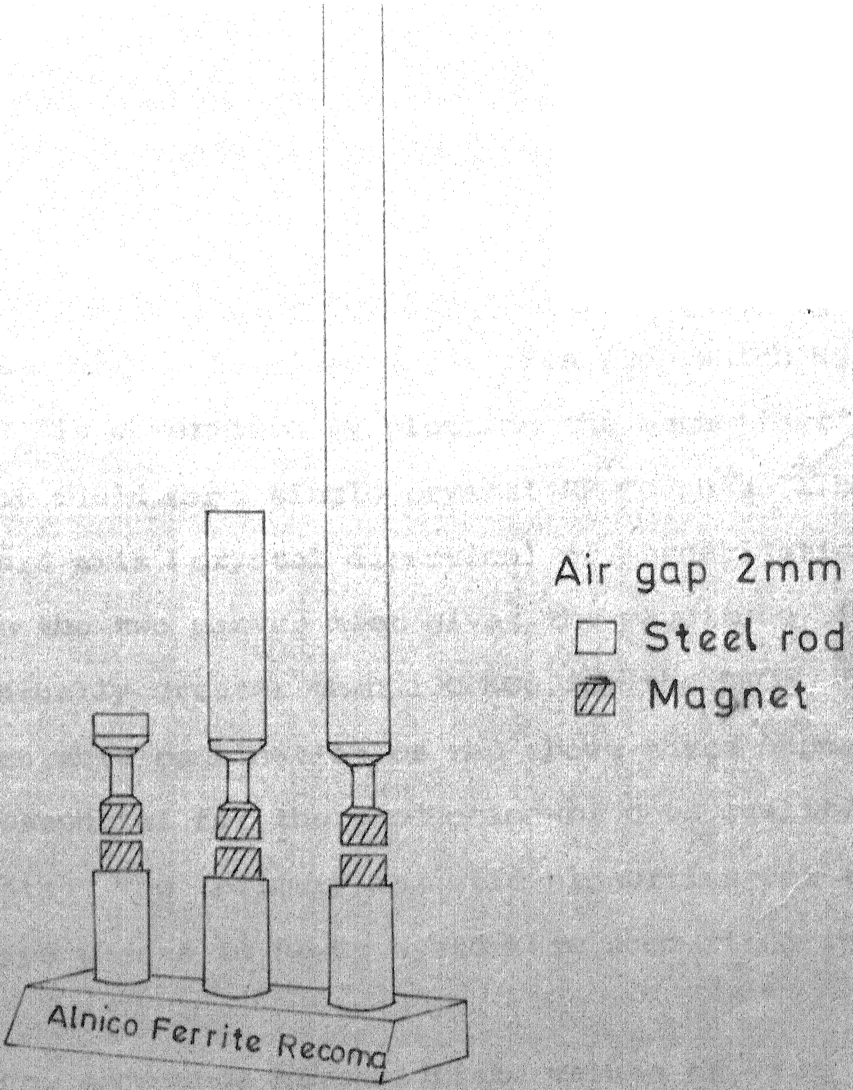

FIG.1.3 DEMONSTRATING THE REPELLING FORCES OF TWO IDENTICAL MAGNETS OF ALNICO 8, STRONTIUM FERRITE AND RECOMA (Ref. 3)

The supporting strength of the three materials are in ratios of 1:6.5:37 respectively.

A Recoma magnet supports 74 times its own weight

1.2 Primary Magnetic Properties of RE-Co Phases

The three primary magnetic properties that determine the suitability of a RE-Co phase for permanent magnet potential are (1) the magnetocrystalline anisotropy constant (K_1) (2) saturation magnetisation ($4\pi M_s$) and (3) Curie temperature (T_c). The magnetocrystalline anisotropy constant (K_1) is related to magnetocrystalline anisotropy field (H_A) by $H_A = 2K_1/M_s$ where H_A is the field necessary to rotate the magnetisation in a perfect single domain crystal. The H_A and M_s are the experimentally determined quantities from which K_1 is deduced. The H_A is determined by plotting the magnetisation as a function of field for a single crystal RE-Co phase along its easy and hard axis (crystal direction) of magnetisation. The point where the two curves meet gives the magnitude of H_A and it is usually greater than 100 KOe for the $RECo_5$ type phases. A favourable combination of the above three magnetic properties is essential for the production of good quality permanent magnets. The primary magnetic properties for the 1:5 and 2:17 type phases in RE-Co systems are summarised in Table 1.1.[2]

The $RECo_5$ compounds have moderate values of $4\pi M_s$ ($\sim$1 T) but extremely large values of K_1 ($\gg$1 MJ/m^3). The latter property is primarily responsible for the exceptionally large coercivity. In this regard $SmCo_5$ is the most outstanding of all $RECo_5$ magnets by virtue of having the largest value of K_1 (17 MJ/m^3). The RE_2Co_{17} compounds have higher $4\pi M_s$

TABLE 1.1 MAGNETIC PROPERTIES OF RCo_5 AND R_2Co_{17} COMPOUNDS: $4\pi M_s$ AND K_1 VALUES AT 25°C ARE GIVEN

Rare earth	RCo_5			R_2Co_{17}		
	$4\pi M_s$ (T)	T_c (°C)	K_1 (MJ/m^3)	$4\pi M_s$ (T)	T_c (°C)	K_1 (MJ/m^3)
Ce	0.85	374	5.3	1.15	800	-0.6
Pr	1.12	612	8.1	1.38	890	-0.6
Nd	1.20	630	0.7	1.39	900	-1.1
Sm	0.97	724	17.2	1.20	920	3.3
Gd	0.19	735	4.6	0.73	930	-0.5
Tb	0.24	707		0.68	920	-3.3
Dy	0.30	6930		0.70	910	-2.6
Ho	0.53	727	3.6	0.83	920	-1.0
Er	0.63	713	3.8	0.90	930	0.41
Tm	0.67	747		1.13	920	0.50
Yb						-0.38
Lu				1.27	940	-0.20
La	0.91	567	5.9			
Y	1.06	648	5.2	1.25	940	-0.34
Th			2.6			-0.53

T = 10 KG.

values than the corresponding RCo_5 series and hence might have greater energy products. However, as Table 4.1 shows, the magnitude of K_1 for the 2:17 compounds is considerably smaller than that for the corresponding 1:5 series. Furthermore, with the exception of Sm, Er and Tm, all 2:17 binary compounds have $K_1 < 0$, that is, an easy (0001) plane. For these compounds, magnetisation reversal becomes relatively easy and low coercivity is expected. There has been some success at modifying the sign and magnitude of K_1 by partial substitution for Co by other transition metals such as Fe, Cr and Mn.[4]

The magnetism of the RE-Co compounds is due to the interatomic exchange between the spins of the two sublattices plus the spin-orbit coupling within the rare earth atoms. In the lighter rare earth series-Ce, Pr, Nd and Sm - the spins of the RE and Co atoms are aligned parallel. The value of $4\pi M_s$ are thus high. In the other they are aligned antiparallel, and the values of $4\pi M_s$ tend to be low. Yttrium is nonmagnetic and hence the magnetic induction comes from Co alone. The magnetocrystalline anisotropy also comes from two sources, one originating in the itinerant electrons of the Co sublattice and one due to the crystalline electric field of the rare earths. A broad summary ranging from basic magnetism to the technology of the rare earth magnets is given by Menth et.al.[5]

1.3 RE- 3d Metal Phase Diagrams and Structures of Their Intermetallic Compounds

1.3.1 RE- 3d Metal Phase Diagrams

The binary phase diagrams of Ce-Co,[6,7] La-Co,[8] Ce-Fe[9] and Ce-Cu[7] are shown in Figures 1.4a to 1.4d and the compound formation in the high transition metal side in these systems is shown in Figure 1.5. The phase diagrams of Nd-Co and Pr-Co systems are similar to that of Ce-Co systems.[8] It is seen from Figure 1.4a that all the intermetallic phases in the Ce-Co system form through peritectic reaction. The temperatures of peritectic reaction for the intermetallic phases in the RE-Co systems (RE = Cr, La, Nd and Pr) are shown in Table 1.2.

TABLE 1.2 PERITECTIC TEMPERATURES OF INTERMETALLIC PHASES IN RE-Co SYSTEMS[7,8]

System	Peritectic temperature (°C)				
	1:3	2:7	5:19	1:5	2:17
Ce-Co	1091	1130	1134	1193	1209
La-Co	Does not exist	843	868	1124	Does not exist
Nd-Co	1105	1161	1166	1266	1301
Pr-Co	1057	1118	1125	1229	1271

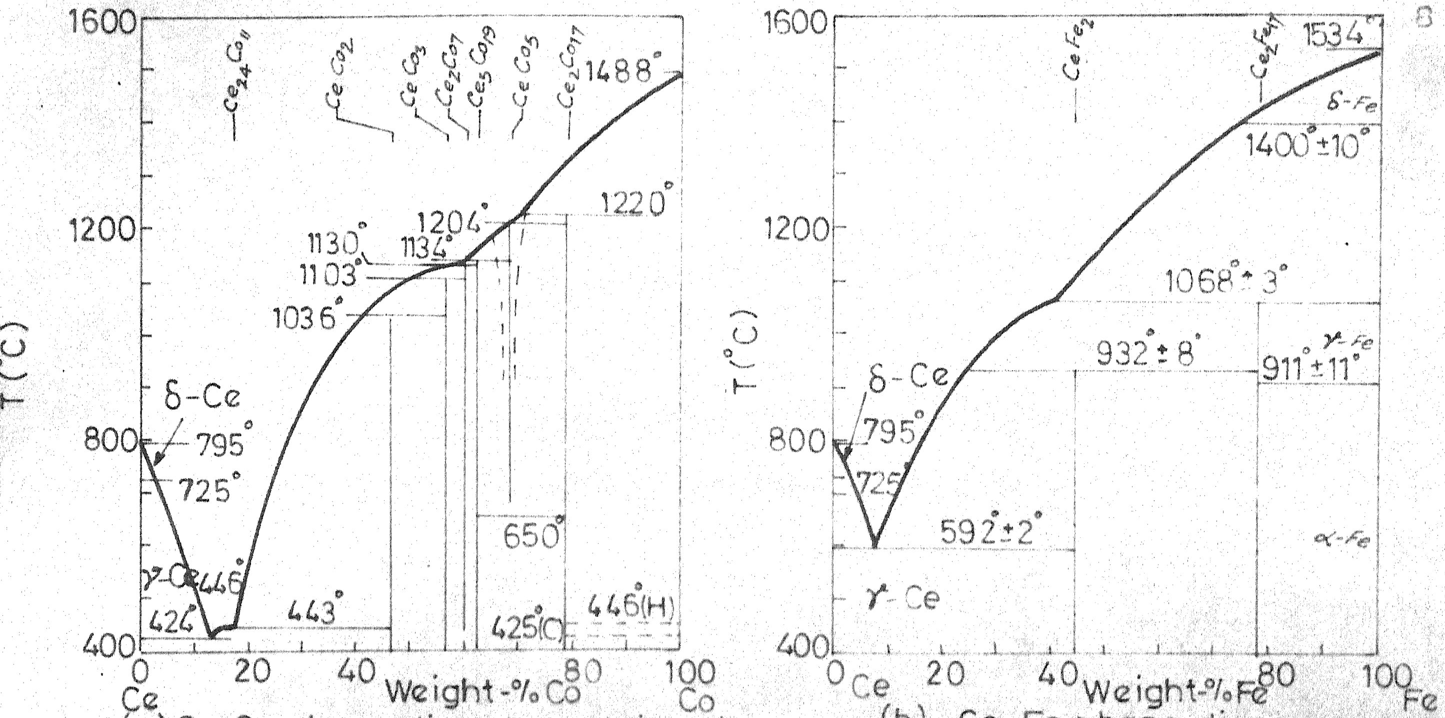

(a) Ce-Co phase diagram as given by Gschneidner (7) with slight modifications according to Martin et al (Ref. 6)

(b) Ce-Fe phase diagram according to Buschow and van Wieringen (Ref. 9)

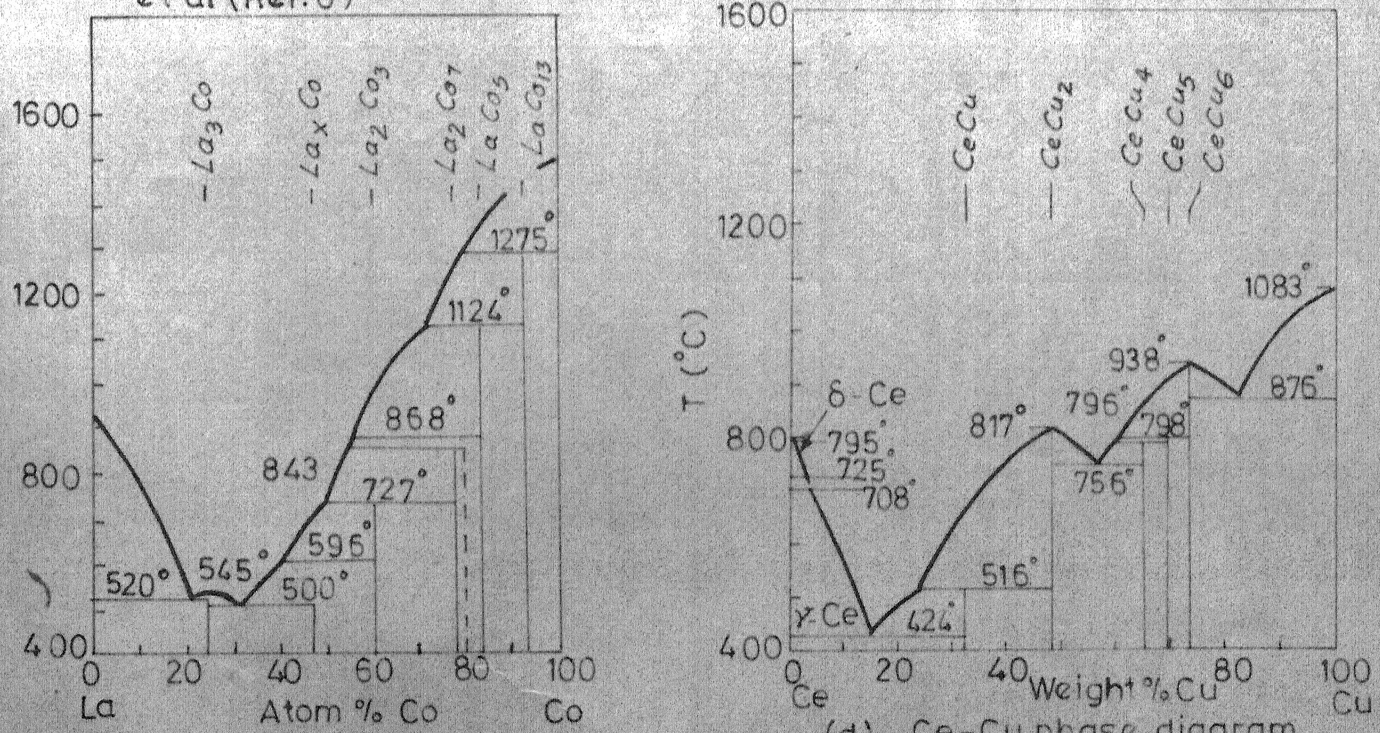

(c) La-Co phase diagram (Ref. 8)

(d) Ce-Cu phase diagram after Gschneidner (Ref. 7)

FIG. 1.4 PHASE DIAGRAMS OF RE-T SYSTEMS RE = Ce and La, T = Co, Fe and Cu

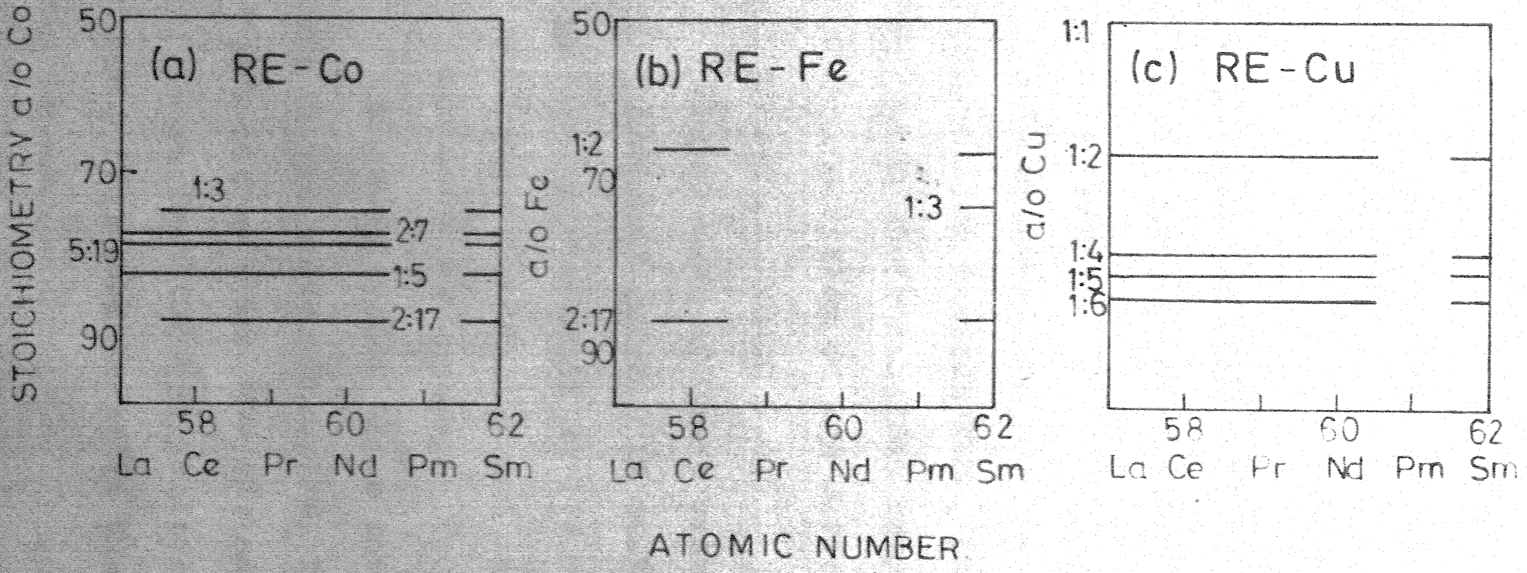

FIG. 1.5 COMPOUND FORMATION IN (a) RE-Co (b) RE-Fe AND (c) RE-Cu SYSTEMS

In the case of La-Co system the $LaCo_3$ and La_2Co_{17} phases do not exist. Also for the La_2Co_7 and La_5Co_{19} phases the peritectic temperatures are lower by about 300° C than that corresponding to these phases in the other RE-Co systems (Table 1.2). In Ce-Co system (Figure 1.4a) two features could be noted for the 1:5 phase. It shows a homogeneity region[6] at high temperatures ($\gg$ 700° C) and undergoes an eutectoid type reaction at temperature below about 650° C.[6,10] This was observed for other RE-Co systems also and the eutectoid decomposition temperatures for various $RECo_5$ phases are shown in Figure 1.6 together with their liquidus temperatures.[11] The effect of Fe and Al impurities on the eutectoid reaction temperatures is also shown in Figure 1.6.

In the case of Ce-Fe system only 1:2 and 2:17 intermetallic compounds exist. In Sm-Fe system in addition to these phases, the existence of an 1:3 phase is reported.[12] The 2:7, 5:19 and 1:5 phases found in the RE-Co systems are absent in the RE-Fe system.

In Ce-Cu system[7] five intermetallic phases corresponding to the stoichiometries, 1:1, 1:2, 1:4, 1:5 and 1:6 are seen, out of which the 1:2 and 1:6 phases form congruently and the rest form through peritectic reaction. The 2:7, 5:19 and 2:17 phases found in the Ce-Co system do not exist in this system.

Besides the binary systems, the isothermal sections of Sm-Co-Cu phase diagram reported by Perry et.al.[13] at 800° C

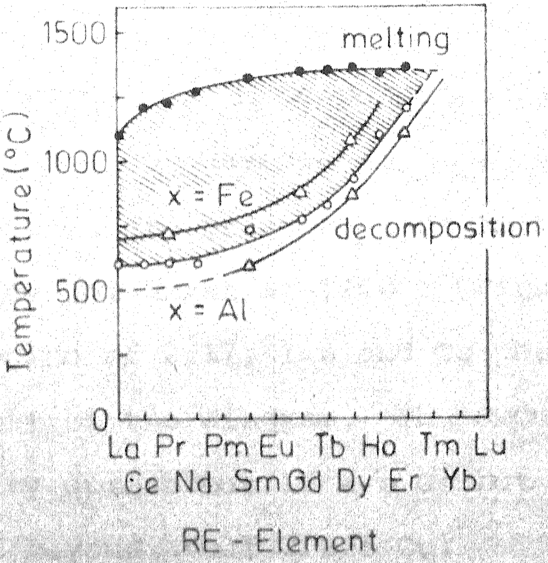

Fig 1·6 Melting temperature and decomposition temperature for various members of the $\mathrm{RECo_5}$ compound The curves denoted by X = Fe and X = Al show the decrease or increase of the stable $\mathrm{CaCu_5}$ - type region that can be obtained by adding 3 at. % X as an impurity (Ref 11)

1200°C are shown in Figures 1.7a and 1.7b. It is seen from Figure 1.7a that at 800°C, the 1:5 phase could exist as a stable phase with 100% solid solubility for Cu. The Sm_2Co_7 phase extends into the ternary upto about 38 a/o Cu but the $SmCo_3$ and Sm_2Co_{17} phases extend only upto a few a/o Cu into the ternary. Two narrow three-phase regions, one containing the 1:5, 2:17 and Co phases and the second containing 2:7, 1:5 and 2:17 phases are present close to the Sm-Co binary line. These regions do not exist at 1200°C (Figure 1.7b). A third three-phase region of 2:17, 1:6 and Co phases is present in the Cu rich part of the diagram. The $SmCu_6$ phase extends into the ternary upto about 16 a/o Co but the $SmCu_4$ phase does not exist beyond about 2 a/o Co.

1.3.2 Structures of Intermetallic Phases in RE-Co Systems

The technically relevant alloy compositions range from the REM_2 to the RE_2M_{17} intermetallics (RE = Ce, Nd, Pr and Sm, M = Co). The compounds in this range can be arranged into two groups, hexagonal and rhombohedral, which derive from the hexagonal $CaCu_5$ type structure of the REM_5 alloys.[14-17] The structure of the 1:5 alloy consists of an infinite stacking sequence of two-atom layers in the direction of c-axis: a hexagonal arrangement of M atoms followed by a mixed layer of RE and M atoms (Figure 1.8a).[18] The hexagonal unit cell contains a three rhombohedral unit cells (Figure 1.8b).[14] By an orderly exchange of an M atom against a RE atom in every

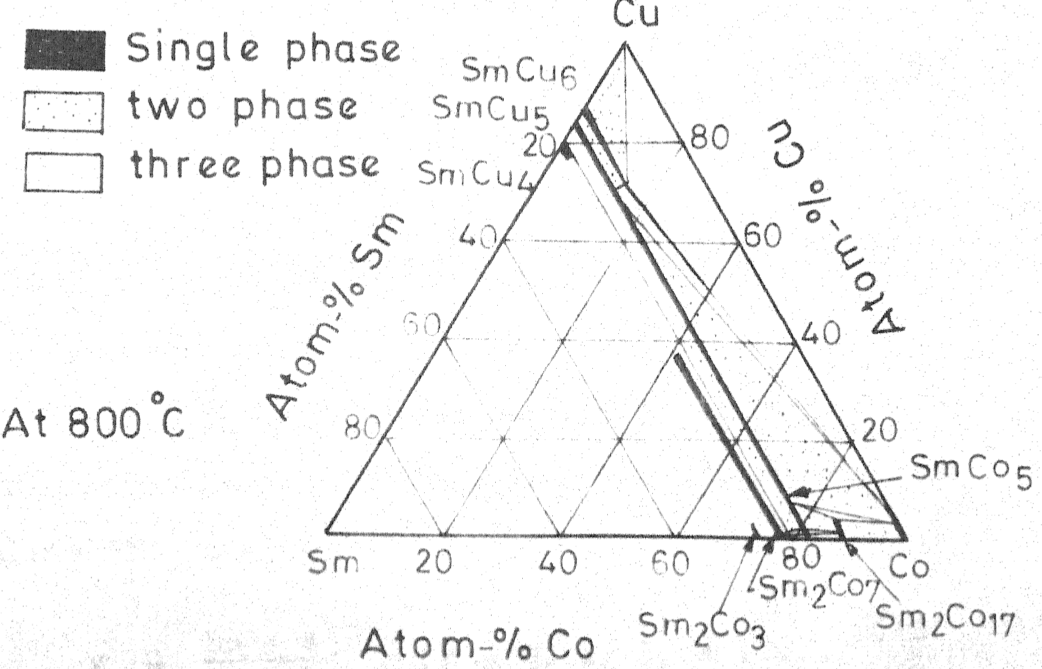

(a) At 800 °C

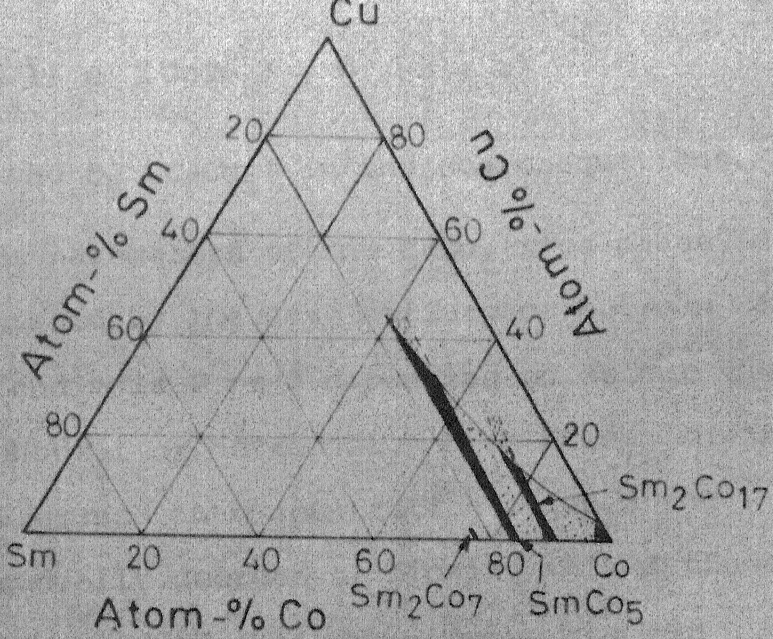

(b) At 1200 °C

FIG. 1.7 ISOTHERMAL SECTIONS OF THE Sm-Co-Cu PHASE DIAGRAM AFTER PERRY (Ref. 13)

first, second, third etc. unit cell, a simultaneous shift of the newly formed building blocks in the hexagonal basis and minor rearrangements of the RE atoms, the compounds REM_2, REM_3, RE_2M_7 etc. are formed.[14,15,17] The respective atom positions for REM_3 are shown in Figure 1.8c; the mode of formation of the other compounds is schematically given in Figure 1.9. The stoichiometries of the possible intermetallics in the series REM_x can be calculated from

$$X = \frac{5n + 4}{n + 2} \qquad (n = 0, 1, 2, 3 \ldots\ldots)^{15}$$

and the theoretically possible Cromer-Larson phases in RE-Co system are shown in Table 1.3. The lattice parameters of these phases are given by[19,20]

$$a_o = a_o\,(CaCu_5) + d_a\,(n + 1)$$

$$c_o = m\,(n + 1)\,c_o\,(CaCu_5) + d_c/(n + 1)$$

where $a_o\,(CaCu_5)$ and $c_o\,(CaCu_5)$ in the above equations. refer to the lattice parameters of the $CaCu_5$ type phase, d is the distortion caused by the size difference between RE and 3d metal atoms and m is 2 or 3 depending on wether the structure is rhombohedral or hexagonal. From RE_2M_7 onwards (Table 1.3) the difference in concentration between the predicted phases gradually decreases; finally this difference becomes indistinguishable and the series converges for $n = \infty$ against the $RECo_5$. Strnat et.al.[17] have reported thermomagnetic

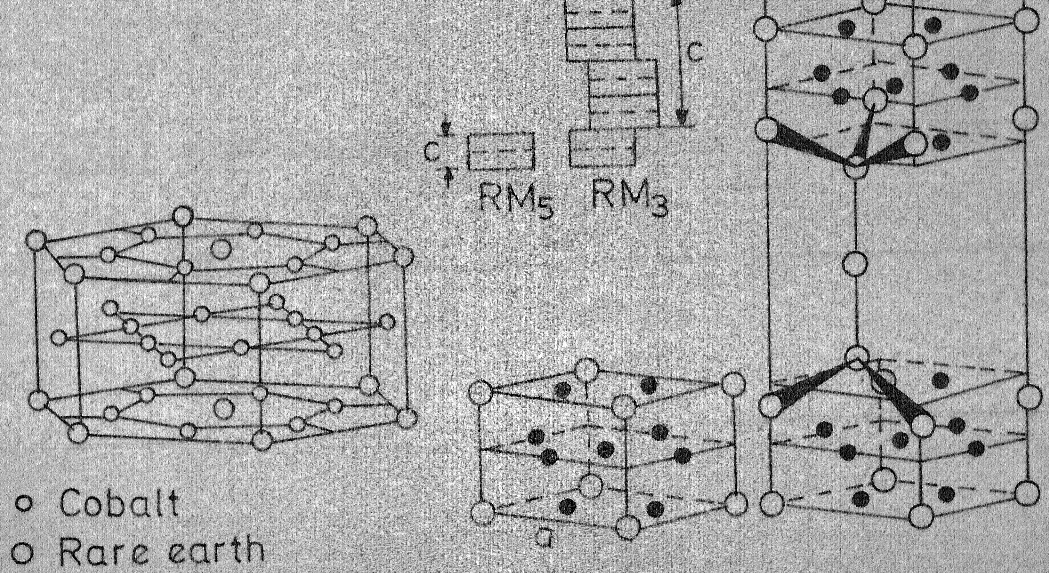

(a) (b) (c)

Fig.1·8

a) Hexagonal unit cell of the $CaCu_5$ structure after (Ref. 18)

b) Rhombohedral unit cell of the $CaCu_5$ structure after (Ref. 14)

(c) Substitution of one RE against one M atom in every second $CaCu_5$ unit cell minor displacements of RE atoms and layer shifts in the hexagonal basis plane lead to the REM_3 structure (Ref. 14)

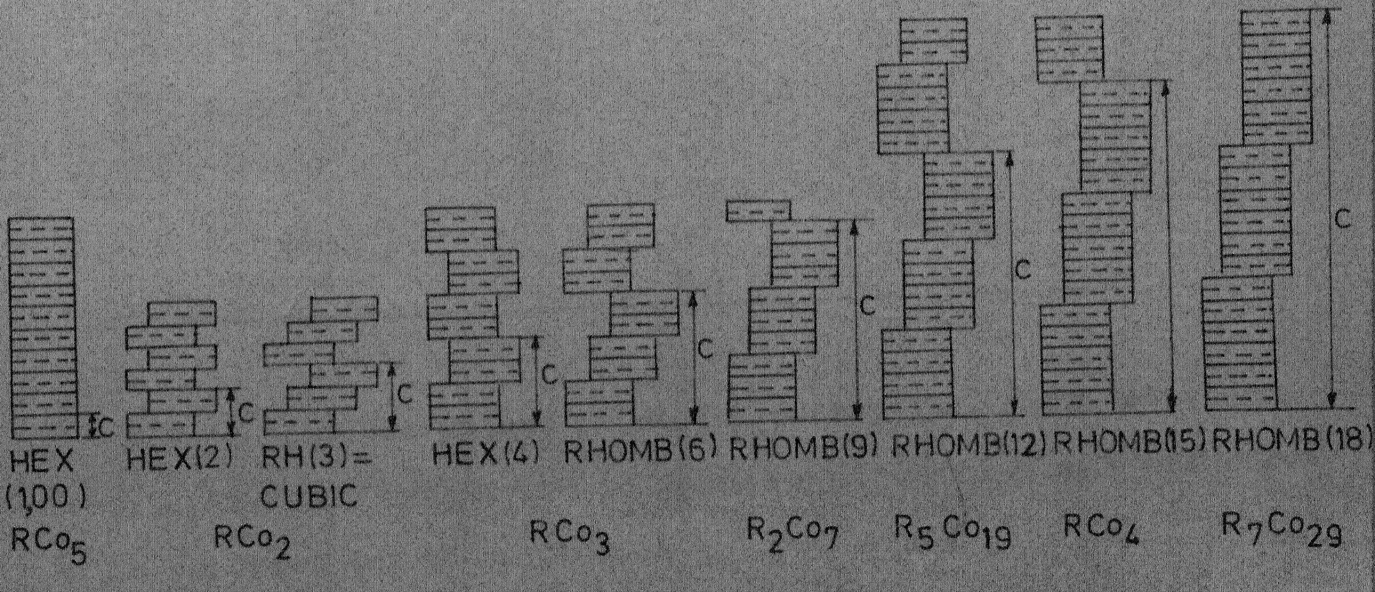

Fig. 1·9 Schematic diagram of the mode of formation of hexagonal and rhombohedral $R_x Co_y$ alloys out of the RCo_5 structure by layer shifts in the hexagonal base plane after (Ref. 14,15,17)

TABLE 1.3 THEORETICALLY POSSIBLE CROMER-LARSON PHASES IN RE-Co SYSTEMS

n	Phase RE_xCo_y	Co/RE ratio
0	1:2	2
1	1:3	3
2	2:7	3.5
3	5:19	3.8
4	1:4	4.0
5	7:29	4.14...
6	4:17	4.25
7	3:13	4.33..
. . .	. . .	. . .
. . .	. . .	. . .
10^4	1:4.99...	4.99...
. . .	. . .	. . .
. . .	. . .	. . .
∞	1:5	5.0

evidence for the phases of stoichiometry 1:4, 7:29, 4:17 and 3:19 in Pr-Co system but no X-ray or microstructural evidence is reported for these phases.

1.4 Structure Sensitive Magnetic Properties

The magnetocrystalline anisotropy[21] field H_A, and the coercivity[22] of the $RECo_5$ alloys depend on the microstructure of the alloy. It is seen from Figure 1.10 that the H_A of 1:5 phase peaks at composition corresponding to 1:5 stoichiometry and falls steeply on either side where the 1:5 coexists with either 2:7 or 2:17 phases. In Figure 1.11 the dependence of ${}_iH_c$, ${}_bH_c$ and $(BH)_{max}$ on the composition of Sm-Co alloy is shown. The coercivity peaks on the slightly Sm richer side of $SmCo_5$ phase but it drops steeply on the Co rich side of 1:5 composition.[22] This indicates that the presence of small amount of 2:7 phase with the 1:5 phase is not detrimental to ${}_iH_c$ as the presence of 2:17 phase with the 1:5 phase.

In Figure 1.12 the effect of heat treatment on the ${}_iH_c$ of $SmCo_5$ magnet is shown. When the $SmCo_5$ magnet is heated around 750°C for 30 minutes, the ${}_iH_c$ falls from about 35 KOe to about 5 KOe. This drastic drop in ${}_iH_c$ is attributed to an eutectoid reaction in $SmCo_5$[23] where the 1:5 phase decomposes into the adjacent 2:7 and 2:17 phases.

1.5 Technology of RE-Co Magnet Processing and Permanent Magnet Properties of $RECo_5$ Type Magnets

1.5.1 Flow Chart of RE-Co Magnet Processing

Powder metallurgy techniques are employed in the manufacture of rare-earth cobalt permanent magnets. The basic process consists of preparing powder by one of several

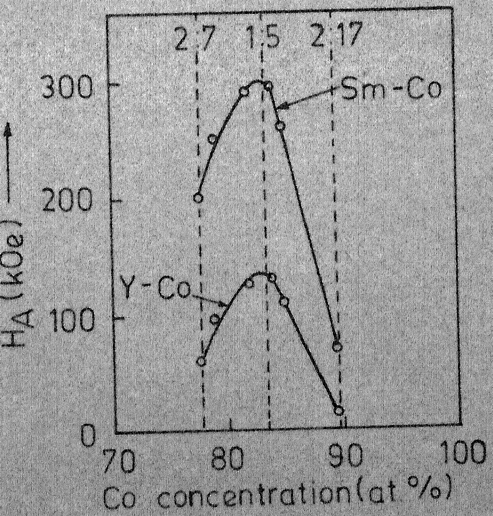

Fig. 1·10 Magnetocrystalline anisotropy of RE-Co materials as a function of composition. (Ref 21)

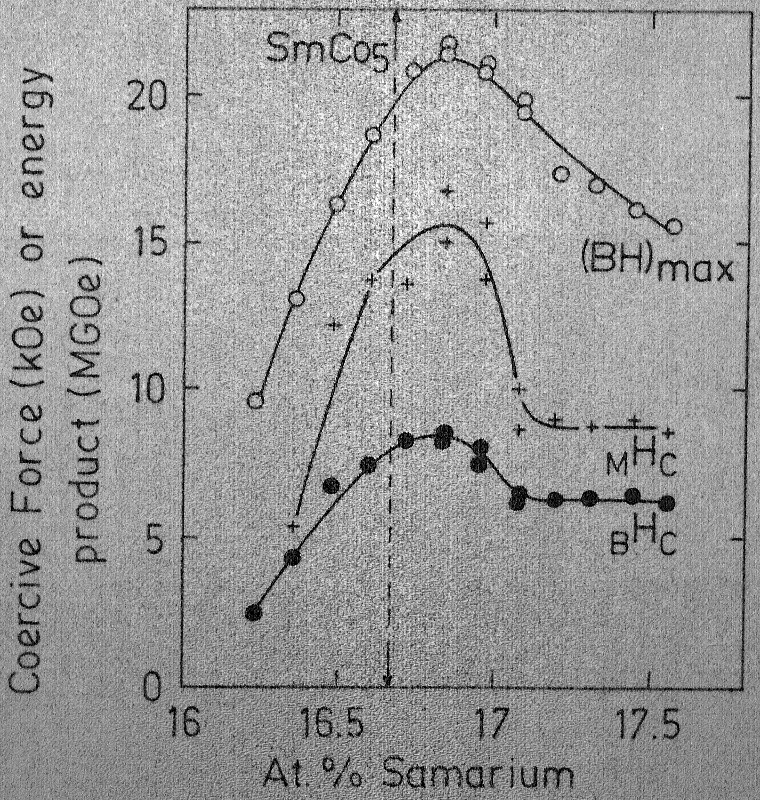

Fig. 1·11 Dependence of intrinsic as well as induction coercivity, $_MH_C$ and $_BH_C$ and energy product, $(BH)_{max}$, of $SmCo_{5 \pm x}$ magnets on cobalt content. (Ref. 22)

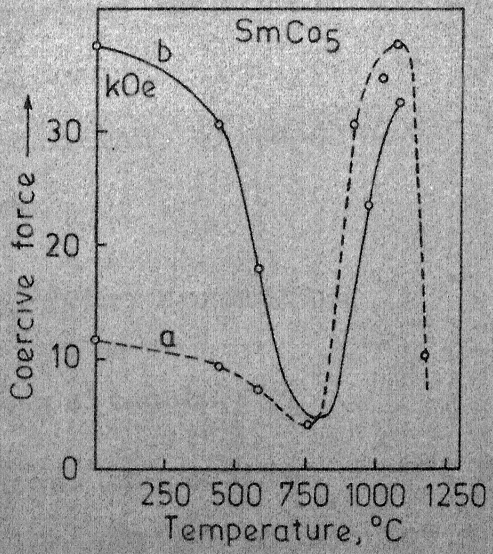

Fig. 1.12 Coercivity measured at room temperature as a function of heating temperature; samples were heated for 30 minutes; reaction with oxygen was avoided. Curve a: ground material. Curve b: ground material heated at 1080°C; second time heated at indicated temperature. (Ref 23)

methods, pressing the powder in a magnetic field, sintering the compacts and heat treating the sintered product. The overall process flow diagram is illustrated in Figure 1.13. Close control is required throughout and the most important factors are chemical composition, oxygen content, powder particle size distribution, aligning field and sintering and heat treating cycles.

1.5.2 Magnet Processing Parameters

1.5.2.1 Alloy Compositions

The chemical composition of the alloy determines its phase composition and the properties of the magnet produced depends on its microstructure. Therefore, a close control of the chemical composition of the alloy is necessary during magnet processing. The change in composition can occur during melting due to the loss of RE elements by evaporation or during powder preparation and sintering due to oxidation of RE elements. Thus the final composition of the magnet may turn out to be different from the starting composition of the alloy. The extent of shift in composition will depend on the melting method (arc or induction melting), milling procedure, and sintering process (solid or liquid phase sintering). Thus for each material system and for each set of process parameters adopted, the composition shift may be different. Therefore the right composition of the sintered magnets that gives the best properties is to be determined by a

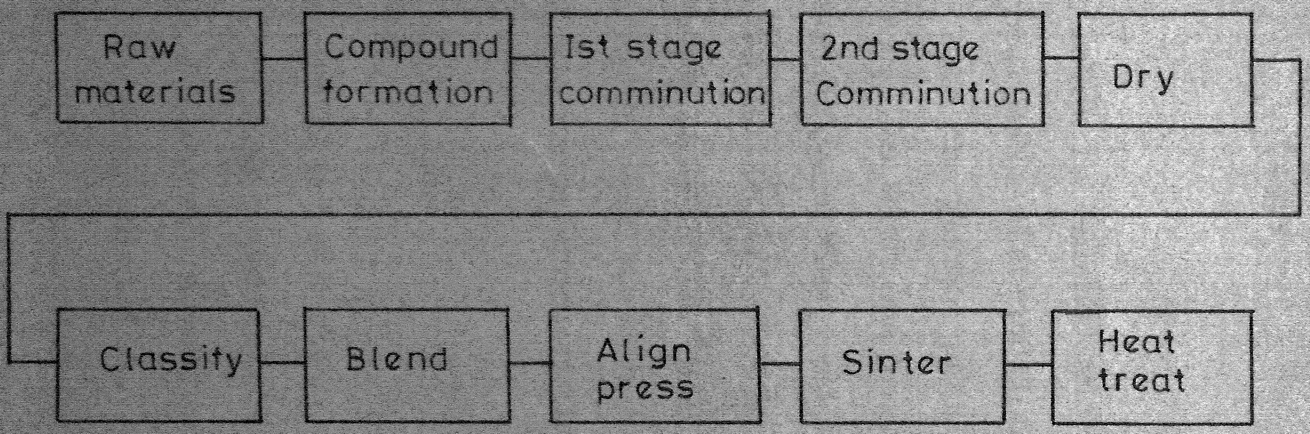

FIG. 1·13 PROCESS FLOW DIAGRAM FOR SINTERED RARE EARTH COBALT PERMANENT MAGNETS (Ref. 26) systematic study of these variables. It has always been reported that in the production of $RECo_5$ type magnets a RE-rich composition is used.[24,25]

1.5.2.2 Comminution

The cast ingot is crushed and ground to produce a powder with the proper size distribution and flow characteristics. In Figure 1.14 the proper particle size distribution (dashed curve) is compared with one that is too bad (solid curve). The large-size particles tend to be multi-grained and do not align or sinter properly. Under sized particles pick up an excessive amount of oxygen, which reacts with the metallic components to form oxide resulting in an overall shift of the composition out of the range where optimum properties are achieved.

1.5.2.3 Compaction

The properly sized and dried powder is pressed in the presence of an applied magnetic field not less than 10 KOe.[26] Homogeneous fields are necessary to produce a high level of uniformly aligned particles. It has been found that the application of a field in a direction perpendicular to the pressing direction leads to a better alignment of particles. Finished magnets are anisotropic with the direction of magnetisation determined during the pressing aligning step.

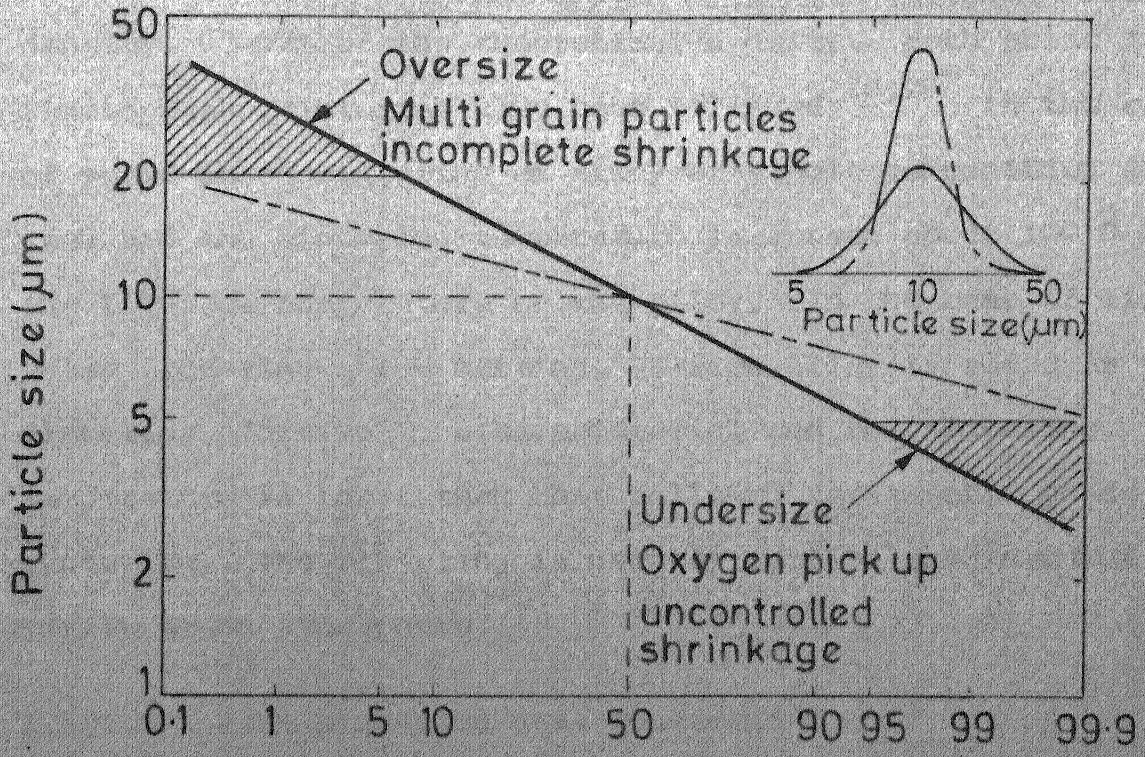

FIG. 1·14 COMPARISON OF OPTIMUM PARTICLE SIZE DISTRIBUTION (DASHED CURVE) WITH BROAD PARTICLE SIZE DISTRIBUTION (SOLID CURVE) (Ref. 26)

1.5.2.4 Sintering

The pressed powder compacts are sintered to high density, 93–97% of the theoretical density. Both solid and liquid phase sintering have been followed.[28,29] In the case of solid phase sintering an alloy of single composition is used and the sintering temperature is chosen about 100°C below the liquidus temperature of the alloy. In the case of liquid phase sintering a low melting, RE-rich alloy is added as the sintering additive to a base material and the sintering temperature is lower than that followed for a solid phase sintering. The sintering is usually carried out in a high purity argon atmosphere.

1.5.2.5 Post-sintering Heat Treatment

The sintered magnets are usually annealed at low temperature ($\leqslant$900°C) to optimise overall second quadrant characteristics of the hysteresis loop.[29-31] The shape of the demagnetisation curve as well as the magnitude of the coercivity can be considerably altered by suitable heat treatment procedure.[31] This heat treatment is found to be associated with change in microstructure of the magnets.

1.5.2.6 Magnetising and Characterisation

The permanent magnet properties are characterised by measuring its hysteresis curve particularly its second quadrant (demagnetisation curve). Two methods of representation are used; the intrinsic magnetisation curve and the BH hysteresis curve (Figure 1.15). The intrinsic magnetisation curve is more suited to describing the physical properties of the material while the BH curve is used for all practical purposes. The latter curve can be obtained from the former by the relation $B = H + 4\pi M$. The B_r, bH_c and $(BH)_{max}$ are obtained directly from the demagnetisation curve. The field applied for magnetising the samples during measurement should be sufficiently high to saturate the material, otherwise there is the risk of tracing the minor hysteresis loop. The field level is normally determined by the intrinsic coercivity in the case of $RECo_5$ type magnets. In practice the magnets are magnetised prior to magnetic measurements in a pulse field of 60-100 KOe and then their demagnetisation curves are traced in a magnetic field sufficiently higher than the intrinsic coercivity of the magnet.

1.5.3 Processes and Properties of Selected $RECo_5$ Type Magnets

Procedures followed in magnet processing and the properties developed for a selected number of $RECo_5$-type magnets are summarised in Table 1.4.

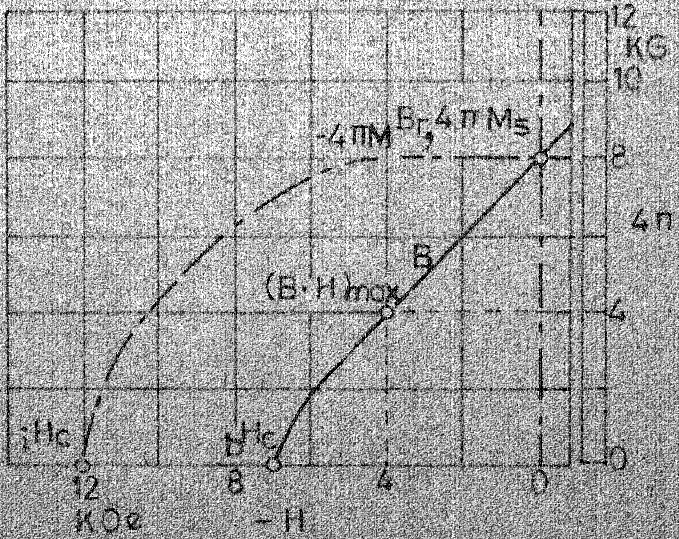

FIG. 1.15 TWO REPRESENTATIONS OF THE HYSTERESIS CURVE OF A PERMANENT MAGNET (Ref. 3)

$4\pi M$ = Intrinsic magnetization curve

B = Induction curve

The relationship between the two curves is given by

$B = 4\pi M + H$

in the Gaussian system of units

$4\pi M$ = Saturation magnetization

B_r = Remanence

$_iH_c$, $_bH_c$ = Coercive field of magnetization and induction respectively

TABLE 1.4 PROCESSES AND PROPERTIES OF SELECTED $RECo_5$ TYPE MAGNETS

System	Process	Properties	Reference
$SmCo_5$	(a) Induction melted, ground to $\nless 25\mu$ size particles by vibrating grinders in toluene. Compacted at 10 KOe. Sintered 1000°C for 60 m in an inert atmosphere.	B_r : 9000 G bH_c : 9000 G $_iH_c$: 25000+ Oe $(BH)_{max}$: 20 MGOe	D. Das[28]
	(b) Sinter additive: 60% Sm, 40% Co Base material: 66.7% Co. 33.3% Sm Induction melted, Fluid energy-milled to 6-8 μ size in nitrogen. Average composition of the blended powder: 62.6% Co, 37.4% Sm. Axially aligned at 60-100 KOe at 200 Kpsi to 6.8 g/cc sintered for 30 m at 1100°C in high purity Argon to 7.7 g/cc	$4\pi M_s$: 9.4 KG B_r : 8.1 KG bH_c : 7.7 KOe $_iH_c$: 16.4 KOe $(BH)_{max}$: 15.7 MGOe	M.G. Benz et.al.[29]
$Sm_{0.5}MM_{0.5}Co_5$	Base material: 66 w/o Co, 17 w/o MM and 17 w/o Sm. Additive: 40 w/o Co, 60 w/o Sm. Induction melted. Fluid energy-milled to ~10 μ in nitrogen. Aligned in 60 KOe field and compacted at 200 K psi. Sintered at 1000-1075°C for 30-60 m and magnetised in 100 KOe field prior to measurement	$4\pi M_s$: 9.6 KG B_r : 9 KG bH_c : 7.6 KOe $_iH_c$: 15.2 KOe $(BH)_{max}$: 20 MGOe	M.G. Benz et.al[25]

Contd....

TABLE 1.4 (contd.)

System	Process	Properties	Reference
$MMCo_5$ (MM: 53 a/o Ce, 30 a/o La, 13 a/o Nd and 4 a/o Pr)	Induction melted in Argon atmosphere. Alloys with MM richer than in $MMCo_5$ were jet-milled in nitrogen. Powder aligned in 50 KOe field at 6000 atmosphere. Sintered at 1040°C, heat treated at ~ 900°C and at ~300°C	${}_iH_c$: 9 KOe B_r : 8.1 KG $(BH)_{max}$: 14 MGOe	H. Nagel et.al.
$MM(Co,Cu,Fe,Mg)_5$ (MM: 52.1-57.8 w/o Ce, 23.4-33.4 w/o La, 10.8-17.9 w/o Nd and 3.4-6.6 w/o Pr)	35.5 w/o MM, 53.5 w/o Co, 6 w/o Fe, 4.9 w/o Cu and 0.1 w/o Mg. Alloys milled in Spex Shatter box at -60°C in Toluene to 3 µ size, aligned in a magnetic field of 8 KOe and compacted at 45,000 psi. Sintered in He at 980°C for 2 hours.	${}_iH_c$: 5.6 KOe ${}_bH_c$: 4.4 KOe B_r : 6.9 KG $(BH)_{max}$: 10.3 MGOe	J.W. Walkiewicz et.al.[32]

REFERENCES

1. I.S. Jacobs, J. Appl. Phys. 50, 7294 (1979).
2. G.Y. Chin and J.H. Wernick, in Encyclopedia of Chemical Technology, Wiley-Interscience, N.Y., ed. 3, in press.
3. K. Bachmann, Brown Boveri Review No. 9, 3 (1972).
4. H.A. Leupold, F. Rothwarf, J.J. Winter, A. Tauber, J.T. Breslin and A. Schwartz, Proceedings of the Second International Symposium on Magnetic Anisotropy and Coercivity in Rare Earth Transition Metal Alloys, p. 87, July 1, 1978, San Diego, CA, U.S.A.
5. A. Menth, H. Nagel, and R.S. Perkins, Annu. Rev. Mater. Sci. 8, 21 (1978).
6. D.L. Martin and J.G. Smeggil, W. Hatfield and R. Bolon, IEEE Trans. Magn. MAG-11, 1420 (1975).
7. K.J. Gschneidner Jr. and M.E. Verkade, Selected Cerium Phase Diagrams, Rare Earth Information Centre Publications IS-RIC-7, Iowa State University, Ames/Iowa (1974).
8. A.E. Ray, A.T. Biermann, R.S. Harmer and J.E. Davison, Cobalt 4, 103 (1973).
9. K.H.J. Buschow and J.S. Van Wieringen, Phys. Stat. Sol. 42, 231 (1970).
10. K.H.J. Buschow, J. Less-Common Metals 29, 283 (1972).
11. K.H.J. Buschow, J. Less-Common Metals 37, 91 (1974).
12. K.H.J. Buschow, J. Less-Common Metals 25, 131 (1971).
13. A.J. Perry, J. Less-Common Metals 51, 153 (1977).
14. K.H.J. Buschow, Phys. Stat. Sol. (a) 7, 199 (1971).
15. Y. Khan, Z. Metallkd. 65, 489 (1974).
16. D.T. Cromer and A.G. Larson, Acta Cryst. 12, 55 (1959).
17. K.J. Strnat and A.E. Ray, AIP Conf. Proc. 24, 680 (1975).

18. J.H. Wernick and S. Geller, Acta Cryst. 12, 662 (1959).

19. Y. Khan, Acta Cryst. B, 30, 1533 (1974).

20. Y. Khan, Phys. Stat. Sol.(a) 23, 425 (1974).

21. Y. Khan, Phys. Stat. Sol.(a) 23, 151 (1974).

22. D.L. Martin, M.G. Benz and A.C. Rockwood, AIP Conf. Proc. 1, 583 (1972).

23. F.F. Westendorp, Solid Stat. Commn. 8, 139 (1970).

24. C.J. Fellows and R.E. Johnson, Cobalt 56, 141 (1972).

25. M.G. Benz and D.L. Martin, J. Appl. Phys. 42, 2786 (1971).

26. A.E. Paladino, N.J. Dionne, P.F. Weirauch and E.C. Wettstein, Goldschmidt Informiert 63, 4/75, Nr. 35 (1975).

27. H. Umebayashi and Y. Fujimura, Japan Journal of Appl. Phys. 10, 1585 (1971).

28. D.K. Das, IEEE Trans. Magn. MAG-5, 214 (1969).

29. M.G. Benz and D.L. Martin, Appl. Phys. Letters 17, 176 (1970).

30. H. Nagel, H.P. Klein and A. Menth, J. Appl. Phys. 47, 3312 (1976).

31. Y. Iwama and T. Nishio, Proceedings of the Fifth International Workshop on Rare Earth-Cobalt Permanent Magnet and Their Applications, Roanoke, VA, June 1981, p. 443.

32. J.W. Walkiewicz and M.M. Wong, IEEE Trans. Magn. MAG-15, 1757 (1979).

2. STATEMENT OF THE PROBLEM

The review given in Chapter 1 under Section 1.1 shows that permanent magnets of outstanding technical properties (${}_iH_c$ and $(BH)_{max}$) much superior to other types of permanent magnets could be produced from Rare-Earth Cobalt alloys. Among the family of Rare-Earth Cobalt magnets, alloys containing Sm as the RE have maximum values for permanent magnet properties. But at the same time Sm is costly and this hinders the large volume production of its magnets for widespread application. In many of the permanent magnet applications a high resistance to demagnetisation is not necessary. In such cases a material which is cheap and at the same time has relatively large values for ${}_iH_c$ and $(BH)_{max}$ compared to the conventional commercial permanent magnets such as alnico and ferrites, may be preferred.

While the technology of production of $SmCo_5$ magnets has been widely studied and reported,(1-8) only a few studies have been reported on the development of magnets utilising mischmetal (a cerium rich mixture of light Rare-Earths) as the only RE.(9-11) Also the composition of mischmetal differs depending on the mineral source and the extraction method. In India there is a vast deposit of Rare-Earth minerals (in Travancore beach sand, Kerala) and it is the third largest producer of Rare-Earth in the world. The Indian mischmetal employed in this study contains about 6 w/o Fe as impurity introduced during the electrolytic process. Cobalt is less abundant than RE and is a scarce material.[12] Its partial replacement with other transition elements like Fe and Cu would certainly be preferred if the loss in magnetic properties as a result of their introduction is not much. Hence a study was undertaken to develop permanent magnets utilising the cheap commercial grade Indian mischmetal and cobalt with partial addition of Fe and Cu in place of Co.

The present study was undertaken with two broad objectives. Firstly to study the relation between structure, microstructure and composition and establish the phase relationships in the MM-Co-Fe and MM-Co-Cu systems. Secondly to select the suitable phase compositions in these systems and study the influence of various process parameters on the permanent magnet properties.

Magnetic properties (${}_{i}H_{c}$ and B_r) are very sensitive to phase composition[13-16] and a knowledge of phase relationship in the RE-Co system is essential to select the right composition for the magnet production. Phase relations study in the RE-Co system is complicated because of the close structural similarity among the various intermetallic phases.[17-19] In addition to the conventional experimental tools like metallography and X-ray diffraction, additional experimental techniques such as thermo-magnetic analysis (TMA) and electron probe micro-analysis (EPMA) are imperative to confirm the identity of the phases. Some of the phases like 5:19 in the binary RE-Co system were discovered only lately by the TMA technique and by very careful thermal analysis. The mischmetal itself contains atleast four RE elements, Ce, La, Nd and Pr and the alloying behaviour of La with Co is quite different from that of the other RE elements with Co. The La-Co system does not contain stable phases like 1:3 and 2:17.[21] Hence a systematic study was undertaken to establish the phase relationships in the technologically important composition region at 900°C using X-ray, metallography and TMA extensively and the EPMA to a limited extent.

An estimation of the primary magnetic properties, magneto-crystalline anisotropy field (H_A), saturation magnetisation ($4\pi M_s$) and the Curie temperature (T_c) is essential to decide the suitability of a RE-Co phase for permanent magnet potential. The MM-Co-Fe and MM-Co-Cu phases were studied for their $4\pi M_s$ and T_c using a vibrating sample magnetometer.

In the process of magnet production the parameters to be studied are: (i) composition of the alloy, (ii) size and size distribution of the powder (iii) compacting method (iv) sintering temperature and time and (v) post-sintering annealing temperature and time. These parameters affect both the B_r and ${}_iH_c$ and hence the $(BH)_{max}$. The selection of right combination of the above parameters is essential to maximise the permanent magnet properties. Obviously, a systematic study varying all the above parameters will be a lengthy process and may not be necessary. Composition, powder characteristics, sintering temperature and sintering time are the parameters investigated in the present study. only MM-Co alloys were tried in this connection. The powder production and the sintering are the most important steps in the magnet processing as the RE-Co alloy powders are highly susceptible to oxidation. The quality of the powder produced was checked by measuring their ${}_iH_c$ rather than their average particle size since no single available technique has been found to give correct estimation of the particle size of the micron-size RE-Co magnetic powders.[22]

REFERENCES

1. K.H.J. Buschow, P.A. Nastepad and F.F. Westendorp, J. Appl. Phys. 40, 4029 (1969).

2. D.K. Das, IEEE Trans. Magn. MAG-5, 214 (1969).

3. M.G. Benz and D.L. Martin, Appl. Phys. Letters 17, 176 (1970).

4. M.G. Benz and D.L. Martin, J. Appl. Phys. 43, 3165 (1972).

5. A.E. Paladino, N.J. Dionne, P.F. Weihrauch and E.C. Wettstein, Goldschmidt Informiert 4/75, Nr. 35, 63 (1975).

6. Proceedings of the Second International Workshop on Rare Earth Cobalt Permanent Magnets and Their Applications, Dayton, Ohio, U.S.A., June 8-11, 1976, New magnet materials and production methods, Session VI.

7. Proceedings of the Third International Workshop on Rare Earth Cobalt Permanent Magnets and Their Applications, San Diego, CA, U.S.A., June 27-30, 1978, Session VII, New Materials and Processes.

8. Proceedings of the Fourth International Workshop on Rare Earth Cobalt Magnets and Their Applications, Hakone National Park, Japan, May 22-24, 1979, Sessions IX, XI and XII Permanent Magnets (I), (II) and (III).

9. C.J. Fellows and R.E. Johnson, Cobalt 56, 141 (1972).

10. H. Nagel, H.P. Klein and A. Menth, J. Appl. Phys. 47, 3312 (1976).

11. K. Narita and H. Yamamoto, IEEE Trans. Magn. MAG-14, 785 (1978).

12. G.Y. Chin, S. Sibley, J.C. Betts, T.D. Schlabach, F.E. Werner and D.L. Martin, IEEE Trans. Magn. MAG-15, 1685 (1979).

13. D.L. Martin and M.G. Benz, AIP Conf. Proc. 5, 970 (1972).

14. P.A. Nastepad, F.J.A. Den Broeder and R.J.K. Wassink, Powder Metall. Int. 5, 61 (1973).

15. A. Benz and K. Bachmann, AIP Conf. Proc. 10, 578 (1973).

16. P.F. Weihrauch and D.K. Das, AIP Conf. Proc. 18, 1149 (1974).

17. D.T. Cromer and A.C. Larson, Acta Crystallogr. 12, 855 (1959).

18. K.H.J. Buschow, Phys. Status Solidi A7, 198 (1971).

19. Y. Khan, Z. Metallkd. 65, 489 (1974).

20. K.J. Strnat and A.E. Ray, AIP Conf. Proc. 24, 680 (1975).

21. A.E. Ray, A.T. Bierman, R.S. Harmer and J.E. Davison, Cobalt 4, 103 (1973).

22. H. Augustin, Goldschmidt Informiert, 2/79, Nr. 48, 64 (1979).

3. EXPERIMENTAL

The experimental methods followed in the present study are grouped into four sections, 1) alloy preparation, 2) phase analysis, 3) characterisation of magnetic properties and 4) magnet processing.

3.1 Alloy Preparation:

3.1.1 Raw Materials:

Indian mischmetal used in the study has the compositio (analysed by x-ray fluorescence and complexometric methods[1]) 52 pct. Ce, 20.1 pct. La, 15.7 pct. Nd, 4.8 pct. Pr and 6 pct. Fe (all in w/o) and the balance ($\sim$1.4 pct.) unidentified impurities. The Co, Fe and Cu used are of $>$99.9 pct. purity. The specifications of these materials are given in appendix I.

3.1.2 Melting:

The mischmetal ingot (Fig. 3.1) was cut into small pieces and ground to remove the outer oxidised surface. An effective gm. at. wt. of 140.06 gms. was computed for MM based on chemical analysis[1]. The component elements MM, Co, Fe or Cu were weighed in the required proportions. The computation procedure of alloy composition is given in appendix II. The allo were prepared by arc melting in a water cooled Cu crucible in an ultra high purity argon atmosphere. Three or four meltings each lasting for 20 to 30 seconds were given and the alloy button weighing about 30 gms. was broken to small pieces and placed inverted after each melting to ensure uniformity in composition through out the ingot. The weight loss during

① Mischmetal(Indian) Ingot

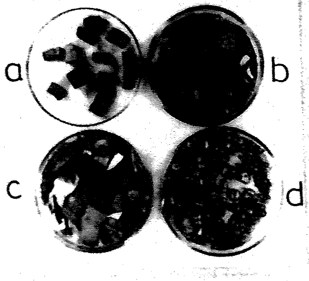

②Raw materials:
(a) Cut and polished MM
(b) Co (c) Fe and (d) Cu

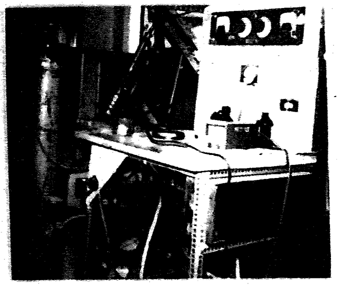

③ Arc melting unit

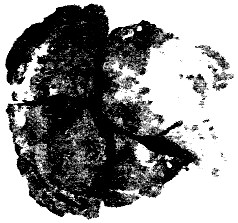

④ Arc melted alloy button

PHASE ANALYSIS: EXPERIMENTAL

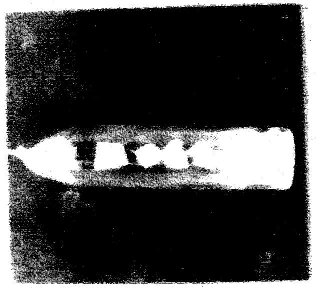

⑤ Encaptulation in quartz ampoule under vacuum (10μ) for 300 °C annealing

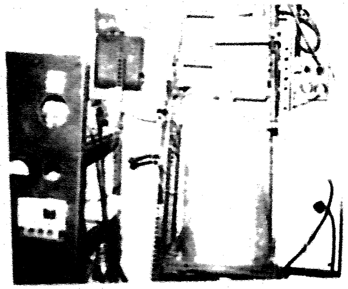

⑥ Annealing furnace set-up

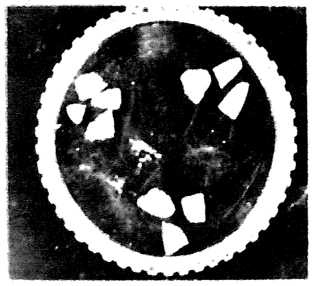

⑦ Homogenised alloy pieces

PHASE ANALYSIS

1. Microstructure
2. X-ray diffraction
3. Thermomagnetic analysis (T.M.A.)
4. Electron probe micro-analysis (E.P.M.A.)

Fig.31 Materials, equipments, and methods employed in phase analysis

melting due to evaporation of the RE elements was typically of 0.5 to 1 w/o.

3.1.3 Annealing

As the molten alloy is cooled very fast and most of the phases in RE-Co systems form through peritectic reactions segregation is inevitable. To homogenise the alloys small lumps of the as-cast alloy buttons were sealed in evaluated (10) quartz ampoules (Figure 3.1), annealed at 900°C for 4 to 10 days and quenched in water at the end of the annealing to retain the equilibrium phases corresponding to the annealing temperature. These homogenised alloy pieces were used for phase analysis.

3.1.4 Chemical Analysis

In arc melting of the alloys, the loss of RE due to evaporation is unavoidable and it varies depending on the arc pressure, melting time, amount of the alloy melted etc. Hence it was necessary to check the composition of the alloys melted. The alloys were analysed for total RE, Co, Fe and Cu. As the Fe caused interference in the determination of RE and Co, it was precipitated quantitatively as Fe (111) hydroxide and analysed while the RE and Co were determined from the filtrate by visual complexometric method. The Cu in the alloys were determined either by complexometric method or by iodimetry. The detailed procedure of the chemical analysis is reported in Reference 1.

3.2 Phase Analysis:

Four techniques, metallography, x-ray diffraction, thermomagnetic analysis (TMA) and electron probe microanalysis (EPMA) were employed to study the phases.

3.2.1 Metallography:

A small piece of the homogenised alloy was taken and its surface for microstructural observation was prepared by standard procedures[2,3]. The brittle alloys were hand ground carefully to avoid the introduction of cracks and then polished with fine alumina (0.1μ) powder. The polished surfaces were then etched with 2 pct. nital solution for 2 to 3 seconds and the microstructure was observed with a Carl Zeiss NU-2 universal microscope in bright field.

3.2.2 X-ray Diffraction:

X-ray diffraction of the annealed samples was carried out with G.E. XRD-5 and 6 and a Philips PW 1730/10 x-ray diffractometers. For MM-Co-Fe alloys Cr, Co or Fe K_α radiation was used but for high Cu containing alloys Cu K_α radiation gave better results. Because of the close structural similarities[4-6] of the different RE-Co phases, their strongest reflections have close 'd' spacings and occur at close 2θ values. In order to resolve them Cr K_α radiation was used as the preferred one. powder samples were prepared by crushing the brittle alloys to -325 mesh size. The high Co and high Cu containing alloys were less brittle and tougher than the less Co or Cu bearing alloys. Hence Co or Cu rich alloy powders were annealed at 600°C for 10 minutes to remove the strain prior to x-ray diffraction.

diffractograms were obtained by scanning at a rate of 2^{o}/min. In those cases where the lattice parameters of the phases were to be determined, the peaks were scanned at a slower speed (0.2^{o}/min).

3.2.3 Thermomagnetic Analysis (TMA)

TMA was found particularly necessary to study the low cobalt phases with stoichiometry lower than 1:5 in the RE-Co systems (RE=Ce, La, Nd and Pr). The melting points of the peritectic 2:7 and 5:19 phases in these systems differ by less than 10^{o}C and their standard x-ray diffraction data calculated based on their lattice parameters have the strong lines occurring at nearly the same position leaving only a few weak lines characteristic of these phases[7,8]. Hence with conventional techniq such as thermal analysis and x-ray diffraction commonly used in determining phase diagrams, possibilities exist to misinterpret them. Also, when the phases 5:19, 1:5 and 2:17 coexist in a non-equilibrium condition in a case such as the partially decomposed 1:5 alloy, then the identification of 1:5 by x-ray diffraction is not possible as all the strong lines of 1:5 are common either to 5:19 or 2:17 phases[8-10]. Since these phases are ferromagnetic and have sufficiently different Curie temperature (T_c)[11], TMA was used to identify the phases and to obtain evidence for both the decomposition products of $MMCo_5$. The TMA was used as a general tool like metallography or x-ray diffraction for phase identification in the present study. The experimental procedure is described under section 3.3.3.

3.2.4 Electron Probe Microanalysis:

A model microsonde Electronic-MS-46 electron probe microanalyser was used to analyse the samples with an accelerating voltage of 20 KV and an x-ray emergence angle of 18°. The specimens were mounted in a perspex mold and their surfaces were prepared as for optical metallography. The polished surfaces were faintly etched with 1 pct. nital solution just to reveal the phase boundaries. This facilitated to select the right site for microanalysis of the elements. The phases were analysed for the five RE elements (Ce, La, Nd, Pr and Sm) and the three 3d transition elements (Fe, Co and Ni). Metals of the above elements with purity $\geqslant$ 99.9 pct. were mounted separately in different sample holders and used as standards to compare the x-ray intensities emitted from the samples. Both point and line scanes cutting across many grains were carried out.

3.3 Characterisation of Magnetic Properties:

3.3.1 Primary Magnetic Properties:

The three primary magnetic properties that determine the suitability of a RE-Co phase for permanent magnets are 1) the magnetocrystalline anisotropy field (H_A), 2) saturation magnetisation ($4\pi M_s$) and Curie temperature (T_c)[12,13].

3.3.1.1 Magnetocrystalline anisotropy field, H_A:

The H_A is experimentally determined by tracing the magnetisation curves along the magnetic easy and hard directions of a single crystal. The magnetic field corresponding to the point of intersection of the two curves gives the H_A[12]. In the case of polycrystalline material the same is obtained using a magnetically aligned powder specimen in which each powder particle is assumed to be a single grain. In practice the hard-axis magnetisation curve is plotted only upto $<$ 100 KOe owing to the limitation of the field and then extrapolated as the H_A of the $RECo_5$ phases is much higher than 100 KOe. This gives in many cases unrealistic values. Hence the H_A values estimated for oriented powder specimens in low magnetic field have to be treated with caution as they can give only an idea of the magnitude of the value. In the present study because of the non-availability of magnetic field greater than 11 KOe, the estimation of H_A was not attempted for MM-Co intermetallic phases.

3.3.1.2 Saturation magnetisation, $4\pi M_s$:

A PAR Model 155 vibrating sample magnetometer was used to estimate the specific magnetisation, σ (emu/gm) at ambient temperature. The magnetometer was calibrated with a standard PAR Ni sample which has a σ of 55 emu/gm at 298°K. All the magnetisation results reported in this work are based on this value. As the MM-Co phases are expected to have $H_A \gg 10$ KOe the alloy specimens were ground to powders of a few micron size under toluene. The powder was mixed into a paste with an epoxy resin and was filled in glass ampoules. Then they were aligned in a magnetic field (11 KOe) for few minutes and allowed to set in air in the absence of the field as they took 10 to 15 hrs for setting. The resin to powder weight ratio was typically of 0.5, the powder weight in the samples being in the range of 0.06 to 0.1 gm. Samples thus prepared have M_r/M_s ratio of about 90 pct. and can be saturated with a 11 KOe field. When the magnetisation is reported for stoichiometric MM-Co phases, annealed samples were used in which the presence of the second phase as estimated by optical microscopy was $\leq$ 5 pct.

3.3.1.3 Curie Temperature, T_c:

As-cast as well as annealed alloys were used for thermomagnetic analysis (TMA). The samples studied were of about 0.2 gm. The TMA was carried out by measuring the magnetic moment (emu) of the sample as a function of temperature in a low magnetic field (40 Oe). A PAR model 155 vibrating sample magnetometer coupled with model 151 high temperature oven assembly was used (Fig. 3.2). The alignment of the oven assembly was checked by measuring the T_c of the standard PAR Ni sample which had a value of 356°C. The samples were taken in a boron nitride crucible and kept in a vacuum of 10^{-3} Torr during the test to avoid oxidation. The output terminals of the Cr-Al thermocouple and the magnetometer were connected to the x and y axis, respectively, of an x-y recorder and the magnetic moment of the sample was continuously traced as a function of temperature. As the upper limiting temperature of he oven was 727°C, the phases having T_c greater than 700°C were ot studied.

Since the thermocouple of the PAR high-temperature oven ndicates only the oven temperature and the sample takes some ime to equilibriate with the changing oven temperature, a hermal hysteresis was observed between the heating and the cooling urves which decreased with decreased rate of heating or cooling.

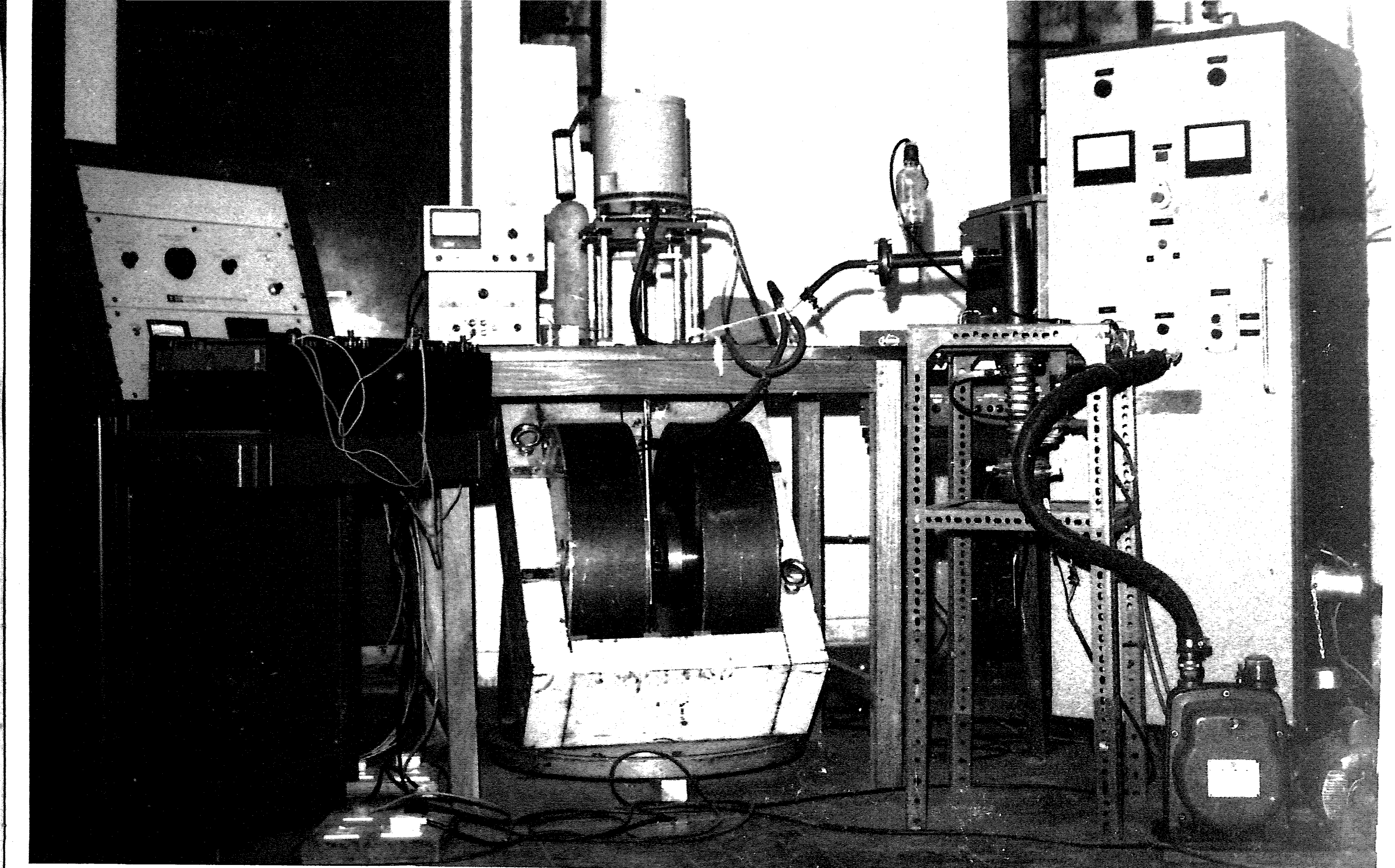

Fig. 3·2 Experimental set-up for thermomagnetic analysis

(1)PAR model 155 vibrating sample magnetometer (2)Model 151 high-temperature oven assemply (3) Polytronic electromagnet (8″ pole gap, 2″ air gap and 11 KOe peak field)(4) Vacuum system-mechanical and diffusion pumps

At a rate of 2°C/min a thermal lag of 10–15°C was persistent. Hence both the heating and the cooling curves were traced at the sa rate, especially near the magnetic transition regions and the mean of the transition temperatures read from these two curves was taken as the ferromagnetic Curie temperature of the phases studied.

3.3.2 Permanent magnet properties:

The permanent magnet properties of technical importanc are Br, $_iH_c$, $_bH_c$ and $(BH)_{max}$. These parameters are obtained from the demagnetisation curve (II quadrant of the magnetic hysteresis loop) of the magnet samples. The experimental procedure to evaluate these properties is described under section 3.4.6,.

3.4 Magnet Processing:

The magnet processing involves the following steps, alloy preparation, comminution, compacting, sintering, magnetisin and characterisation of the magnets for their physical and magnetic properties (Figure 3.3).

3.4.1 Alloy Preparation:

MM-Co alloys were prepared by arc melting method described in section 3.1. Each melt was about 30 to 40 gms. The as-cast arc melted buttons were used as such for powder production.

① Arc melted alloy button

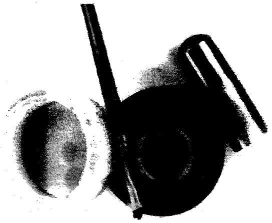

② Crusher, sieve (-100 mesh) and brush

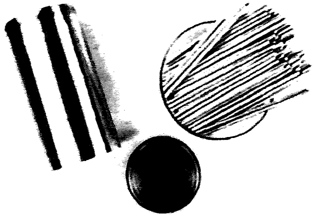

③ Stainless steel grinding jar and rods

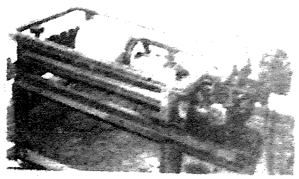

④ Pot mill

MAGNET PROCESSING: EXPERIMENTAL

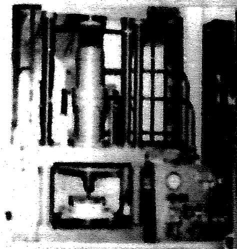

⑤ Field pressing facility (20 ton press and 30 kG pulse magnetiser)

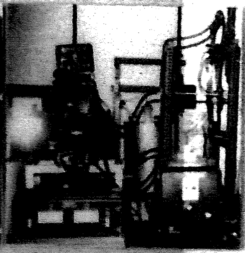

⑥ Sintering furnace set-up

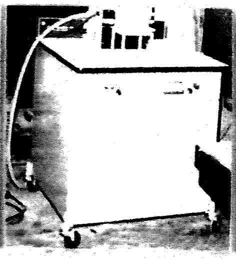

⑦ 60 kG pulse magnetiser

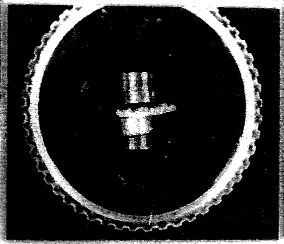

⑧ Sintered and magnetised pellets

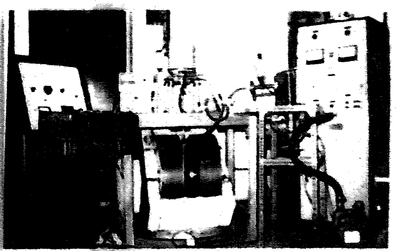

⑨ Magnetic characterisation: vibrating sample magnetometer and electromagnet

Fig. 3·3 Materials, equipments, and methods employed in magnet processing

3.4.2 Comminution:

The comminution of the as-cast alloys was carried out in two stages. First the alloy was hand crushed in a steel crusher to -100 mesh size in air and sieved into a small stainle jar (volume of 125 cc) containing toluene. Fine grinding was carried out by rod milling the -100 mesh powder in the stainless steel jar with stainless steel rods as the grinding media under sodium gettered toluene. The rods were of 2 mm dia and 9.5 cm long; the jar was of 4 cm dia and 10 cms in length. After milling, the wet powder was dried in a dessicator under vacuum (500μ). The optimum parameters to be selected in grinding are the feed size, feed volume and the milling time. In the present the feed size was fixed at -100 mesh as feeds finer than this may lead to severe oxidation of the powder. The effectiveness of the grinding and the optimum parameters of feed volume and milling time were determined by measuring the $_iH_c$ of the powder rather than their average particle size. A feed volume of 5 gms was used in the present study.

3.4.3 Compaction:

The powders were field-pressed in a pulse magnetic fiel of 13 KOe applying a load of 14 Tons/cm^2. A 20 Ton Bemco Hydraulic press and an RFL model 747-6 magnet charger fitted with a charging fixture of 3½" i.d. and 2" length was used (Fig. 3.3). The direction of the field and the pressing was parallel. Pellets of 0.96 cm dia and 0.3 to 0.6 cm thickness were formed wi a green density of 5.6 gm/cm^3 which is about 65 pct. of the theoretical density for MM-Co phases. The powder compacts were sintered immediately after pressing.

3.4.4 Sintering:

The sintering of the powder compacts was carried out in a flowing argon (ultra high pure - IOLAR Grade) atmosphere at temperatures between 970°C and 1050°C in an alumina crucible. The sintering set up is shown in Fig. 3.3. One end closed alumi tube of 2.5 cm in i.d. and ∼45 cms in length was fitted with a brass flange with an inlet and an outlet gas-leads of zirconia tubes of 3 mm bore. An alumina crucible containing the green pellets was placed inside the tube assembly and the end was closed vacuum tight. The chamber was evacuated to 20μ pressure and then flushed with argon. This was repeated 2 or 3 times. Then the alumina tube assembly was lowered into a furnace kept at any desired sintering temperature. It normally takes 10 to 15 minutes for the pellets to reach the sintering temperature. Sintering time was counted from the time the set sintering temperature was reached. At the end of the sintering period the alumina tube assembly was taken out and cooled in air. The cooling takes less than 3 min to reach 500°C and about 30 minute to come to room temperature.

3.4.5 Magnetising:

The sintered pellets were magnetised prior to magnetic measurements in an RFL model 747-6 magnet charger fitted with a charging fixture of 1" i.d. and 4" length. This can give a pulse field of 60 KOe with a pulse width of 100 to 200 milliseconds. The field was applied in a direction parallel to the pressing direction.

3.4.6 Characterisation:

The permanent magnet properties B_r, ${}_iH_c$, ${}_bH_c$ and $(BH)_{max}$ of the sintered pellets were measured and compared with the density and phase and chemical composition of the pellets studied.

3.4.6.1 Permanent magnet properties:

The B_r and ${}_iH_c$ are obtained directly from the intrinsic demagnetisation curve ($4\pi M$ vs. H) while the ${}_bH_c$ and $(BH)_{max}$ are obtained from the induction (B vs. H) demagnetisation curve. The latter curve is derived from the former using the relation $B = H + 4\pi M$ where H is a negative quantity (demagnetising field).

A PAR model 155 vibrating sample magnetometer (VSM) coupled with a Polytronic type RTB-200 electromagnet which can give a peak field of 11 KOe, was used. The field was measured with a Hall probe - Gaussmeter. The output terminals of the Gaussmeter and the VSM were connected to an x-y recorder and the I and II quadrants of the hysteresis loop of the sintered and magnetised pellets were traced.

3.4.6.2 Density:

The density of the sintered pellets was determined by geometrical as well as liquid (toluene) displacement methods.

3.4.6.3 Phase composition:

To relate the magnetic properties observed to the structure of the sintered pellets, metallography and x-ray diffraction were performed. The techniques are the same as described under section 3.2. For x-ray diffraction the smooth sintered

I. I. T. KANPUR
CENTRAL LIBRARY
A 70494

pellet surface was used as such with no necessity of powder preparation.

3.4.6.4 Chemical composition:

Chemical analysis was carried out for a given alloy composition at three stages, 1) as-cast alloy, 2) powder compact and iii) sintered pellet. This was necessary to check any evaporation loss or oxidation of rare earth during the course of magnet processing. The procedure is the same as given under section 3.1.4.

REFERENCES

1. T.A. Padmavathi Sankar, H.O. Gupta, E.C. Subbarao, K.P. Gupta, N.R. Bonda, D.K. Goel, S.N. Kaul, A.K. Majumdar, R.C. Mittal, G. Sarkar, M.V. Satyanarayana, K.S. Prasad, J. Subramanyam and E.M.T. Velu, Bull. Mater. Sci. 2, (3), 167 (1980).

2. G.L. Kehl, Metallographic Laboratory Practice, McGraw-Hill, N.Y. (1949).

3. C. Herget and H. Altenhoff, Practical Metallography 11, 599 (1974).

4. D.T. Cromer and A.C. Larson, Acta Crystallogr. 12, 855 (1959).

5. K.H.J. Buschow, Phys. Status Solidi A7, 198 (1971).

6. Y. Khan, Z. Metallkd. 65, 489 (1974).

7. E.F. Bertaut, R. Lemaire and J. Schweizer, Bull. Soc. Fr. Mineral Cristallogr. 88, 580 (1965).

8. Y. Khan, Acta Crystallogr. B30, 1533 (1974).

9. J.H. Wernick and S. Geller, Acta Crystallogr. 12, 662 (1959).

10. Y. Khan, Acta Crystallogr. B29, 2502 (1973).

11. K.J. Strnat and A.E. Ray, AIP Conf. Proc. 24, 680 (1975).

12. J.J. Becker, K. Strnat, G. Hoffer, J. Olson and W. Ostertag, J. Appl. Phys. 38, 1001 (1967).

13. J.J. Becker, IEEE Trans. Magn. MAG-4, 239 (1968).

4. PHASE RELATIONS IN MM-Co-Fe SYSTEM IN Co-RICH REGION

4.1 Introduction

Intermetallic phases of 1:5 and 2:17 stoichiometry in binary RE-Co (RE = Ce, La, Nd and Pr) systems have attractive magnetic properties: magnetocrystalline anisotropy field (H_A), saturation magnetisation ($4\pi M_s$) and Curie temperature (T_c).[1-5] These phases are used for the production of high energy density permanent magnets.[6-12] The properties, ${}_iH_c$ and B_r of these magnets are very sensitive to phase composition.[13-16] Hence a knowledge of phase relations near the 1:5 and 2:17 stoichiometry becomes important for selecting the right composition that gives a single phase alloy and for knowing how a slight change in composition alters the microstructure of these alloys. Although details of phase relations near 1:5 and 2:17 stoichiometries are available for pure binary RE-Co systems[17-20] phase relationships in a multicomponent MM-Co-Fe system are not investigated in detail. Mischmetal itself contains at least four RE elements (Ce, La, Nd and Pr). While the binary RE-Co phase diagram for RE = Ce, La and Nd are similar[18] the La-Co system differs from the rest. It does not contain 1:3 and 2:17 phases.[21] A phase diagram for MM-Co system[22] and detailed phase relationships in the Co-rich regions of the MM-Co system[23] have been reported previously.

The Indian mischmetal also contains about 6 w/o Fe as impurity. The effects of Fe addition on the magnetic properties of MM-Co and RE-Co phases have been studied[24-25] but no systematic study on the phase equilibria of RE-Co-Fe and MM-Co-Fe systems have been reported. Also the 1:5 and 2:17 phases in binary systems have been reported to have homogeneity region[17,19,20] and the former phase (1:5) undergoes an eutectoid reaction at low temperature (700°C).[29] Hence a systematic study was undertaken (i) to identify the different phases occurring in the MM-Co-Fe system (ii) to obtain their crystallographic details (iii) to establish the 900°C isothermal section of the MM-Co-Fe phase diagram (iv) to find the homogeneity region of the phases and (vi) to confirm the phase stability of the $MMCo_5$ phase.

For the purpose of drawing the phase diagram all the RE elements in mischmetal were assumed to constitute as a single component as far as their effect on phase-formation is concerned. However, wether this assumption leads to any violation of the phase rule was considered carefully in this study.

4.2 Experimental

The alloys were prepared using Indian mischmetal and 99.9% pure Co and Fe. The composition of mischmetal is the same as given under Section 3.1.1. The melting and annealing procedure of the alloys are described under Sections 3.1.2 and 3.1.3. The materials used and the methods followed in the phase analysis are illustrated in Figure 3.1 (Chapter 3). The alloys homogenised at 900°C for 4 to 10 days were taken for phase analysis. The alloys studied for the stability of $MMCo_5$ were annealed at 700°C for 15 to 30 days. The phases were studied by metallography, X-ray diffraction, thermomagnetic analysis (TMA) and electron-probe micro-analysis. The experimental procedure is given under Section 3.2.

4.3 Results and Discussion

The chemical and phase composition of the MM-Co-Fe alloys studied are given in Table 4.1 and the 900°C isothermal section of the MM-Co-Fe phase diagram is given in Figure 4.1. Excepting the D-group alloys, the alloy compositions plotted in the MM-Co-Fe phase diagram were analysed by TMA and by the conventional metallography and X-ray diffraction techniques. Six phases, 1:3, 2:7, 5:19, 1:5, 2:17 and β-Co were identified between 75 and 95 a/o Fe (Figure 4.1) close to the MM-Co binary line. In addition to them, a new phase designated as X, with a T_c of about 340°C was present between 5:19 and 1:5 stoichiometries. The 2:7, 5:19, 1:5 and 2:17 phases were found to extend to considerable extent into the MM-Co-Fe ternary. At greater than 15 a/o Fe an S phase has been reported[30] to exist on the RE-rich side of 2:17 stoichiometry.

4.3.1 Identity and Crystallographic Details of Different Phases in the MM-Co-Fe System

4.3.1.1 2:7 and 5:19 Phases

The alloy A-1 (Table 4.1) with composition on the

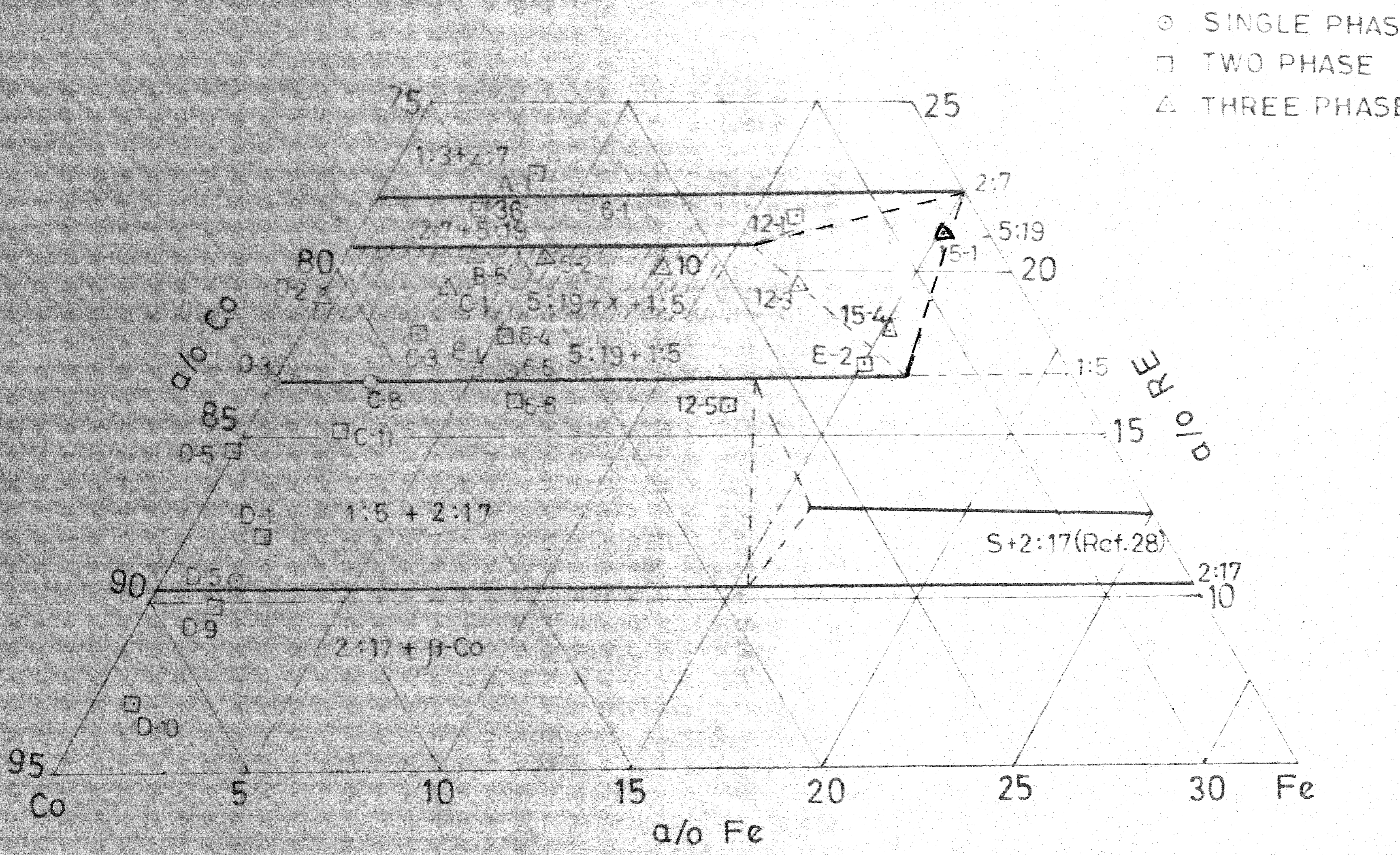

FIG. 4.1 900 °C ISOTHERMAL SECTION OF MM - Co - Fe PHASE DIAGRAM

TABLE 4.1 CHEMICAL AND PHASE COMPOSITION OF ALLOYS SELECTED FOR THE STUDY OF PHASE RELATIONS IN MM-Co-Fe SYSTEM

Alloy	Composition (a/o, analysed)			Phases (900°C, 4-10 d)		
	MM[a]	Co	Fe	Micro-structure (No. of phases)	X-ray diffraction	TMA[d] (T_c, °C)
A-1	22.8	73.4	3.8	2	1:3 + 2:7	<20, 67
A-2	22.6	73.7	3.7	2		
A-3	22.3	74.0	3.7	1	2:7	
A-4	22.6	74.3	3.7	2	2:7 + 5:19	
A-5	21.8	74.6	3.6	2		
B-1	21.3	75.2	3.5	2		
B-2	21.1	75.4	3.5	2		
B-3	20.9	75.6	3.5	1	5:19	
B-4	20.6	76.0	3.4	3	5:19 + (X) + 1:5	
B-5	20.4	76.4	3.2	3		270 340 520
C-0	20.0	76.8	3.2	3		270 340 520
C-1	19.5	77.4	3.1	3		280 340 530
C-2	18.8	78.2	3.0	3		
C-3	18.1	79.0	2.9	2	5:19 + 1:5	280 480
C-4	17.4	79.7	2.9	2		
C-5	17.5	79.6	2.9	2		
C-6	17.2	80.0	2.8	1	1:5	
C-7	16.9	80.3	2.8	1		
C-8	16.4	81.0	2.6	1		
C-9	16.2	81.2	2.6	2	1:5 + 2:17	
C-10	15.9	81.6	2.5	2		
C-11	15.1	82.5	2.4	2		520 >700
C-12	14.6	83.1	2.3	2		
C-13	14.1	83.6	2.3	2		
C-14	13.6	84.1	2.3	2		
C-15	13.2	84.6	2.2	2		

Contd...

TABLE 4.1 (contd.)

Alloy	Composition (a/o, analysed)			Phases (900° C, 4–10 d)				
	MM[a]	Co	Fe	Micro-structure (No. of phases)	X-ray diffraction	TMA[d] (T_c, °C)		
D-1	11.9	86.2	1.9	2	1:5 + 2:17			
D-2	11.6	86.5	1.9					
D-3	11.4	86.8	1.8					
D-4	11.1	87.1	1.8					
D-5	11.0	87.2	1.8	1	2:17			
D-6	10.9	87.4	1.7	2	2:17 + β-Co			
D-7	10.8	87.5	1.7					
D-8	10.5	87.8	1.7					
D-9	10.0	88.4	1.6					
D-10	7.0	92.0	1.0					
E-1[b]	16.7	78.3	5.0	2	5:19 + 1:5	280		550
E-2[b]	16.6	68.2	15.2	2	5:19 + 1:5	220		600
O-1[c]	19.4	80.6	0	3	5:19 + (X) + 1:5			
O-2[c]	19.2	80.8	0	3	5:19 + (X) + 1:5	230	500	490
O-3[c]	16.6	83.4	0	1	1:5		500	
O-4[c]	15.8	84.2	0	2	1:5 + 2:17			
O-5[c]	14.6	85.4	0	2	1:5 + 2:17			
4-1	20.6	75.0	4.4	3	5:19 + (X) + 1:5			
4-2	20.2	75.6	4.2	3	5:19 + (X) + 1:5			
4-3	18.8	76.8	4.4	3	5:19 + (X) + 1:5			
4-4	17.6	77.9	4.5	3	5:19 + (X) + 1:5			
4-5	16.6	79.1	4.3	1	1:5			
4-6	15.9	79.9	4.2	2	1:5 + 2:17			

Contd...

TABLE 4.1 (contd.)

Alloy	Composition (a/o, analysed)			Phases (900° C, 4–10 d)				
	MM[a]	Co	Fe	Micro-structure (No. of phases)	X-ray diffraction	TMA[d] (T_c, °C)		
6–1	22.3	72.3	5.4	2	2:7 + 5:19	130		240
6–2	20.5	74.4	5.1	3	2:7 + (X) + 1:5	270	320	540
6–3	19.5	75.3	5.2	3	2:7 + (X) + 1:5			
6–4	18.0	76.7	5.3	2	5:19 + 1:5	260		525
6–5	16.6	77.0	6.4	1	1:5			530
6–6	16.2	77.3	6.5	2	1:5 + 2:17			
12–1	21.3	67.3	11.4	3	2:7 + 5:19 + 1:5	184	280	
12–3	19.4	68.3	12.3	3	2:7 + 5:19 + 1:5	170	290	>600
12–5	15.8	71.9	12.3	2	1:5 + 2:17		580	700
15–1	21.5	63.3	15.2	3	2:7 + 1:5? +5:19?	200		>600
15–4	18.0	66.7	15.3	3	2:7 + 5:19 + 1:5	184	290	>600

a : MM represents only the total RE (Ce, La, Nd and Pr) content and does not include the Fe and the impurities present (1.4 w/o) in mischmetal. The Fe present as impurity in MM plus the Fe added intentionally is shown in a separate column. The analysed compositions (w/o) of the alloys for RE, Co and Fe were normalised to 100% and then converted to a/o. The average at. wt. of MM was taken to be 140.82 based on the X-ray fluorescence analysis.[31]

b : E-1 and E-2 were prepared with synthetic MM of composition: 49.4% Ce, 22.8% La, 19.5% Nd, 4.9% Pr and 3.4% Sm (all in w/o).

c : Alloys O-1 to O-5 were prepared with synthetic MM of composition: 48.4% Ce, 22.6% La and 29.0% Pr (all in w/o).

d : The Curie temperatures shown in this table are indicative only for the purpose of identification of phases and the actual T_c may differ by ±10° C.

rare-earth-rich side of the stoichiometry 2:7 shows two phases (Figure 4.2) and the alloy A-3 is a single phase. In the B-group, the alloy B-5 on the cobalt-rich side of the stoichiometry 5:19 has three phases and the alloy B-3 is a single phase. The X-ray diffraction data of the alloys A-3 and B-3 are given in Tables 4.2 and 4.3. Interestingly, both the alloys have all their strong lines occurring at nearly the same 2θ position, leaving only a few weak lines which are characteristic of the phases. Thus it was ambiguous to conclude wether the phase in B-3 was different from that in A-3. To investigate this further, the alloys A-1 and B-5 were studied by thermomagnetic analysis and their thermomagnetic curves are shown in Figure 4.3.

The alloy A-1 shows one magnetic transition near 60° C whereas the alloy B-5 has a major transition near 270° C, two weak transitions near 340°C and 520°C and none near 60°C. The magnetic transition observed at 60°C for the alloy A-1 is attributed to the MM_2Co_7 phase (Figure 4.3). The magnetic transition of the second phase present in A-1 ($MMCo_3$) is not observed as it should have a ferromagnetic transition temperature, T_c much less than room temperature (20° C). Similarly the magnetic transition seen at 270° C for the alloy B-5 is attributed to MM_5Co_{19} phase and the other transitions are attributed to minor phases. These results confirm that the matrix phases in the alloys A-1 and B-5 are MM_2Co_7 and MM_5Co_{19} respectively.

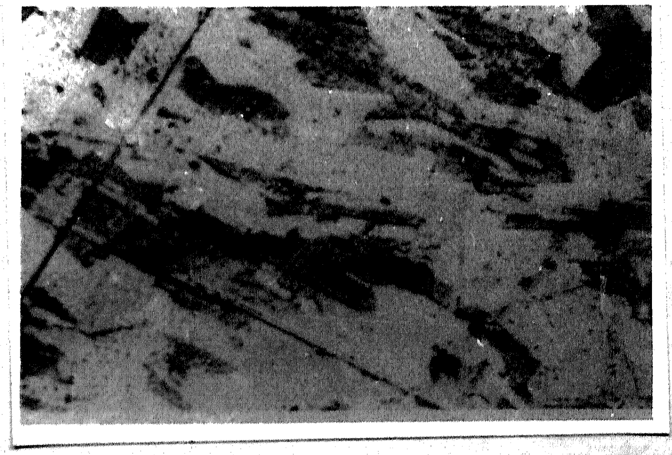

Figure 4.2 The microstructure of the alloy A-1. The areas are $MMCo_3$ and the matrix is MM_2Co_7.

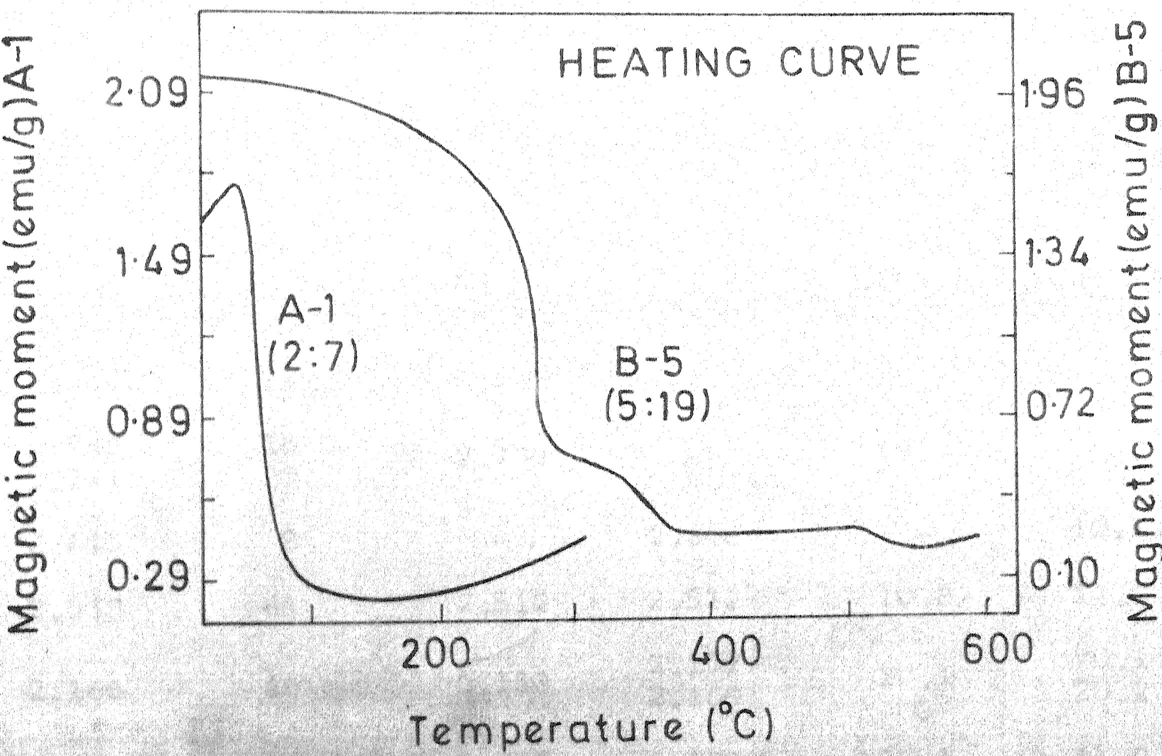

FIG. 4·3 THE LOW FIELD MAGNETIC MOMENT AS A FUNCTION OF TEMPERATURE FOR THE ALLOYS A-1 AND B-5 AFTER ANNEALING AT 900 °C FOR 10 DAYS

TABLE 4.2 X-RAY DIFFRACTION DATA FOR MM_2Co_7 PHASE

Hexagonal	a : 4.99$_0$	Rhombohedral	a : 5.02$_4$
	c : 24.69$_9$		c : 36.71$_3$

$d_{obs.}$ (Å)	% $I_{obs.}$	$d_{cal.}$ (Å)		(hkl)	
		hex.	rhomb.	hex.	rhomb.
2.804	11	-	2.806	-	10.10
2.745 2.724	18 20	2.733	-	10.7	-
2.645	8	-	2.648	-	10.11
2.513	61	2.512	2.512	10.8	11.0
2.166	46	2.153	2.172 2.160	20.1	20.1 20.2
2.136	100	2.144	2.139	10.1	11.9
2.034	23	-	2.039	-	00.18
1.938	6	1.941	1.934	11.8	10.17
1.745	7	1.739	1.748	10.13	00.21 11.15
1.581	4	-	1.583	-	11.8
1.451	7	1.454	1.475	10.16	21.11
1.433	7	1.427	1.445	20.13	20.19 30.0
*1.367	35	1.367	1.367	20.14	30.9
*1.256	31	1.256	1.256	20.16	22.0

* Lines taken for the calculation of lattice parameters.

- Denotes not present.

TABLE 4.3 X-RAY DIFFRACTION DATA FOR MM_5Co_{19} PHASES
Rhombohedral - a: 5.01_8; c : 48.65_7

$d_{obs.}$ (Å)	% $I_{obs.}$	$d_{cal.}$ (Å)	(hk.l)
2.831 2.798	9 16	2.836	10.13
2.714	13	2.714	10.14
2.509*	43	2.509 2.492	11.00 10.16
2.166	39	2.171 2.164	20.1[illegible] 20.20
2.134	100	2.134	11.2[illegible]
2.027*	23	2.027	00.24
1.578	4	1.577	11.24
1.449	8	1.448	30.00
1.364	26	1.364	30.12
1.254	23	1.254	22.1[illegible]

* Lines taken for the calculation of lattice parameters.

The X-ray diffraction lines of the alloy A-3 were indexed based on the hexagonal Th_2Co_7 type structure.[32] However, some of the lines could not be accounted for based on this structure. Khan[33] has reported that for RE_2Co_7 (RE = Ce, Pr, Nd and CeMM) the rhombohedral modification (Gd_2Co_7 type) is the stable low temperature form whereas Buschow[32] has reported that both the modifications could coexist. In the present study the observed diffraction lines for the alloy A-3 could be accounted for only if both the modifications were assumed to be present(Table 4.2). The lattice parameters calculated for both the modifications are shown in Table 4.4. All the X-ray diffraction lines of the alloy B-3 could be indexed on the basis of the rhombohedral Ce_5Co_{19}-type structure[34] and the lattice parameters calculated for the MM_5Co_{19} phase in the alloy B-3 are in close agreement with the values reported for $CeMM_5Co_{19}$ by Khan[33] (Table 4.4).

Alloys 6-1, 12-1 and 15-1 (Figure 4.1) lie between the 2:7 and 5:19 stoichiometries and the Fe content increases from 5.4 a/o in alloy 6-1 to 15.2 a/o in alloy 15-1 (Table 4.1). Their microstructures show two phases. These alloys were also analysed by TMA and the Curie temperature of the phases (Table 4.1) show a gradual increase from 67°C in alloy A-1 to 200°C in alloy 15-1 for the 2:7 phase. Similarly for the 5:19 phase the T_c was found to increase from 220°C in alloy 36[35] to 280°C in alloy 12-1. This increase

TABLE 4.4 COMPARISON OF LATTICE PARAMETERS OF STOICHIOMETRIC PHASES OF MM-Co SYSTEM WITH THOSE OF Ce-Co AND CeMM-Co SYSTEMS

Phases	Structure type	Crystal symmetry	Lattice parameters (Å)					
			MM-Co		Ce-Co[33,34]		CeMM-Co[33]	
			a	c	a	c	a	c
2:7	Gd_2Co_7	rhomb.	5.02_4	36.71_3	4.95_6	36.5_{25}	5.02_3	36.7_{47}
	Ce_2Ni_7	hex.	4.99_0	24.6_{99}	4.94_4	24.4_{70}	-	-
5:19	Pr_5Co_{19}	rhomb.	5.01_8	48.6_{57}	4.94_7	48.7_{43}	5.01_2	48.7_{16}
1:5	$CaCu_5$	hex.	4.98_0	4.00_8	4.92_2	4.03_0	4.99_1	4.00_4
2:17	Th_2Zn_{17}	rhomb.	8.47_2	12.14_5	8.37_8	12.20_6	-	-

is attributed to the presence of Fe in these phases.[35] The 2:7 phase does not exist in the RE-Fe binary system.[36] The present study indicates the 2:7 phase extends into the ternary as a stable phase at least upto 15 a/o Fe. The 5:19 phase was not observed in alloy 15-1 and the alloy 12-3 contains three phases. The 5:19 phase does not seem to extend to greater than 10 a/o Fe into the MM-Co-Fe ternary.

4.3.1.2 1:5 Phase

The alloy c-6 (Table 4.1) was found to be a single phase and its X-ray diffraction pattern could be indexed on the basis of the $CeCo_5$-type structure.[37] The X-ray diffraction data of the $MMCo_5$ phase is given in Table 4.5. This

TABLE 4.5 X-RAY DIFFRACTION DATA FOR $MMCo_5$ PHASE

Hexagonal

$\underline{a}$: 4.98_0 Å

$\underline{c}$: 4.00_8 Å

$d_{obs.}$ (Å)	% $I_{obs.}$	$d_{cal.}$ (Å)	(h k.l)
4.007	3	4.008	0 0.1
2.930	38	2.936	1 0.1
2.483	29	2.489	1 1.0
2.154	41	2.156	2 0.0
2.113	100	2.115	1 1.1
2.003	19	2.004	0 0.2
1.898	17	1.899	2 0.1
1.562	16	1.561	1 1.2
1.509	14	1.510	2 1.1
1.468*	21	1.468	2 0.2
1.437	5	1.438	3 0.0
1.352	24	1.353	3 0.1
1.245*	31	1.245	2 2.0

* Lines taken for the calculation of lattice parameters.

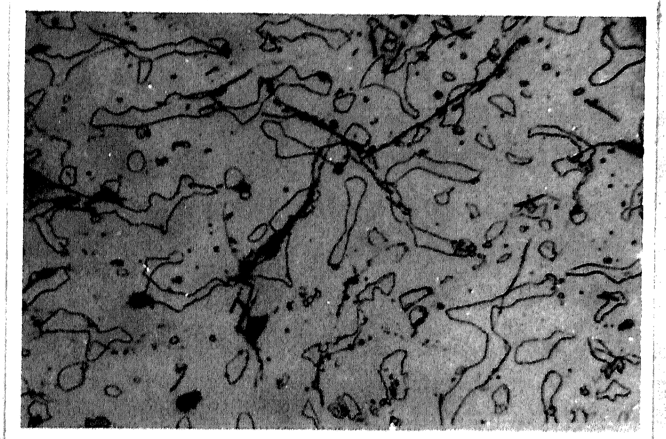

Figure 4.4 The microstructure of the alloy C-4. The islands are MM_5Co_{19} and the matrix is $MMCo_5$.

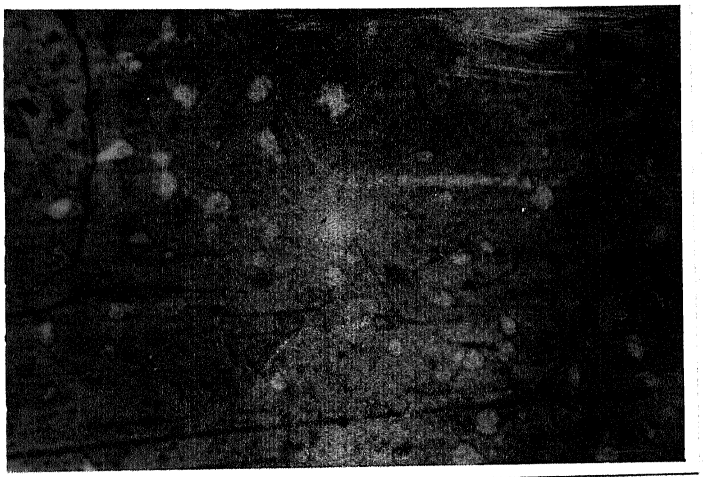

Figure 4.5 Microstructure of alloy 6-6. The matrix is $MMCo_5$ and the minor phase is MM_2Co_{17}.

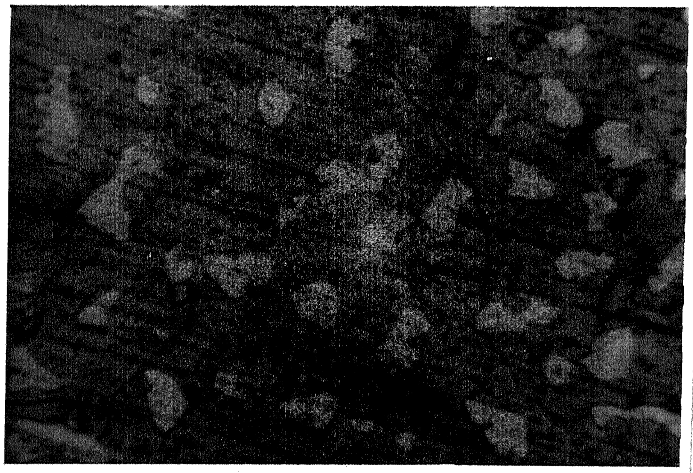

Figure 4.6 Microstructure of alloy 12-5. The matrix is $MMCo_5$ and the minor phase is MM_2Co_{17}.

phase appeared initially in the alloy B-4 and then increased in quantity with increasing cobalt concentration. The microstructure of the alloy c-4, which contains MM_5Co_{19}, and $MMCo_5$ (matrix) is shown in Figure 4.4. The alloys c-6, c-7 and c-8 showed a single-phase ($MMCo_5$) structure (Table 4.1), indicating the presence of a homogeneity region for this phase. This is discussed further in the next section.

Alloy O-3 was prepared with synthetic mischmetal and contains no Fe. This alloy shows single phase, 1:5 both in the microstructure and in the TMA. A number of alloys, c-8, 4-5, E-1, 6-5, 12-5 and E-2 (Figure 4.1 and Table 4.1) containing different amount of Fe along the 1:5 stoichiometric line were prepared. Alloys c-8, 4-5 and 6-5 show microstructurally single phase with a trace of second phase while the rest contain 1:5 as the predominant phase with small amount of the second phase. The second phase present in the alloy E-2 was the 5:19 phase as evidenced by its TMA.[38] The TMA pattern of the alloy 12-5 (Figure 5.6, Chapter 5) does not show any magnetic transition corresponding to the 5:19 phase. Hence the second phase seen in the microstructure of alloy 12-5 is attributed to 2:17 phase (Figure 4.5). Similarly the second phase seen in the alloy 6-6 (Figure 4.6) which gets etched brighter than the matrix 1:5 phase is attributed to the 2:17 phase. In an earlier study[30] the composition of 1:5 phase was reported to deviate towards higher Co content as the Fe content in the 1:5 increased. But the present study shows no such deviation from the ideal stoichiometric line and the 1:5 phase exists as a stable phase at 900°C at least upto 17 a/o Fe in the MM-Co-Fe ternary system.

4.3.1.3 2:17 Phase

A phase having a crystal structure of the Th_2Zn_{17} type first appeared in the alloy C-9 and increased in quantity with increasing Co concentration (Table 4.1). A single phase of stoichiometry 2:17 was obtained for the alloy D-5, the X-ray diffraction data of which is given in Table 4.6. In between C-9 and D-5, $MMCo_5$ and MM_2Co_{17} are present. The microstructure of the alloy C-11 in which the bright MM_2Co_{17} is precipitated along the grain boundaries of $MMCo_5$, is shown in Figure 4.7. The binary La-Co system does not have the La_2Co_{17} phase. However, in the present study it was found that natural mischmetal, which contains about 20 w/o La, forms a stable MM_2Co_{17} phase and the observed X-ray diffraction lines for this phase could be indexed on the basis of the Th_2Zn_{17} rhombohedral structure.[39] This phase extends far into the ternary system and possibly upto the binary MM-Fe.[30]

4.3.1.4 β-Co Phase

In addition to the stoichiometric phases, a Co-Fe phase was found to coexist with MM_2Co_{17} on the Co-rich side of 2:17 stoichiometry. Unlike the other alloys, the alloy D-10 (Figure 4.8), which contained about 40% of this

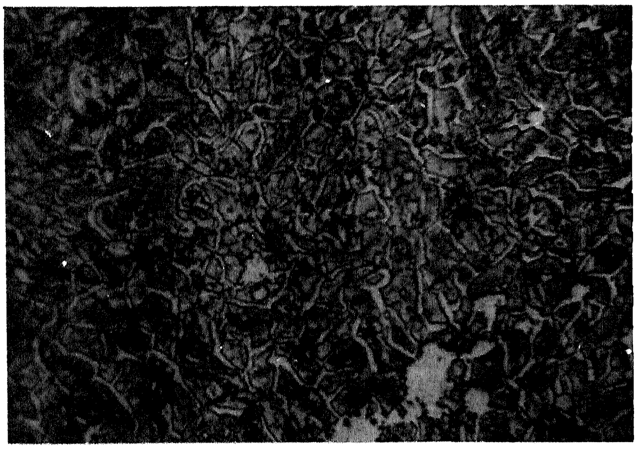

Figure 4.7 The microstructure of the alloy C-11. The matrix is $MMCo_5$ with MM_2Co_{17} at the grain boundaries.

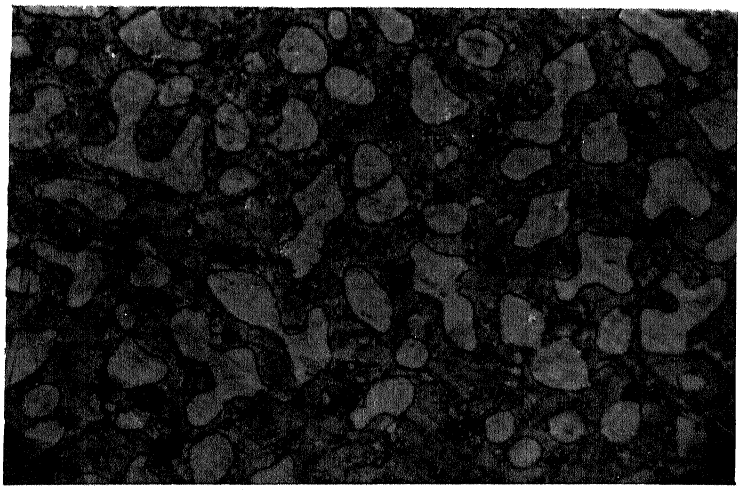

Figure 4.8 The microstructure of the alloy D-10. The matrix is MM_2Co_{17} with islands of β-Co.

TABLE 4.6 X-RAY DIFFRACTION DATA FOR MM_2Co_{17} PHASE

Rhombohedral $\underline{a}$: 8.47_2 Å

$\underline{c}$: 12.14_5 Å

$d_{obs.}$ (Å)	% $I_{obs.}$	$d_{cal.}$ (Å)	(hk.l)
3.138	4	3.139	20.20
2.929	41	2.926	11.30
2.837	8	2.806	10.40
2.689	8	2.703	21.10
2.513	9	2.523	21.20
2.431	36	2.446	30.00
2.347	34	2.339	20.40
2.102	60	2.118	22.00
2.085	100	2.093	31.30
2.042	41	2.047	21.40
2.031	44	2.024	00.60
1.870	31	1.877	22.30
1.833	8	1.826	11.60
1.804	5	1.814	40.10
1.745	5	1.737	22.40
1.611	6	1.606	11.70
1.562	5	1.559	30.60
1.480	15	1.489	41.30
1.476	15	1.471	21.70
1.464*	25	1.464	40.50 32.40
1.403	5	1.412	33.00
1.326	15	1.333	33.30
1.315	5	1.321	50.4
1.256	8	1.256	41.60
1.214*	31	1.214	00.10
1.209	8	1.222	60.00
1.203	6	1.217	60.10
1.200	8	1.200	10.10

* Lines taken for the calculation of lattice parameters.

phase, was not brittle. The X-ray diffraction results confirmed that it existed as f.c.c., β-Co. The β-Co phase was analysed using electron probe micro-analyser (EPMA) for the presence of any rare earth elements. Figure 4.9 shows an EPMA trace of β-Co and the MM_2Co_{17} phase of the alloy D-10; it was analysed for the three 3d elements, cobalt, iron and nickel, and for the five rare earth elements cerium, lanthanum, neodymium, praseodymium and samarium. For both the phases, except for Co, the elements were probed at the same X-ray intensity scale (300 counts per second). It can be seen that the β-Co phase contains predominantly Co with small amounts of Fe and Ni and contains no detectable amount of RE elements. The binary phase diagrams of the RE-Co systems[18] also show the absence of terminal solid solubility of rare earths in cobalt.

4.3.1.5 X-phase

A phase having a T_c about 340°C was observed for a number of alloys adjacent to 5:19 stoichiometric line on the Co rich side and the region where it was detected is shown in hatched form in the MM-Co-Fe phase diagram (Figure 4.1). This phase was initially suspected for the 1:4 type phase based on similar such evidence reported by Strnat for Pr-Co system.[40] In order to confirm this $MMCo_{4.0}$ alloy (C-0) was prepared and its TMA curve was obtained which is shown in Figure 4.10. It is seen from this figure, that the

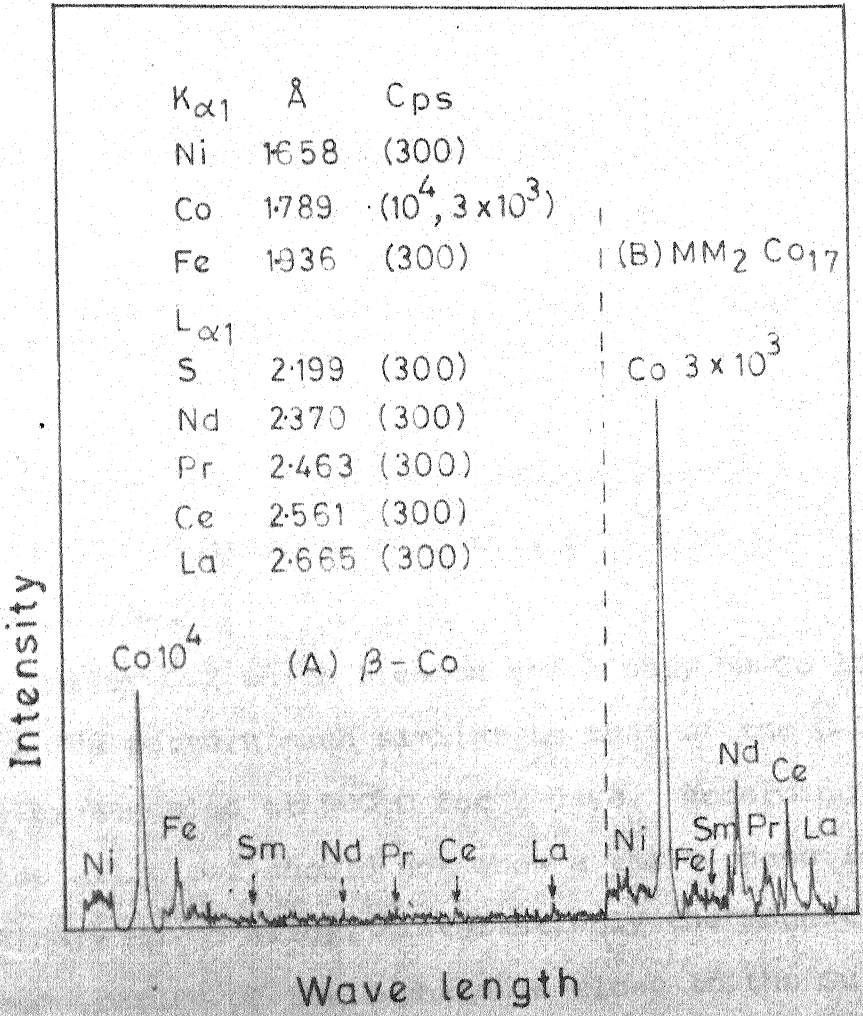

$K_{\alpha 1}$	Å	Cps
Ni	1·658	(300)
Co	1·789	(10^4, 3×10^3)
Fe	1·936	(300)
$L_{\alpha 1}$		
S	2·199	(300)
Nd	2·370	(300)
Pr	2·463	(300)
Ce	2·561	(300)
La	2·665	(300)

FIG·4·9 AN EPMA TRACE OF THE ALLOY D-10 ANALYSED FOR 3d AND RARE EARTH ELEMENTS IN β-Co AND MM_2Co_{17}

340°C transition still remains a minor one. It occurs in the 900°C annealed alloy and is absent in the as-cast and 1000°C annealed alloys (Figure 4.11). $MMCo_{4.0}$ alloy annealed at 700°C had similar TMA pattern as that of the 900°C annealed alloy. Also this phase was not present in alloy C-3, 6-4 and E-1 which are close to the 1:5 stoichiometric line (Figures 4.1 and 4.10) suggesting that this could not be due to 1:4 type of phases.

Alloy O-2 which lies on the binary MM-Co line also shows a TMA pattern much similar to that of the C-0 alloy for its alloy annealed at 900°C for 7 days. According to phase rule the alloy O-2 should not show a third phase if it were a true binary MM-Co alloy. Interestingly the magnetic transition temperature of the X-phase is close to the Curie temperature of the La_5Co_{19} phase[40] (343°C). A comparison of the peritectic temperatures of the different intermetallic phases in the RE-Co system for RE = Ce, La, Nd and Pr (Section 1.3.1, Chapter 1) indicates that for La_5Co_{19} and La_2Co_7 the peritectic temperatures are lower by about 300°C from the other RE_5Co_{19} and RE_2Co_7 phases. Wether this will have any effect on phase separation of La_5Co_{19} from the MM_5Co_{19} is not known for certain. The X-ray diffraction results of $MMCo_{4.0}$ did not reveal this phase possibly because the La_5Co_{19} and MM_5Co_{19} have very close lattice parameters. However, in the microstructure an evidence could be obtained for the presence of small amount of a third phase. But wether it

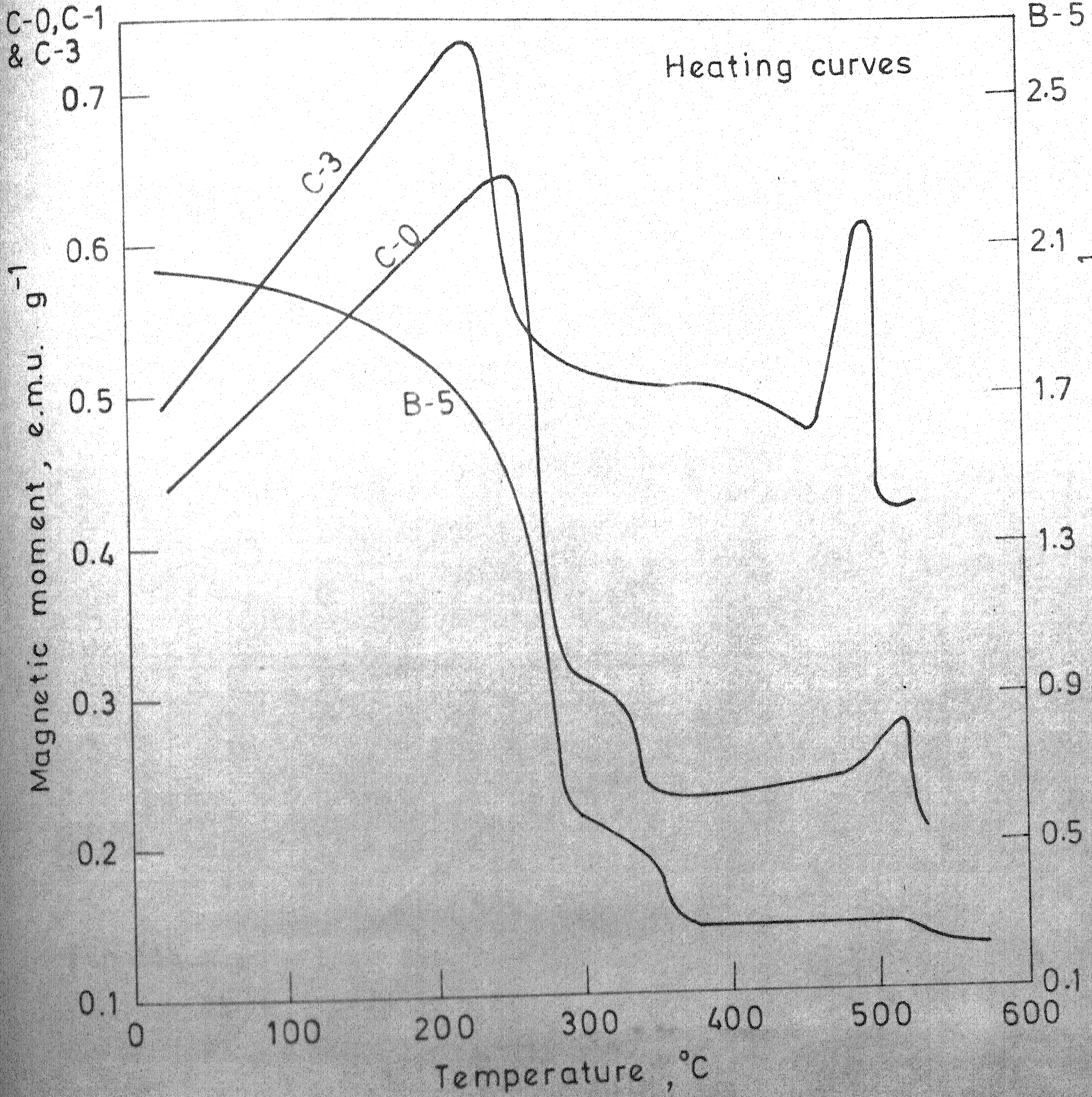

FIG. 4.10 MAGNETISATION VS TEMPERATURE AT LOW FIELD FOR ALLOYS B-5, C-0 AND C-3, 900 °C ANNEALED

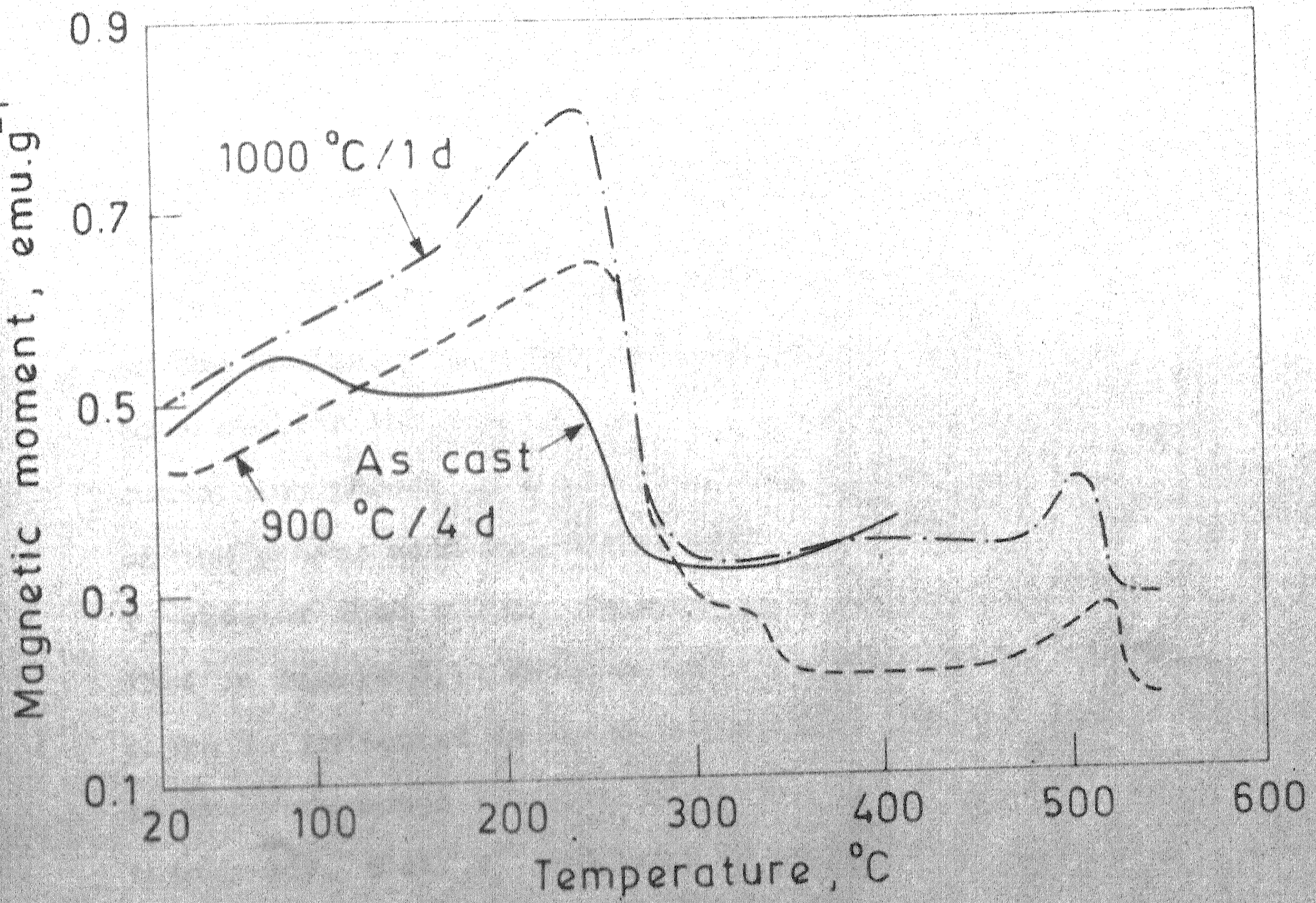

Fig.4.11 Magnetisation versus temperature at 40 Oe for $MMCo_{4.0}$ alloys (C-0)

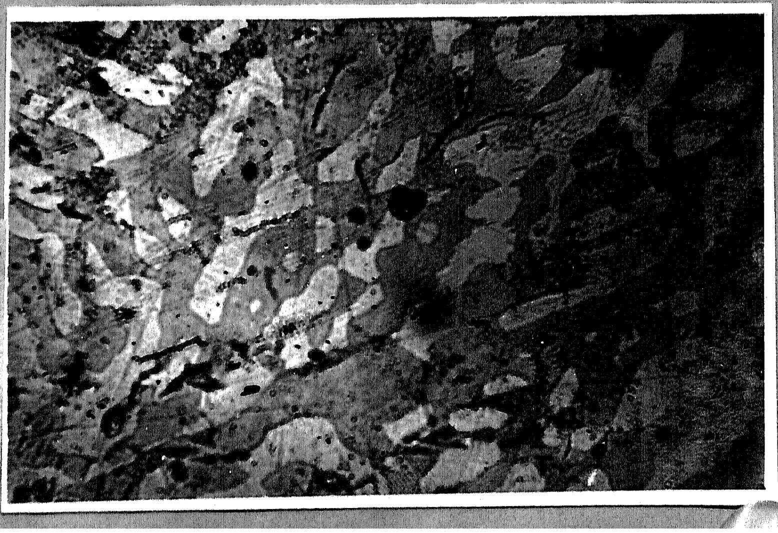

Fig. 4.11b. Microstructure of alloy C-0 900°C, 7 days annealed. 1:5 phase (matrix) coexists with 5:19 phase (white) and X phase (black).

is really due to La_5Co_{19} is yet to be proved by using other techniques like EPMA.

4.3.1.6 High Fe Containing MM-Co-Fe Alloys Between 2:7 and 1:5 Stoichiometries

The phases of alloys present in this region all have closely related crystal structures and their X-ray diffraction results could not give unambiguous evidence for the identity of the phases. Hence TMA was used as a reliable technique to establish the identity of the phases. While the low Fe containing phases in this region had T_c less than 500° C, some of the phases with Fe content greater than about 10 a/o have T_c greater than 600° C. This is shown for alloys 12-3 and 15-4 in Figure 4.12 where a definite evidence for a third phase is indicated in their TMA patterns. However since 600° C is the safe upper limit of the high temperature oven used in this study, their T_c could not be determined. Alloy 15-1 shows 3 phases only in the microstructure. Hence based on the microstructural results and the incomplete TMA results a tentative three-phase region is indicated in the MM-Co-Fe phase diagram.

4.3.2 Homogeneity Region of 1:5 Phase

In the study of the X-ray diffraction patterns of the alloys of near 1:5 stoichiometry, a systematic shift in the 2θ position of the X-ray diffraction lines of the $MMCo_5$ phase was observed. The shift was distinctly visible on

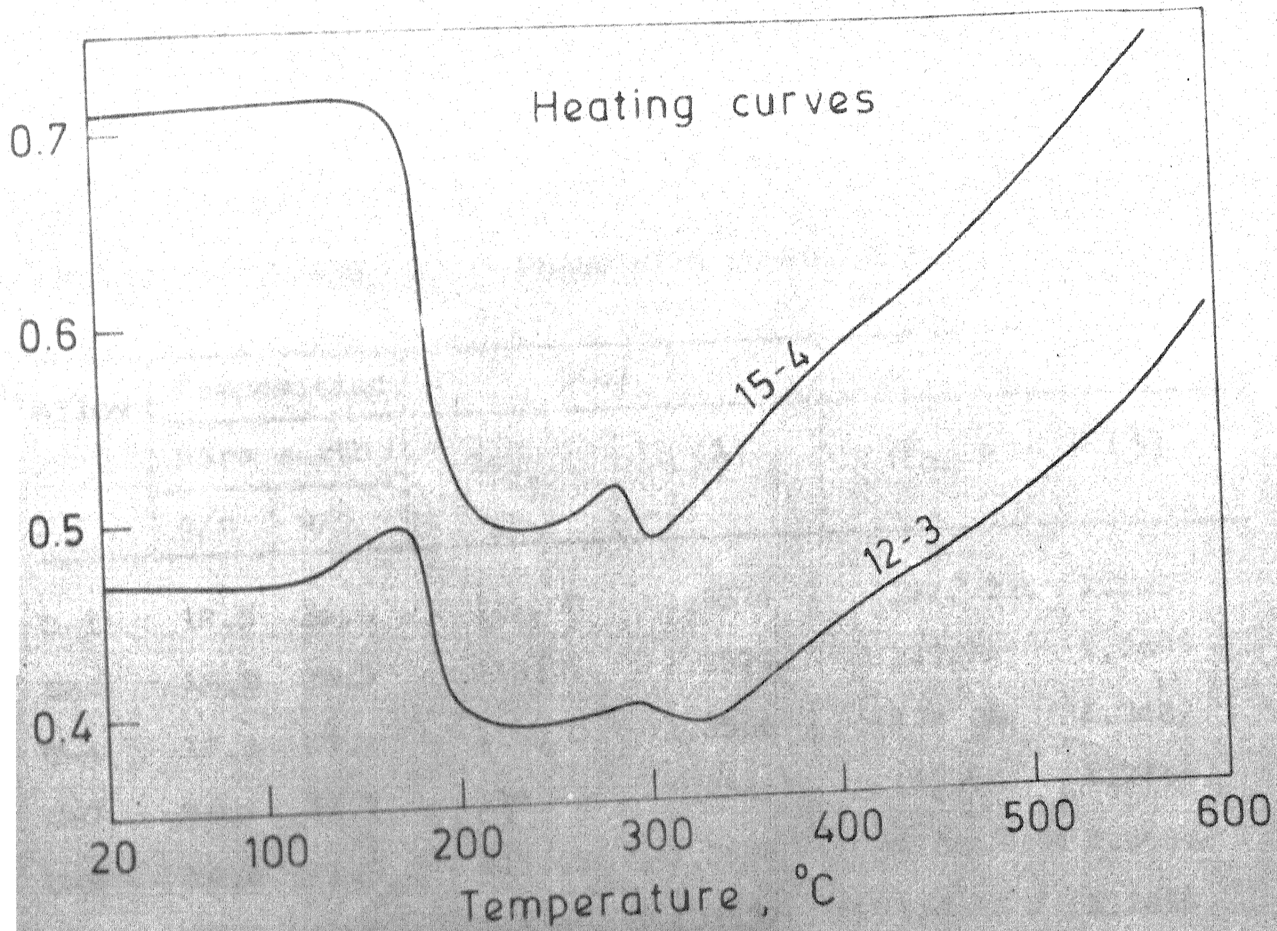

4·12 Magnetisation versus temperature at 40 Oe for alloys 12-3 and 15-4; 900 °C, 7 days annealed.

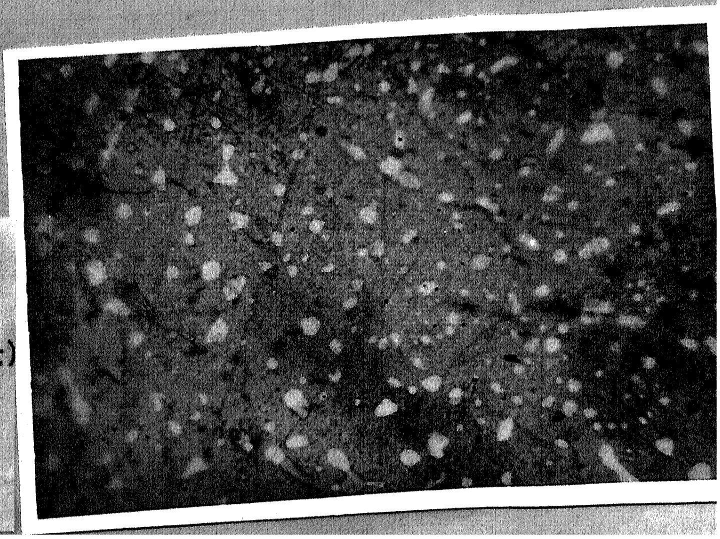

4.12b. Microstructure of alloy 15-1, 900°C, 7 days annealed. The 2:7 phase (matrix) coexists with two other minor phases (white, 1:5? and black, 5:19?).

the high angle (2θ ≥ 100°) side and is given in Table 4.7 for the planes (30.1) and (22.0) of the $MMCo_5$ phase. The X-ray diffraction peaks of these planes were scanned at a slow rate (0.2°/min) in order to read the 2θ value accurately (± 0.02°).

TABLE 4.7 VARIATION IN THE POSITION (2θ) OF X-RAY DIFFRACTION LINES OF 1:5 PHASE WITH COMPOSITION

Alloy	Composition Rare earth a/o	 w/o	30.1 $2\theta_{Cr}$	 d (Å)	22.0 $2\theta_{Cr}$	 d (Å)
C-1	19.5	36.5	115.00	1.3574	132.92	1.2487
C-2	18.8	35.5	115.05	1.3570	132.95	1.2485
C-4	17.4	33.6	115.10	1.3566	133.03	1.2482
C-7	16.9	32.7	115.33	1.3549	133.37	1.2466
C-8	16.4	31.8	115.45	1.3538	133.62	1.2454
C-10	15.9	31.0	115.48	1.3537	133.66	1.2452
C-11	15.1	29.8	115.52	1.3535	133.72	1.2450
C-12	14.6	28.9	115.59	1.3530	133.78	1.2447

The X-ray diffraction and microstructure results given in Table 4.1 also shows that the alloys C-6, C-7 and C-8 are single phase $MMCo_5$. Using the reflections (30.1) and (22.0) (Table 4.7) the lattice parameters a and c of the $MMCo_5$ phase were calculated. The variation of the parameters a and c with composition is shown in Figure 4.13. In the single phase region, between alloys C-4 and C-10 (Table 4.7) a decreases and c increases (with a consequent increase of c/a) with increasing Co content. This is in agreement with the variation of lattice parameters reported by Buschow et.al.[17] and by Khan[19] in the homogeneity region of $RECo_5$ phase (RE = Sm, Ce, Pr and Nd). Khan[19] has reported the existence of a homogeneity region for $CeCo_5$, $PrCo_5$ and $NdCo_5$ near 1100°C. The present study shows that mischmetal which is a mixture of Ce, La, Nd and Pr also has a homogeneity region for the $MMCo_5$ phase extending over 2 w/o (1.5 a/o) rare-earth at 900°C and its width is comparable with that reported by Khan[19] for the $CeCo_5$ phase.

In the present study the homogeneity region was studied only for 1:5 phase alloys containing about 3 a/o Fe. It was not studied closely for low as well as high Fe containing 1:5 alloys.

4.3.3 Phase Stability of $MMCo_5$

The alloy C-6, which is single-phase $MMCo_5$ at 900°C, gave an interesting microstructure when annealed at 700°C for 30 days (Figure 4.14). A bright phase MM_2Co_{17} appeared along the grain boundaries of the $MMCo_5$ phase. Buschow[27] has obtained a similar microstructure for the $NdCo_5$ phase annealed at 620°C for 8 weeks. He has attributed this to a eutectoid reaction in which the $NdCo_5$ phase decomposes into Nd_5Co_{19}

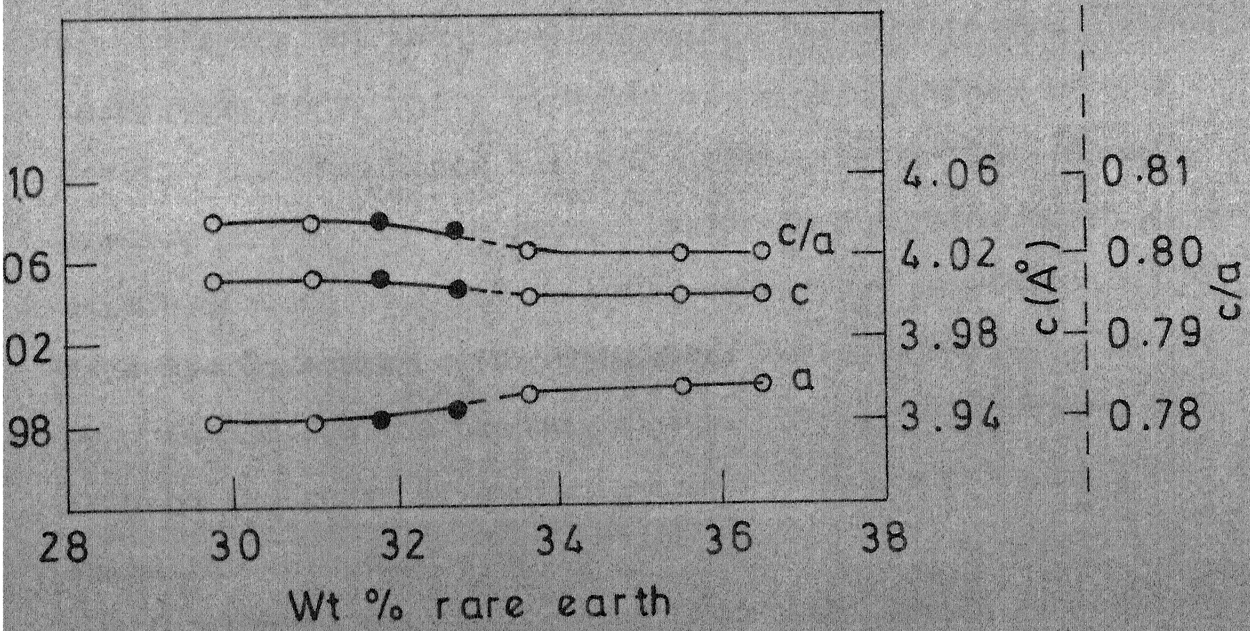

4·13 VARIATION IN THE LATTICE PARAMETERS WITH COMPOSITION OF THE $MMCo_5$ PHASE IN $MMCo_{5 \pm x}$ ALLOYS. ●, Homogeneous alloys; ○, Heterogeneous alloys and Nd_2Co_{17}, the latter appearing as bright grain boundary precipitates and the former appearing as dark parallel lines inside the $NdCo_5$ phase with different orientations in each grain. X-ray evidence has been given only for the Nd_2Co_7 product phase. In the present study it was observed that the extent of decomposition of $MMCo_5$ even after annealing for 30 days was so small ($<$5%) that clear X-ray evidence could not be obtained for the product phases. Since the addition of iron to the phase of stoichiometry 1:5 has been reported to raise the eutectoid reaction temperature,[41] two alloys E-1 and E-2 (Table 4.1) containing 5 and 15.2 a/o Fe respectively, were prepared using synthetic mischmetal and high purity Fe and Co ($>$99.9%). The synthetic mischmetal contained high purity ($\geq$99.9%) rare earth elements in approximately the same ratio as that in natural mischmetal.

In Table 4.8 the X-ray diffraction results of as-cast and annealed alloys of E-1 and E-2 are shown. In the as-cast condition both E-1 and E-2 contain predominantly $MMCo_5$ with a small amount of MM_5Co_{19}. The same alloys on annealing at 700°C for 30 days gave new reflections belonging to the MM_2Co_{17} phase.

The microstructures of the alloys E-1 and E-2 annealed at 700°C for 30 days are shown in Figures 4.15 and 4.16. For the alloy E-1 the bright MM_2Co_{17} phase is precipitated along the grain boundaries and inside the grain (Figure 4.15) whereas in the alloy E-2 they appear as

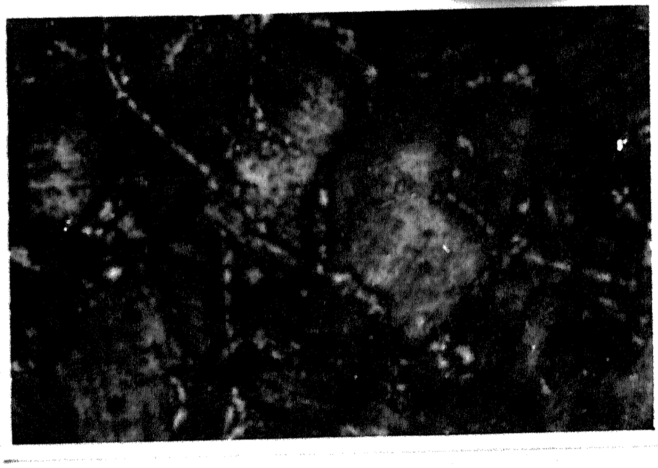

Figure 4.14 The microstructure of the alloy C-6 after annealing at 700° C for 30 days. The matrix is $MMCo_5$ with MM_2Co_{17} at the grain boundaries. The dark parallel lines inside the grains are possibly the phase of stoichiometry 5:19.

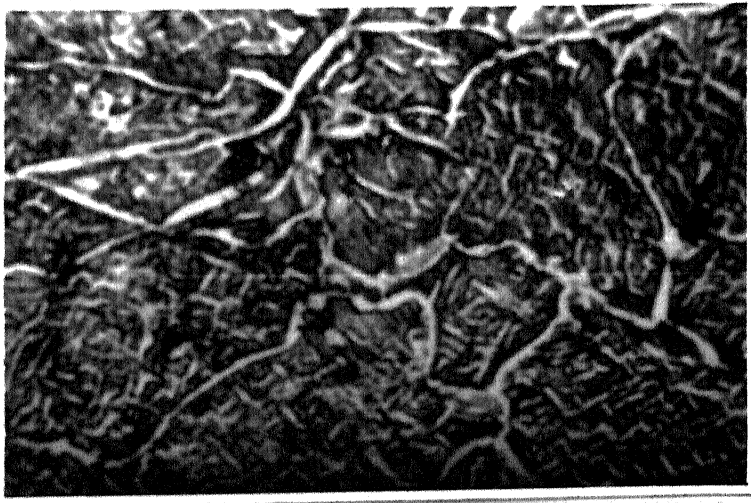

Figure 4.15 The microstructure of the alloy E-1 after annealing at 700° C for 30 days. MM_2Co_{17} is present at the grain boundaries and inside the grains. The dark regions are MM_5Co_{19} and $MMCo_5$.

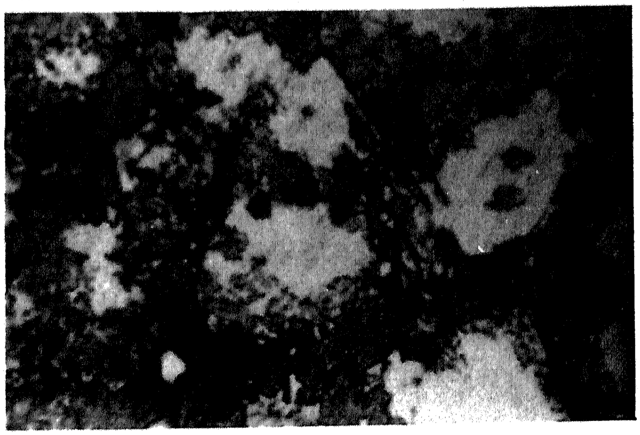

Figure 4.16 The microstructure of the alloy E-2 after annealing at 700° C for 30 days. The bright regions are MM_2Co_{17} and the dark regions are MM_5Co_{19}(?)

separate grains (Figure 4.16). However, it was not possible to prove the absence of the parent $MMCo_5$ phase in these alloys because all the strong X-ray diffraction lines of $MMCo_5$ overlap with those of either the MM_5Co_{19} or the MM_2Co_{17} phase (Table 4.8). In the microstructure also no clear evidence could be obtained for this. Hence these alloys were further studied by thermomagnetic analysis.

In Figure 4.17 the TMA curves for the as-cast alloy of E-1 and for the alloy of E-1 annealed at 700° C for 30 days are shown. For the as-cast alloy a strong magnetic transition near 541° C and a weak magnetic transition at 240° C can be seen, belonging to $MMCo_5$ and MM_5Co_{19} respectively. On annealing, the $MMCo_5$ magnetic transition is greatly reduced and that of MM_5Co_{19} becomes prominent. The magnetic transition corresponding to the MM_2Co_{17} phase could not be seen in this curve because it has a higher ferromagnetic transition temperature, T_c than the upper limit of the high temperature oven used. These results prove that the E-1 alloy annealed at 700° C contains mainly the MM_5Co_{19} and MM_2Co_{17} phase with a small amount of the parent $MMCo_5$ phase.

The TMA curves of the alloy E-2, which contains a greater amount of iron (15.2 a/o) than the alloy E-1 (5 a/o) show a different result (Figure 4.18). The $MMCo_5$-magnetic transition observed for the as-cast alloy was totally absent for the alloy annealed at 700° C for 30 days, proving the absence of the $MMCo_5$ phase. The magnetic transition

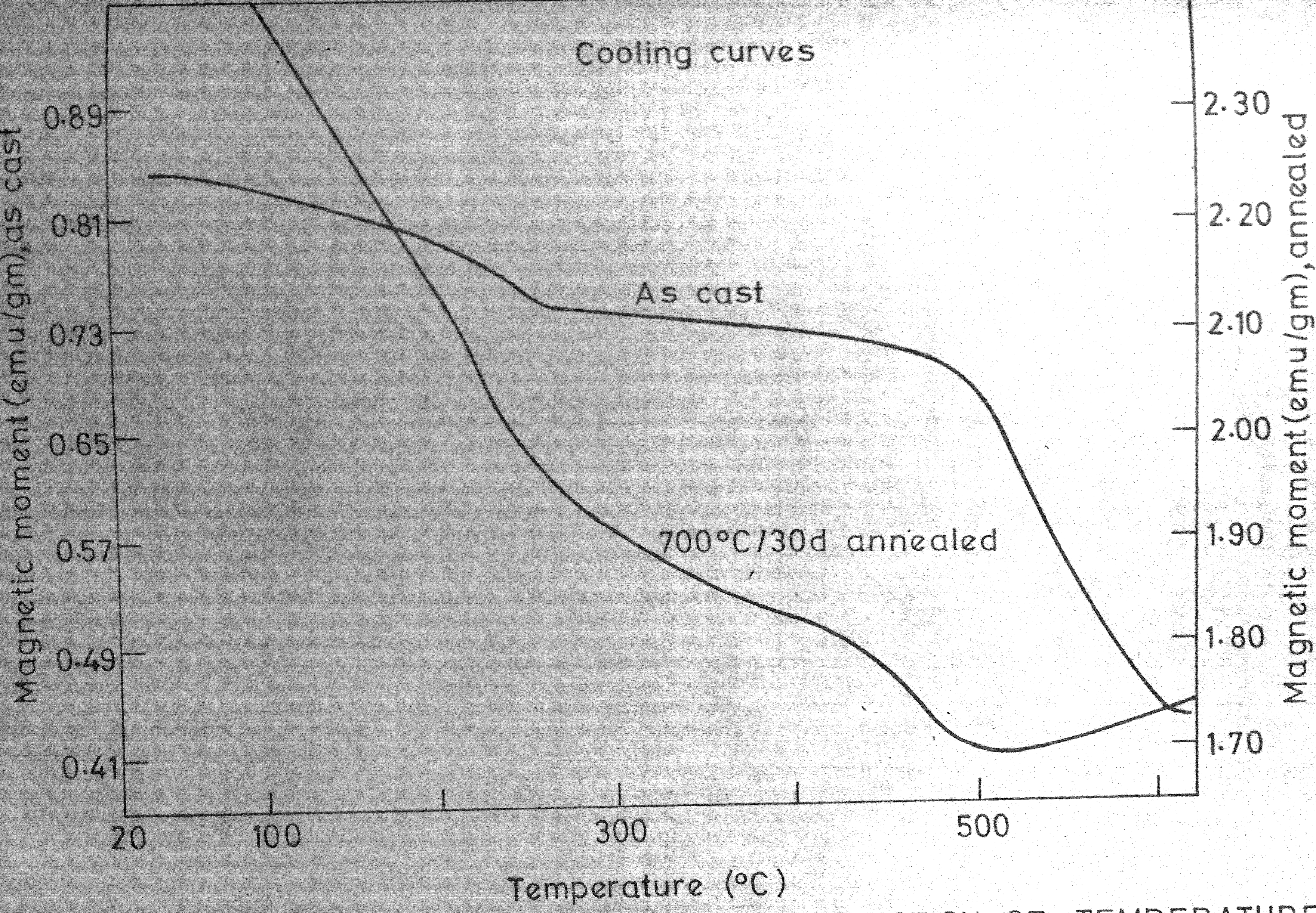

FIG. 4.17 LOW FIELD MAGNETIC MOMENT AS A FUNCTION OF TEMPERATURE FOR ALLOY E-1

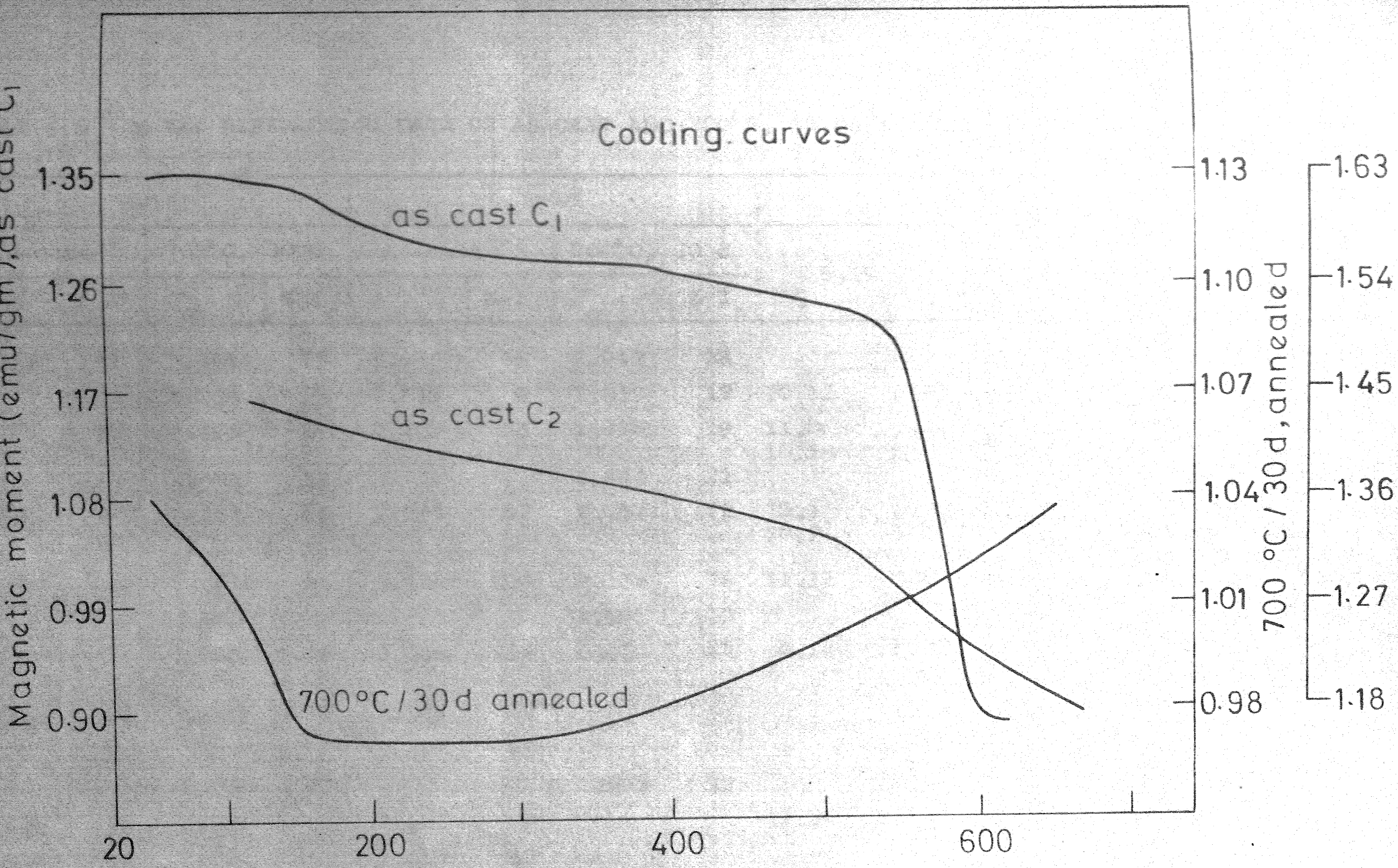

FIG. 4.18 LOW FIELD MAGNETIC MOMENT AS A FUNCTION OF TEMPERATURE FOR E-2 ALLOY

TABLE 4.8 X-RAY DIFFRACTION DATA OF AS-CAST AND 700°C, 30 days ANNEALED ALLOYS OF E-1 AND E-2

E-1				E-2				hk.1 (% I_c)					
As-cast		700°C, 30 d		As-cast		700°C, 30 d		5:19		1:5		2:17	
d_o	% I_o	d_o	% I_o	d_o	% I_o	d_c	% I_o						
2.942	41	2.942	33	2.942	38	2.942	28			10.1	(38)	11.3	(41)
		2.819	17	2.819	9	2.819	17	10.13	(16)			10.4	(8)
2.485	28	2.496	31	2.485	28	2.496	19	11.0 10.16	(43)	11.0	(29)		
		2.441	22			2.441	21					30.0	(36)
2.149	46	2.157	41	2.141	47	2.137	72	20.1 20.2	(39)	20.0	(41)		
2.116	100	2.116	94	2.116	100	2.116	75	11.12	(100)	11.1	(100)	22.0	(60)
		2.093	100			2.101	100					31.3	(100)
		2.040	55	2.048	19	2.055	47	00.24	(23)			00.6 21.4	(44)
2.012	24	2.022	50	2.022	29					00.2	(19)		
1.893	14			1.893	13					20.1	(17)		
		1.869	17			1.875	19					22.3	(31)
1.559	12	1.559	9	1.583	9			11.24	(4)	11.2	(16)	30.6	(5)
1.507	12			1.507	12					21.1	(14)		
		1.486	20			1.483	21					21.7	(16)

Contd...

ABLE 4.8 (contd.)

E-1				E-2				hk.1 (% I_c)					
As-cast		700° C, 30 d		As-cast		700° C, 30 d		5:19		1:5		2:17	
	% I_o	d_o	% I_o	d_o	% I_o	d_o	% I_o						
.469	20	1.469	27	1.473	20	1.473	26			20.2	(21)	40.5	
												32.4	(25)
												22.6	
.345	16	1.345	8	1.350	15	1.363	9	30.12	(26)	30.1	(24)		
		1.324	13			1.330	15					33.3	(15)
		1.248	16			1.248	11					41.6	(9)
.243	10	1.239	11	1.241	12			22.1	(23)	22.0	(31)		

corresponding to the RE-rich phase appeared at a lower temperature for both the annealed alloy and the as-cast alloy. Though this phase could be accounted for 5:19 in the X-ray (Table 4.8) its Curie temperature is much lower (150°C) than that expected for a 5:19 phase (280°C). Also the MM-Co-Fe phase diagram (Figure 4.1) shows that the 5:19 phase does not extend beyond about 10 a/o Fe. It is possible that this phase is of 2:7 type rather than 5:19.

4.4 Conclusions

Phase equilibria in MM-Co-Fe system was studied at 900°C between 73 a/o and 92 a/o Co with Fe content upto 15 a/o. Six different phases $MMCo_3$, MM_2Co_7, MM_5Co_{19}, $MMCo_5$, MM_2Co_{17} and β-Co were identified close to the MM-Co binary line. Thermomagnetic analysis proved to be a better technique than X-ray diffraction for identifying the low cobalt phases, $MMCo_3$, MM_2Co_7 and MM_5Co_{19} the ferromagnetic transition temperature of which were found to be $<$ 20°C, 67°C and 270°C respectively. The 2:7, 5:19, 1:5 and 2:17 phases were also found to exist as stable phases in the MM-Co-Fe ternary system. The 5:19 phase was found to extend to about 10 a/o Fe while the 2:7, 1:5 and 2:17 phases extend to greater than 10 a/o Fe. In addition to the above phases, a phase with a T_c of 340°C was found to coexist with 5:19 and 1:5 phases close to the 5:19 stoichiometric line and the region of its occurrence in the MM-Co-Fe system at 900°C is indicated. The phase on the cobalt rich side of 2:17 stoichiometry had β-Co structure with no solid solubility for RE elements while $MMCo_5$ showed a narrow homogeneity region at 900°C other phases did not show the presence of such region. $MMCo_5$ was unstable at temperatures below about 700°C. The decomposition was found to be sluggish in the low Fe (<3 a/o) containing 1:5 phase and hence evidence could be obtained only for the MM_2Co_{17} product phase. But in high iron 1:5 alloys (>5 a/o) the decomposition at 700°C was rapid and evidence could be obtained for both the 5:19 and 2:17 product phases by TMA.

REFERENCES

1. J.J. Becker, K. Strnat, G. Hoffer, J. Olsen and W. Ostertag, J. Appl. Phys. 38, 1001 (1967).

2. K.J. Strnat, IEEE Trans. Magn. MAG-6, 182 (1970).

3. K.J. Strnat, A.E. Ray and H.F. Mildrum, IEEE Trans. Magn. MAG-13, 1323 (1977).

4. K.J. Strnat, J. Appl. Phys. 37, 1252 (1966).

5. K.J. Strnat, G. Hoffer and A.E. Ray, IEEE Trans. Magn. MAG-2, 489 (1966).

6. K.H.J. Buschow, P.A. Nastepad and F.F. Westendorp, J. Appl. Phys. 40, 4029 (1969).

7. D.K. Das, IEEE Trans. Magn. MAG-5, 214 (1969).

8. M.G. Benz and D.L. Martin, J. Appl. Phys. 43, 3165 (1972).

9. A.E. Paladino, N.J. Dionne, P.F. Weihrauch and E.C. Wettstein, Goldschmidt Informiert 4/75, Nr. 35, 63 (1975).

10. H. Nagel, H.P. Klein and A. Menth, J. Appl. Phys. 47, 3312 (1976).

11. T. Ojima, S. Tomizawa, T. Yoneyama and T. Hori, IEEE Trans. Magn. MAG-13, 1317 (1977).

12. K. Inomata, T. Oshima, T. Ido and M. Yamada, Appl. Phys. Lett. 30, 669 (1977).

13. D.L. Martin and M.G. Benz, AIP Conf. Proc. 5, 970 (1972).

14. P.A. Nastepad, F.J.A. den Broeder and R.J. Wassink, Powder Metall. Int. 5, 61 (1973).

15. A. Benz and K. Bachmann, AIP Conf. Proc. 10, 578 (1973).

16. P.F. Weihrauch and D.K. Das, AIP Conf. Proc. 18, 1149 (1974).

17. K.H.J. Buschow and F.J.A. den Broeder, J. Less-Common Metals, 33, 191 (1973).

18. A.E. Ray, A.T. Biermann, R.S. Harmer and J.E. Davison, Cobalt, 4, 103 (1973).

19. Y. Khan, Phy. Status Sol. (a) 21, 69 (1974).

20. Y. Khan, J. Less-Common Metals, 34, 191 (1974).

21. E.A. Nesbitt and J.H. Wernick, Rare Earth Permanent Magnets, Academic Press, N.Y. (1973).

22. G. Schaffer and W. Spyra, Entwicklung von Daner Magneten auf der Basis Von Seltenerd-Kobalt-Legierungen Forschungsbericht T76-37, Zentralstelle fur Luft und Raumfahrtdokumentation und information, Munich, October (1976).

23. E.M.T. Velu, E.C. Subbarao, H.O. Gupta, K.P. Gupta, S.N. Kaul, A.K. Majumdar, R.C. Mittal, T.A. Padmavathi Sankar, G. Sarkar, M.V. Satyanarayana, K. Shankara Prasad and J. Subramanyam, in G.J. McCarthy, J.J. Rhyne and H.B. Silber (eds.) Rare Earths in Modern Science and Technology, 2, Plenum, N.Y. (1980) p.45 and J. Less-Common Metals 71, 219 (1980).

24. A.E. Ray and K.J. Strnat, IEEE Trans. Magn. MAG-8, 516 (1972).

25. A.E. Ray and R.S. Harmer, Proc. 9th Rare Earth Research Conf., Blacksburg, VA, 1, 368 (1971).

26. F.J.A. den Broeder and K.H.J. Buschow, J. Less-Common Metals, 29, 65 (1972).

27. K.H.J. Buschow, J. Less-Common Metals, 29, 283 (1972).

28. J.G. Smeggil, P. Rao, J. Livingston and E.F. Koch, AIP Conf. Proc. 18, 1144 (1974).

29. D.L. Martin, J.G. Smeggil, W. Hatfield and R. Bolon, IEEE Trans. Magnetics, 11, 1420 (1975).

30. R.C. Mittal, M.V. Satyanarayana, K.P. Gupta, H.O. Gupta, S.N. Kaul, A.K. Majumdar, K. Shankara Prasad, T.A. Padmavathi Sankar, E.C. Subbarao and E.M.T. Velu, J. Less-Common Metals, 78, 245 (1981).

31. T.A. Padmavathi Sankar, H.O. Gupta, E.C. Subbarao, K.P. Gupta, N.R. Bonda, S. Laha, A.K. Majumdar, S. Pandian, J. Subramanyam and E.M.T. Velu, Bull. Mater. Sci. 2, 167 (1980).

32. K.H.J. Buschow, Acta Crystallogr. B, 26, 1389 (1970).

33. Y. Khan, Acta Crystallogr. B, 29, 2502 (1973).

34. Y. Khan, Acta Crystallogr. B, 30, 1533 (1974).

35. E.M.T. Velu, S. Laha, E.C. Subbarao, K.P. Gupta, A.K. Majumdar, T.A. Padmavathi Sankar, S. Pandian and U. Ramakrishna, Paper No. M-11, 15th Rare Earth Research Conference, June 15-18, 1981, Missouri, Rolla, U.S.A. To be published in Rare Earths in Modern Science and Technology, Vol. 3.

36. K.H.J. Buschow and J.S. Van Wieringen, Phys. Stat. Solidi, 42, 231 (1970).

37. J.H. Wernick and S. Geller, Acta Crystallogr. 12, 662 (1959).

38. E.M.T. Velu, E.C. Subbarao, N.R. Bonda, D.K. Goel, K.P. Gupta, A.K. Majumdar, T.A. Padmavathi Sankar and J. Subramanyam, J. Appl. Phys. 51, 3322 (1980).

39. G. Bouchet, J. Laforest, R. Lemaire and J. Schweizer, C. R. Acad. Sci. 262, 1 (1966).

40. K.J. Strnat and A.E. Ray, AIP Conf. Proc. 24, 680 (1975).

41. K.H.J. Buschow, J. Less-Common Metals, 37, 91 (1974).

5. MAGNETIC PROPERTIES OF MM-Co-Fe PHASES

5.1 Introduction

Primary magnetic properties of interest for permanent magnet production are (1) saturation magnetisation ($4\pi M_s$) (2) magnetocrystalline anisotropy field (H_A) and (3) Curie temperature. Materials with high values for all these parameters are excellent candidates for the production of high energy density permanent magnets. Hence it is very essential to characterise the different intermetallic phases occurring in the RE-Co systems for these parameters. Extensive studies[1-2] have been made on the primary magnetic properties of pure binary RE-Co phases and the properties reported for the intermetallic phases in the RE-Co systems RE= Ce, La, Nd, Pr and Sm are summarised in Tables 6.1 and 6.2.

5.2 Experimental

The different intermetallic phases found in the MM-Co-Fe system were characterised for their saturation magnetisation and Curie temperature. The experimental procedure is the same as that described under Section 3.2.3. The H_A, as explained under the Section 3.3.1.1 was not determined in this study.

TABLE 5.1. PRIMARY MAGNETIC PROPERTIES OF $RECo_5$ PHASES

System Properties	Unit	YCo_5	$LaCo_5$	$CeCo_5$	$CeMMCo_5$	$PrCo_5$	$SmCo_5$
$4\pi M_s$ (20° C)	G	10600	9090	7700	8900	12000	9650
T_c	°C	648	567	374	495	612	724
H_A (20° C)	KOe	130	175	170-210	180-195	145-210	210-290
$(BH)_{max}$ (Theoretical)	MGOe	28.1	20.6	14.8	19.8	36.0	23.4
${}_iH_c$	Oe	6700	3600	2800	4750	5750	25000

TABLE 5.2. MAGNETIC SATURATION AND ANISOTROPY AT 20°C OF RE_2Co_7 PHASES

Phase	$4\pi M_s$ (20° C)		H_A (KOe)
	(emu/g)	Gauss	
La_2Co_7	50.4	5193	171
Pr_2Co_7	83.4	8851	105
Nd_2Co_7	85.1	9173	28

5.3. Results and Discussion

5.3.1 Saturation Magnetisation of MM-Co Phases

The specific saturation magnetisation (σ, emu/g) was determined for the stoichiometric phases in the MM-Co system. The amount of the second phase in these alloys was 5% as determined metallographically. The $4\pi M_s$ of MM_2Co_7, MM_5Co_{19} and MM_2Co_{17} phases are shown in Table 5.3.

TABLE 5.3. SATURATION MAGNETISATION OF MM-Co PHASES AT 20° C

Alloy	Phase	Composition (a/o, analysed)			$4\pi M_s$	$4\pi M_r$	M_r/M_s
		RE	Co	Fe	(emu/g)	(emu/g)	
A-3	2:7	22.9	73.4	3.7	29	12	0.41
B-3	5:19	21.5	75.0	3.5	44	29	0.66
C-3	1:5	16.9	80.3	2.8	95	80	0.84
D-4	2:17	11.1	87.1	1.8	114	21	0.18

The $MMCo_5$ phase has a $4\pi M_s$ of 95 emu/g and a density of 8.3 g/cc. This on conversion turns out to be 9.6 KG which is slightly higher than the value reported by Strnat[1] for $CeMMCo_5$ phase (Table 5.1). The $4\pi M_s$ of the individual $RECo_5$ phases differ considerably (Table 5.1). The higher value observed for the $MMCo_5$ may be due to a different distribution of RE elements in the Indian mischmetal and due to the presence of about 6 w/o Fe as impurity in the Indian mischmetal.

The MM_5Co_{19} has a $4\pi M_s$ of 44 emu/g. Though it contains 75.0 a/o Co its $4\pi M_s$ is low by more than twice that of $MMCo_5$ which contains 80.3 a/o Co. The MM_2Co_7 phase which contains 73.4 a/o Co shows a $4\pi M_s$ of 29 emu/g only. However no $4\pi M_s$ value is available for Ce_5Co_{19} and Ce_2Co_7 to compare with the observed values. Both Ce_5Co_{19} and Ce_2Co_7 are paramagnetic at room temperature (25° C). The T_c of Ce_5Co_{19} is 20° C and that of Ce_2Co_7 is -110° C.[4]

The MM_2Co_{17} phase contains 87.1 a/o Co and shows the highest value for $4\pi M_s$ as expected but on the contrary it has the lowest M_r/M_s ratio of 0.18. MM_2Co_{17} phase has been reported to have an easy plane anisotropy[5] in which case this low value is explainable.

5.3.2 Curie Temperature

5.3.2.1 T_c of Stoichiometric Phases in MM-Co System

The chemical and phase composition of the alloys used for the thermomagnetic study are given in Table 5.4.

TABLE 5.4. CHEMICAL AND PHASE COMPOSITION OF MM-Co-Fe ALLOYS USED FOR TMA

Alloy	Composition (a/o, analysed)			Phases (900°C, 4-10 d)	
	RE	Co	Fe	Microstructure (number of phases)	X-ray
A-1	23.4	72.8	3.8	2	1:3 + 2:7
6-1	22.3	72.3	5.4	2	2:7 + 5:19
12-1	21.3	67.3	11.4	2	2:7 + 5:19
15-1	21.5	63.3	15.2	2	2:7 + 5:19
B-5	21.0	75.6	3.4	2	5:19 + 1:5
C-1	19.5	77.4	3.1	2	5:19 + 1:5
C-3	18.1	79.0	2.9	2	5:19 + 1:5
S-1	16.5	83.5	0	1	1:5
O-3	16.6	83.4	0	1	1:5
6-5	16.6	77.0	6.4	1	1:5
12-5	15.8	71.9	12.3	2	1:5 + 2:17

The thermomagnetic curves of alloys A-1, B-5 and S-1 are shown in Figure 5.1. A magnetic transition near 60° C is observed for alloy A-1. Since the composition of this alloy lies on the MM rich side of 2:7 stoichiometry this transition is attributed to the MM_2Co_7 phase. The second phase seen in the microstructure of the alloy should be the 1:3 phase. As this phase is expected to have a T_c much less than room temperature (20° C) its transition could not be observed in the present study. The alloy B-5 with composition on the cobalt rich side of 5:19 stoichiometry shows no magnetic transition near 60° C confirming the absence of a 2:7 phase. A major fall in moment observed at 280° C is attributed to the 5:19 phase. For the alloy S-1, a magnetic transition corresponding to the 1:5 phase only is observed. The T_c values of these phases after correcting for the thermal hysteresis are compared in Table 5.5. with the literature values for low cobalt phases in binary RE-Co systems. It is interesting to note that a simple relation i.e.

$$T_{c\ MM_xCo_y} = [\quad (\text{wt \% RE in MM})(T_{c\ RE_xCo_y})]\ 10^{-2}$$

could be used to predict the T_c of a MM_xCo_y phase from the composition of MM and the T_c of binary RE_xCo_y phases. For example, this equation when applied to the alloy S-1 (Table 5.5) which was prepared with high purity RE elements and Co,

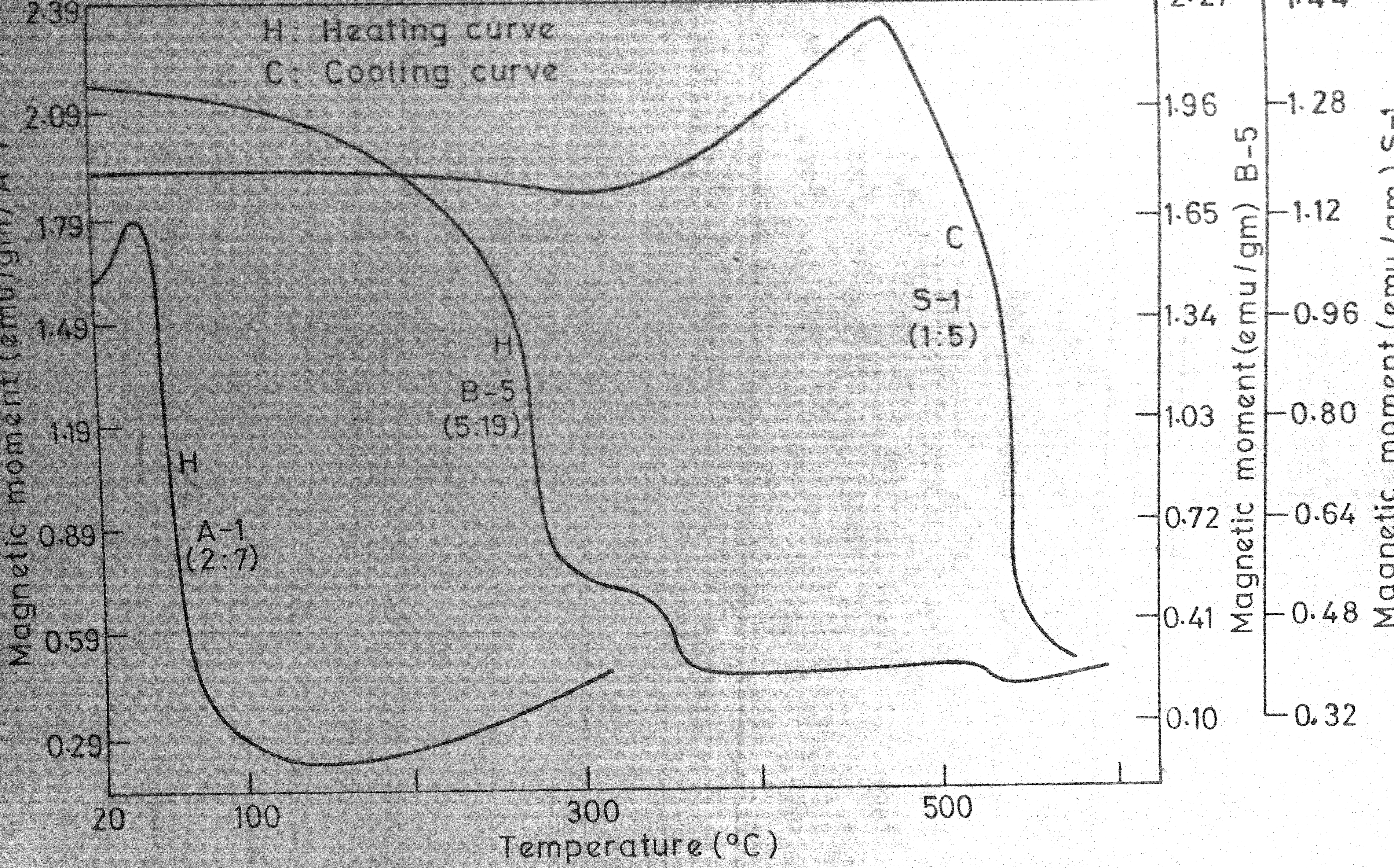

FIG.5·1 LOW FIELD MAGNETIC MOMENT AS A FUNCTION OF TEMPERATURE FOR ALLOYS A-1, B-5 & S-1 900°C ANNEALED

TABLE 5.5. CURIE TEMPERATURES IN °C OF RE-Co COMPOUNDS

RE	$RECo_3$	RE_2Co_7	RE_5Co_{19}	$RECo_5$	RE_2Co_{17}
Ce	-195^a	-110^c	20^d	374^e	810^f
La	Does not exist	220^c	343^d	567^e	Does not exist
Nd	122^a	355^c	441^d	630^c	877^f
Pr	76^a	337^c	417^d	612^e	898^f
Sm	250^b	450^b	$(510\ ?)^{b,d}$	724^e	917^f
MM	$<20^p$	67^p	270^p	541^p	$>735^p$

a : Ref. 7; b : Ref. 8; c : Ref. 4; d : Ref. 3;
e : Ref. 1; f : Ref. 9; p : present work.

predicts a T_c of 491°C, whereas the experimental value is 541°C, the difference being less than 10%.

For the alloy B-5 two more magnetic transitions at 350 and 517°C were observed (Figure 5.1). The latter was due to $MMCo_5$ present as a minor phase in this alloy which was also detected in the X-ray diffraction. The new magnetic transition observed between the T_c of MM_5Co_{19} and $MMCo_5$ was also seen for a number of alloys near 1:4 composition in the MM-Co system[10] and this has been discussed under Section 4.3.1. It is seen from Figures 5.2 and 5.3 that the heating and cooling curves for the alloy C-1 are irreversible. In the heating cycle the magnetic moment increases steadily and peaks near the Curie temperature before falling. On cooling

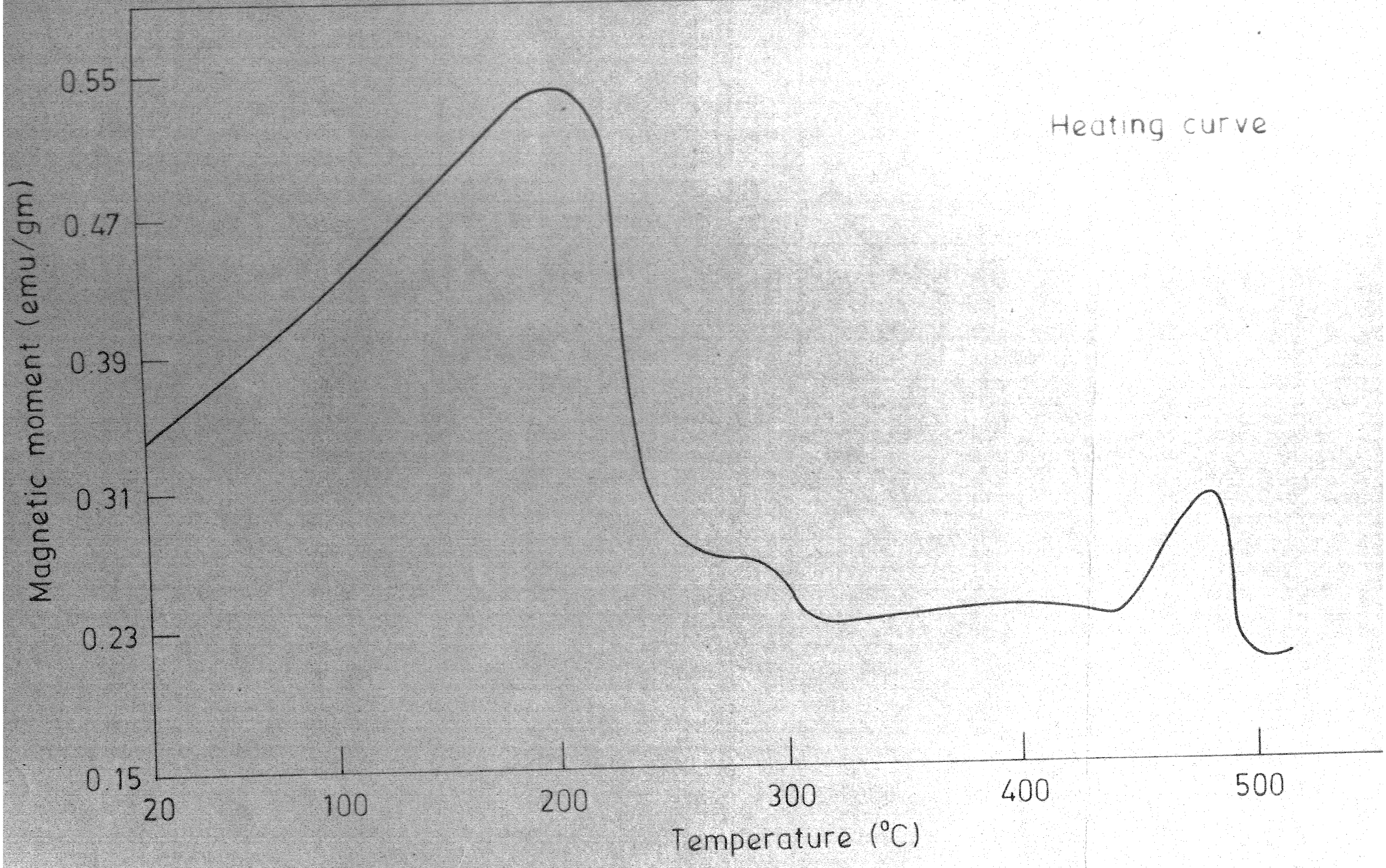

FIG.5·2 Low field magnetic moment as a function of temperature for C-1 alloy,

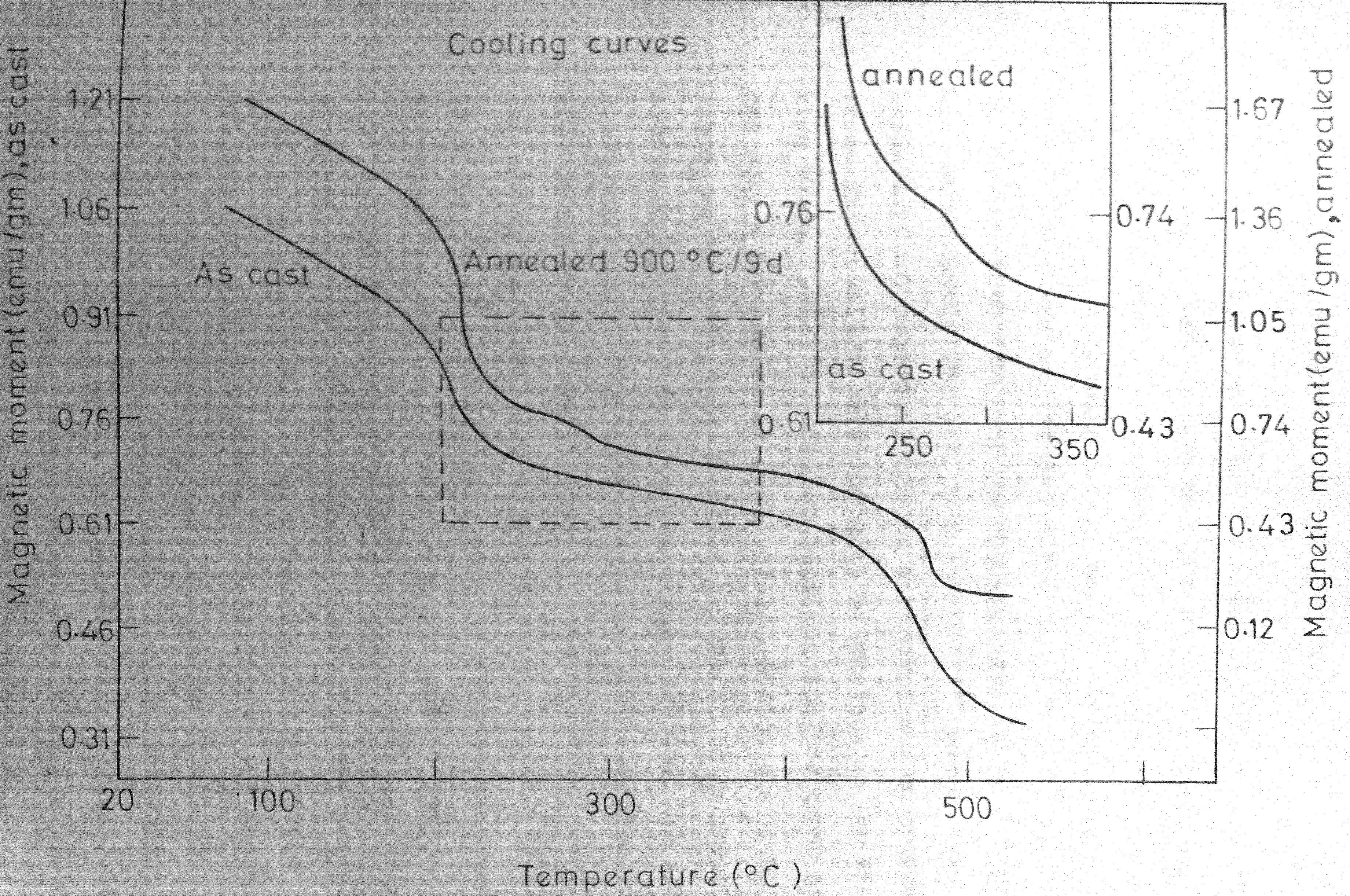

FIG.5.3 LOW FIELD MAGNETIC MOMENT AS A FUNCTION OF TEMPERATURE FOR C-1 ALLOY

it takes a different path and the magnetisation at any given temperature is greater than that observed in the heating cycle. This behaviour was observed for most of the alloys studied and in particular for the as-cast alloys. In subsequent heating and cooling cycles the curves were reversible and the peeking phenomena near the magnetic transition temperature was not observed. The 2:7, 5:19 and 1:5[11,12] phases have large uniaxial magnetocrystalline anisotropy and consequently these phases will be very difficult to saturate at low fields like 40 Oe. Hence the observed magnetisation for these samples are only a few percent of their saturation magnetisation. The H_A of the $MMCo_5$ phase has been reported[13] to decrease monotonically with increasing temperature and vanishes near its Curie point. This might be true for the other phases also in the MM-Co system. Hence as the temperature approaches the transition point where H_A also tends to vanish, a field of 40 Oe should be sufficiently high to increase the magnetisation of the samples giving rise to the peaking phenomena in the heating cycle. On cooling the magnetisation was observed to increase 2 to 3 times the value observed in the heating cycle. This suggests that increased number of magnetic domains get aligned in a direction parallel to the applied magnetic field in the polycrystalline sample during the cooling as a result of domain growth. In the subsequent heating and cooling cycles the curves were reversible and the peaking phenomenon near the T_c was absent. This suggests that the magnetic domain configuration remains essentially the same after the first heating and cooling cycles.

The Curie temperature of the MM_2Co_{17} phase is not reported here as it has a $T_c \gg 700°C$, which is beyond the experimental safety limit of the high temperature oven used.

5.3.2.2 T_c of MM-Co-Fe Phases

The compositions of the alloys A-1, 35^{10}, 6-1, 12-1 and 15-1 lie between the 2:7 and 5:19 stoichiometries. The microstructure of the alloys show 2 phases (Table 5.4). These phases are assigned to MM_2Co_7 and MM_5Co_{19}. The heating TMA curves of the alloys A-1, 6-1, 12-1 and 15-1 are shown in Figure 5.4. Their Curie temperature after correcting for the thermal hysteresis are indicated in Table 5.6. It could be seen that the Curie temperature of both the 2:7 and 5:19 phases increase with increasing concentration of Fe. A three fold increase in the T_c of the 2:7 phase, from 70°C to 218°C, is observed as the Fe content varies from 3.8 a/o in alloy A-1 to 15.2 a/o in alloy 15-1 (Table 5.6). On the contrary only about 60°C raise in T_c is observed for the 5:19 phase as the Fe varies from 3.8 to 11.4 a/o (Figure 5.5). It is to be noted that the concentration of Fe listed in Table 5.6 is only the bulk concentration of the alloy and the actual distribution of the Fe in the two phases when they coexist, need not be the same. Thus the observed lower raise in T_c for the MM_5Co_{19} could possibly be due to the lesser solubility of Fe in it than in the 2:7 phase. There is also indirect indication

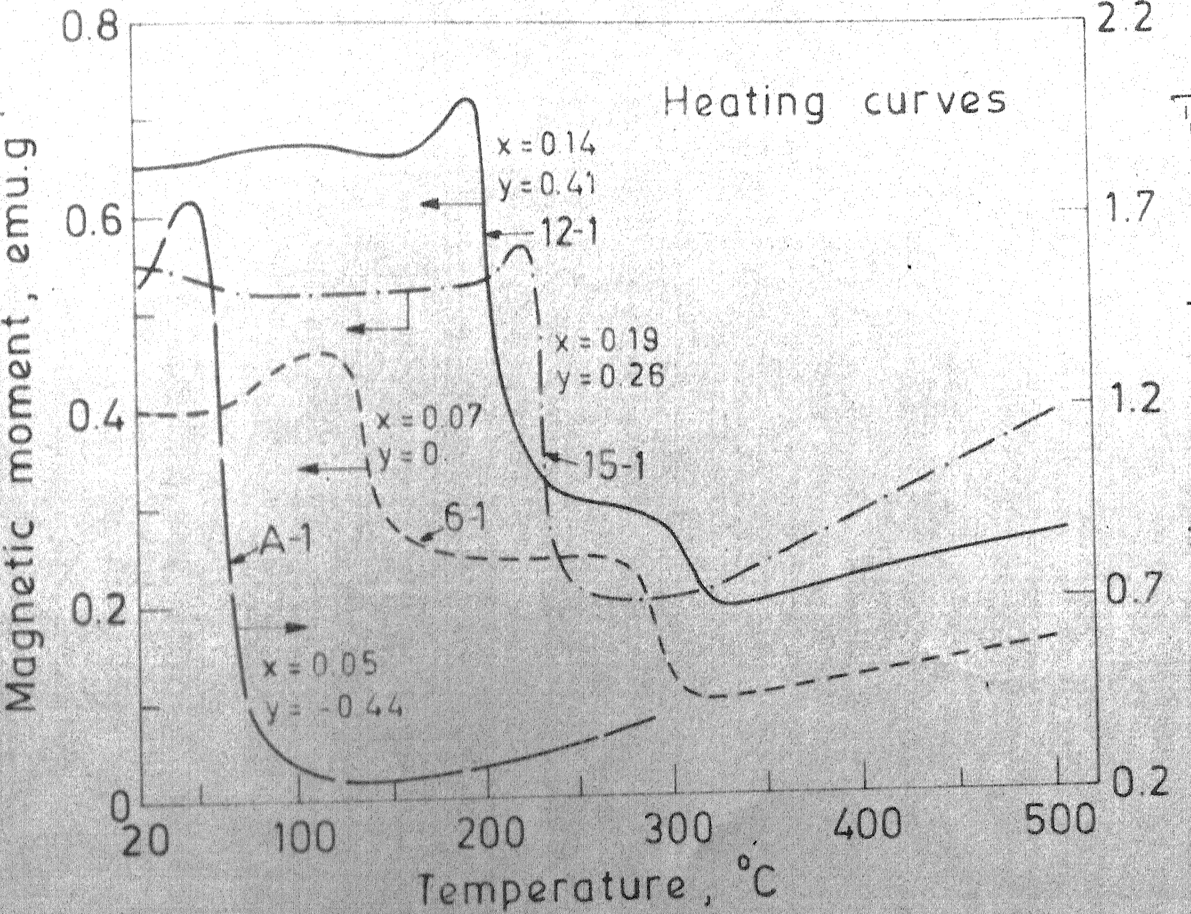

Fig.5·4 Magnetisation versus temperature at 40 Oe for $MM_2(Co_{1-x}Fe_x)_{7+y}$ alloys; 900 °C, 7 days annealed

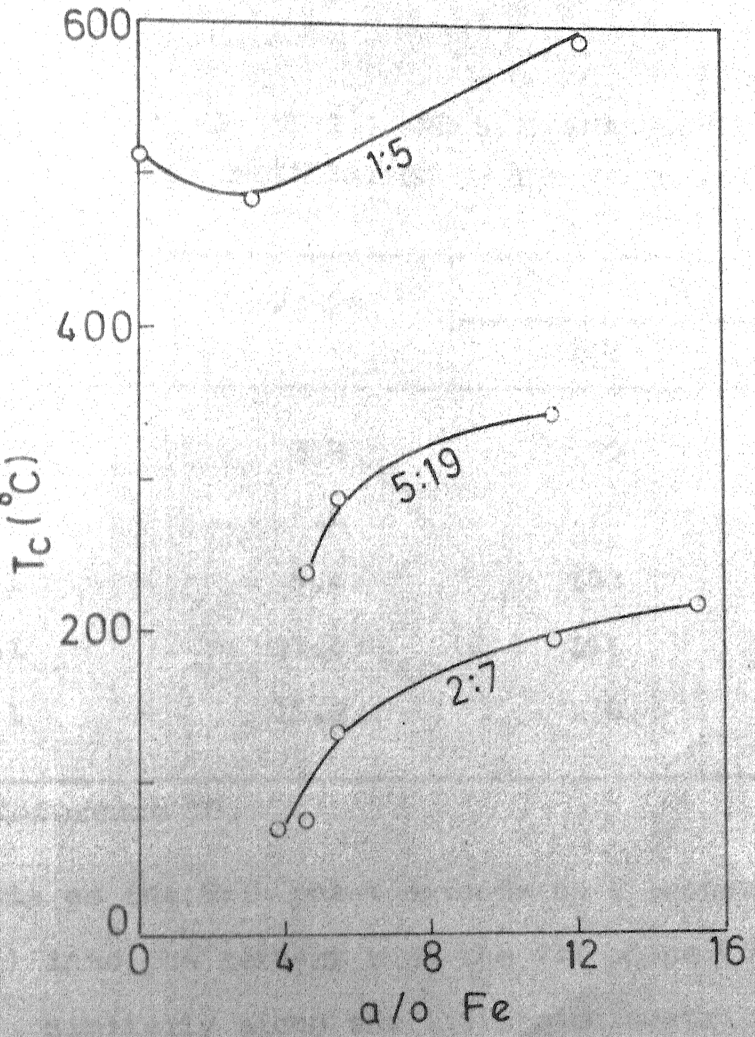

FIG.5.5 VARIATION OF T_c OF 2:7 5:19 AND 1:5 PHASE WITH Fe CONCENTRATION IN MM-Co-Fe SYSTEM

TABLE 5.6. T_c OF THE 2:7 AND 5:19 PHASES WITH THE VARYING Fe CONCENTRATION IN THE MM-Co-Fe SYSTEM

Alloy	a/o Fe	T_c (°C)	
		2:7	5:19
A-1	3.8	70	absent
36[a]	4.6	75	238
6-1	5.4	133	280
12-1	11.4	196	295
15-1	15.2	218	absent

a : Reference 10.

for this as the 5:19 phase extends to a lesser extent ($\sim$11.4 a/o Fe) into the ternary than the 2:7 phase (Section 4.3.1).

Similarly along the 1:5 stoichiometric line alloys 0-3, 6-5 and 12-5 were studied. These alloys contain different amount of Fe and their microstructure revealed (Table 5.4) that the alloys 0-3 and 6-5 to be single phase 1:5 while 12-5 contains some amount of other phase ($\lessdot$ 20%) in addition to the major 1:5 phase. The TMA plots of these alloys are shown in the Figure 5.6 and their T_cs corrected for the thermal hysteresis are shown in Table 5.7. The T_c initially falls to 485°C at 2.9 a/o Fe from 512°C and then rises to 580°C at 12.3 a/o Fe (Figure 5.5).

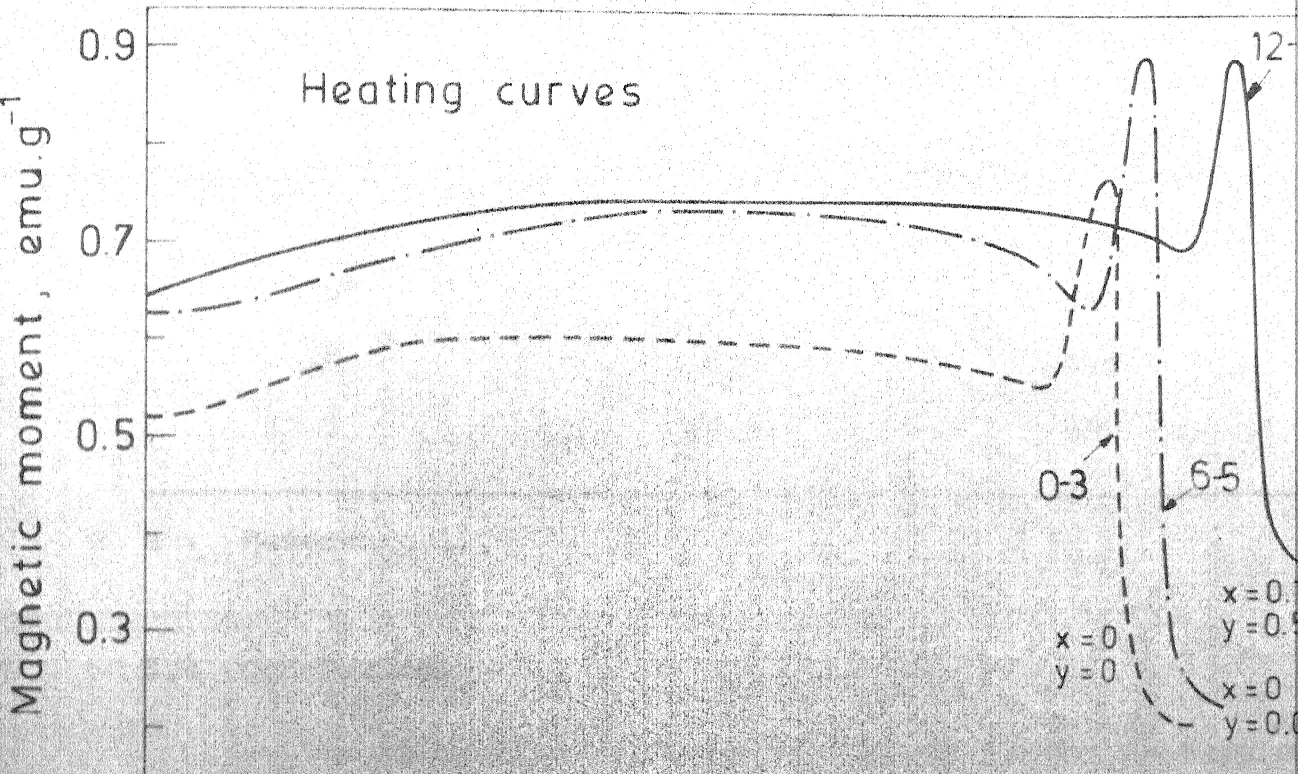

Fig. 5·6 Magnetisation versus temperature at 40 Oe for MM$(Co_{1-x}Fe_x)_{5+y}$ alloys

TABLE 5.7. T_c OF THE 1:5 PHASE WITH THE VARYING Fe CONCENTRATION IN THE MM-Co-Fe SYSTEM

Alloy	a/o Fe	T_c (°C)
0-3	0	512
C-3[a]	2.9	485
6-5	5.4	532
12-5	12.3	580

a : Reference 11.

5.4 Conclusions

The saturation magnetisation and Curie temperature of the intermetallic phases in the MM-Co-Fe system were studied. The $4\pi M_s$ of the 1:5 phase is 95 emu/g and that of the 2:17 phase is 114 emu/g. Both the 2:7 and 5:19 phases have a value less than 45 emu/g. The T_c of the stoichiometric 2:7, 5:19 and 1:5 phases are 67° C, 270° C and 541° C respectively. These values were found to increase with the increasing concentration of Fe.

REFERENCES

1. K.J. Strnat, IEEE Trans. Magn. MAG-6, 182 (1970).

2. K.J. Strnat, A.E. Ray and H.F. Mildrum, IEEE Trans. Magn. MAG-13, 1323 (1977).

3. A.E. Ray and K.J. Strnat, IEEE Trans. Magn. MAG-11, 1429 (1975).

4. K.J. Strnat and A.E. Ray, AIP Conf. Proc. 24, 680 (1975).

5. K.J. Strnat and A.E. Ray, Goldschmidt Informiert, 4/75, Nr. 35, 47 (1975).

6. E.M.T. Velu, E.C. Subbarao, H.O. Gupta, K.P. Gupta, S.N. Kaul, A.K. Majumdar, R.C. Mittal, T.A. Padmavathi Sankar, G. Sarkar, M.V. Satyanarayana, K. Shankaraprasad and J. Subramanyam, J. Less-Common Metals 71, 219 (1980).

7. R. Lemaire, R. Pauthenet, J. Schweizer and I.S. Silvera, J. Phys. Chem. Solids 28, 2471 (1967).

8. Y. Khan and A.H. Qureshi, Phys. Stat. Sol. (a) 28, 169 (1975).

9. J. Laforest, R. Lemaire, R. Pauthenet and J. Schweizer, C. R. Acad. Sc. Paris 262, 1260 (1966).

10. E.M.T. Velu, S. Laha, E.C. Subbarao, K.P. Gupta, S. U. Ramakrishna, A.K. Majumdar, T.A. Padmavathi Sankar, Paper No. M.11, 15th Rare Earth Research Conference, Rolla, Missouri, June 15-18, 1981.

11. E.M.T. Velu, E.C. Subbarao, N.R. Bonda, D.K. Goel, K.P. Gupta, A.K. Majumdar, T.A. Padmavathi Sankar and J. Subramanyam, J. Appl. Phys. 51, 3322 (1980).

6. PHASE RELATIONS AND MAGNETIC PROPERTIES OF MM($Co_{1-x}Cu_x$)$_5$ ALLOYS

6.1 Introduction

Widespread application of $SmCo_5$ permanent magnets is limited by the high cost of Sm and the scarcity of cobalt. Attractive magnetic properties have been reported for $SmCo_5$ alloys containing Cu.[1-2] MM-Co[3] and MM-Co-Fe-Cu[4] alloys also have useful permanent magnet properties of technological importance, but no systematic studies on phase relations and magnetic properties of MM-Co alloys containing Cu have been reported. Hence a systematic addition of Cu in place of Co was made in $MMCo_5$ alloy to know (i) the extent of solid solubility of Cu in $MMCo_5$ (ii) its effect on the phase stability of the 1:5 phase and (iii) its effect on $4\pi M_s$ and T_c of 1:5 phase. The mischmetal used in this study has the same composition as given under Section 3.1.1.

6.2 Experimental

The melting and annealing of the alloys and the procedure of phase analysis are the same as described under Sections 3.1 and 3.2. In X-ray diffraction studies, for Cu rich alloys Cu K_α radiations gave better results than Co K_α radiation. The magnetisation and the Curie temperature were studied with a vibrating sample magnetometer. To measure the $4\pi M_s$, the sample were powdered, magnetically aligned and then fixed in an epoxy resin. A field of 11 KOe was sufficient to saturate the aligned samples. The magnetisation of the alloys as a function of temperature was studied in a low magnetic field of about 40 Oe in order to determine their magnetic phase transitions. Solid pieces of about 0.1 gm were used for this study. The experimental set up is shown in Figure 3.2 and the procedures are given under Section 3.3.1.3.

6.3 Results and Discussion

6.3.1 Phase Relations

The $CaCu_5$ type phase is present in the entire composition range in $MM(Co_{1-x}Cu_x)_5$ alloys ($x = 0$ to 1) (Table 6.1). The low Cu alloys B-1 and B-2, annealed at 900° C contain 2:17 and a new phase in small amounts in addition to the major 1:5 phase. The amount of 2:17 phase increases when these alloys are annealed at 700° C. The X-ray diffraction patterns of alloys B-4 and B-5 show 1:5 phase both in 900° C and 700° C annealed condition whereas their microstructure gives a clear evidence for the presence of a small amount of a second phase also, which gets etched brighter than the matrix. Perry[5] reports that in Sm-Co-Cu system $SmCo_5$ phase coexists with a Co phase on the transition metal rich side of 1:5 stoichiometry for alloys containing greater than 10 a/o Cu at 800° C. It is possible that this phase is Co.

TABLE 6.1 CHEMICAL AND PHASE COMPOSITION OF $MM_{1-z}(Co_{1-x-y}Fe_yCu_x)_5$ ALLOYS

Alloy	$MM_{1-z}(Co_{1-x-y}Fe_yCu_x)_5$			Composition (w/o, analysed)				Phases (X-ray, microstructure)				
								900° C, 4 d			700° C, 4 d	
	X	Y	Z	RE	Co	Fe	Cu	Mic. st.	X-ray	TMA (T_c °C)	Mic. st.	X-ray
B-1	0.1	0.02	0.07	29.3	60.7	2.2	7.8	3	1:5+2:17+x	550, ~100	3	1:5+2:17+x
B-2	0.2	0.02	0.07	29.2	53.8	2.1	14.9	3	1:5+2:17+x	500, ~100	3	1:5+2:17+x
B-3	0.3	0.03	0	31.6	44.7	2.2	21.5	2	1:5+x	320, (~100)	Not observed	
B-4	0.4	0.02	0.07	29.5	38.4	2.1	30.0	2	1:5+(Co)	230	2	1:5+(Co)
B-5	0.6	0.02	0.07	29.5	25.1	2.1	43.3	2	1:5+(Co)	<20	2	1:5+(Co)
B-6	0.8	0.02	0.07	28.7	12.2	2.1	57.0	3	1:5+1:6+(Co)	<20	2	1:5+(Co)
B-7	1.0	0.02	0.07	28.3	0	1.9	69.8	2	1:5+1:6		2	1:5+1:6

However, it could not be confirmed by X-ray since it is present in small amounts. The alloys B-6 and B-7 melted on heating at 900° C and when quenched from 900° C showed 1:5 and 1:6 phases. This is similar to a $CeCu_5$ alloy[6] which at 900° C has a liquid phase in equilibrium with a solid phase (1:6). The $MMCu_6$ phase has a $SmCu_6$ type structure.[7] The orthorhombic lattice constants of $MMCu_6$ are a : 8.132 Å, b : 5.099 Å and c : 10.211 Å. On annealing at 700° C the 1:6 phase observed in alloy B-6 disappears giving rise to 1:5 phase, and a trace of a third phase (Co) observed at 900° C remains at 700° C. The alloy B-7 which contains no Co still shows 1:5 and 1:6 phases at 700° C. In binary Ce-Cu[6] system these phases exist as line compounds with no homogeneity region and a slight deviation from the stoichiometry will result in two phase structure. The $MMCu_5$ and $MMCu_6$ phases differ by less than 4 w/o in their stoichiometries and the presence of two phase structure observed for the B-6 alloy is attributed to its slightly transition metal richer composition than 1:5. The lattice constants a and c of the 1:5 phase in alloys B-1 to B-7 increase linearly with increasing Cu concentration (Figure 6.1). This is similar to the results reported by Lihl[8] for YCo_5-YCu_5 and $SmCo_5$-$SmCu_5$ systems.

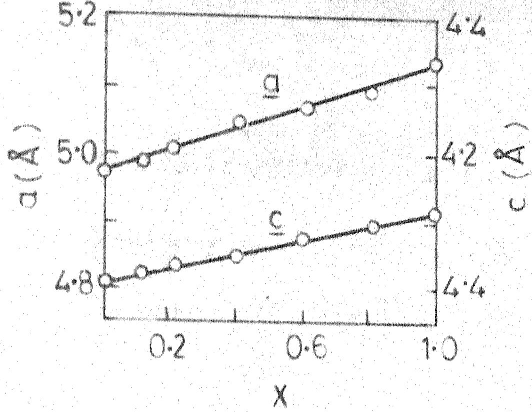

FIG.6·1 LATTICE PARAMETERS VS COMPOSITION OF 1:5 PHASE

$MM_{0.93}\left[Fe_{0.02}Co_{0.98-x}Cu_{x}\right]_{5}$

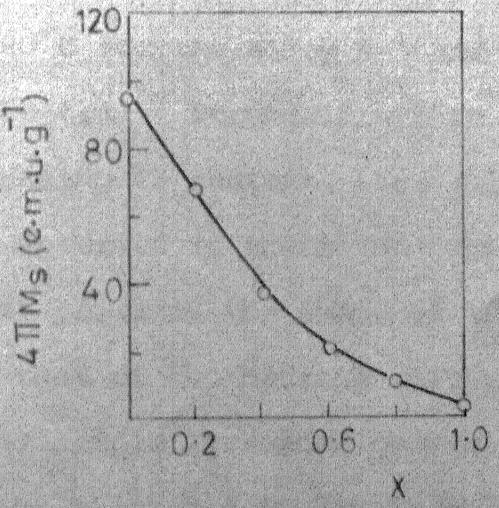

FIG.6·2 $4\pi M_s$ VS COMPOSITION OF

$MM_{0.93}\left[Fe_{0.02}Co_{0.98-x}Cu_{x}\right]_{5}$ ALLOYS

6.3.2 Magnetic Characteristics

The replacement of Co by Cu in $MMCo_5$ lowers the $4\pi M_s$ from 95 emu/g to less than 20 emu/g at 50 w/o Cu (Figure 6.2).

Alloy B-1 which contains 7.5 w/o Cu shows a Curie temperature greater than 500°C (Figure 6.3). MM-Co-Cu alloys close to this composition have been studied by Walkiewicz et.al.[4] and they reported an addition of 0.2 w/o Mg to alloys near this composition increases the ${}_iH_c$ to greater than 24 KOe. On further increasing the Cu content the T_c falls to 500°C at 14.5 w/o Cu (Figure 6.3) for the alloy B-2, to 320°C for the alloy B-3 and to 230°C for the alloy B-4 (Table 6.1). Beyond 15 w/o Cu the fall in T_c is steeper with increasing Cu content. For all the alloys two common features were observed in their TMA curves measured in a low magnetic field: firstly the shape of the cooling curve was different from that of the heating curve, secondly the magnetisation of the sample increased manyfold on cooling. This is shown for the alloy B-4 in Figure 6.3. This was observed for the Cu free MM-Co phases also and it was attributed to the strong temperature dependence of H_A of the phases in those alloys.[9] The H_A of the 1:5 phase decreases with increasing temperature and vanishes near the Curie point.[10] Hence at a fixed magnetic field the magnetisation should be easier at temperature close to the Curie point. A temperature difference of about 10°C is present between the heating and cooling curves

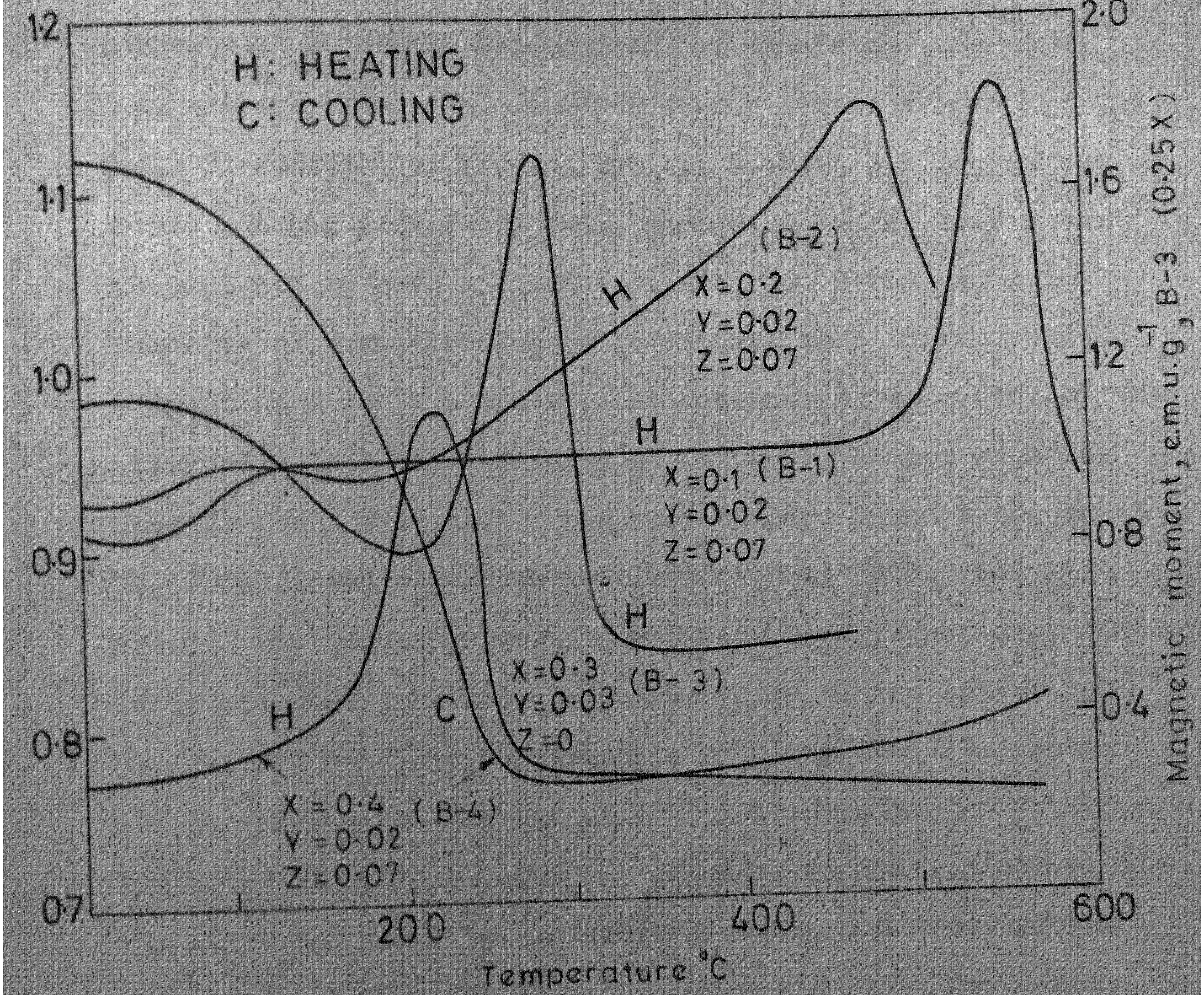

6·3 LOW FIELD MAGNETIC MOMENT VS TEMPERATURE FOR $MM_{1-z}(Co_{1-x-y}Fe_yCu_x)_5$ ALLOYS, 900 °C ANNEALED because of a thermal lag between the sample and the high temperature oven. The microstructures of the alloys B-1 and B-2, in addition to showing the 1:5 contain 2:17 and a new phase (darkly etched) in small amounts. As the 2:17 phase is expected to have a T_c greater than 600° C the magnetic transitions corresponding to it are not seen in Figure 6.3; whereas near 100° C there are indications in TMA curves of the alloys B-1, B-2 and B-3 for a third phase. Based on X-ray results Labulle et.al.[11] reported to have found a new phase $Ce_5(CoCu)_{13}$ and a hexagonal $Ce_5(CoCu)_{19}$ in $CeCo_{3.5}Cu_{1.5}$ alloy. However, no magnetic data have been reported by them. It is possible that the new phase may be of the latter type but it needs further confirmation by X-ray and EPMA study.

Alloys B-5 and B-6 were also studied by TMA upto 600° C and they do not show any magnetic transition above 20° C. The alloy B-7 which is a mixture of $MMCu_5$ and $MMCu_6$ phases show non-zero magnetisation ($\sim$3 emu/g) at 20° C while $CeCu_5$[12] and $CeCu_6$[13] are paramagnetic at room temperature. This is attributed to Fe present as an impurity in the mischmetal used in this work.

6.4 Conclusion

The substitution of Cu for Co in $MM(Co_{1-x}Cu_x)_5$ alloys gives stable 1:5 phase in the entire range of composition. At low Cu concentration (21.5 w/o) 2:17 and a new phase coexist with the matrix 1:5 phase. Cu could be substituted for Co upto 15 w/o in 1:5 with a T_c not less than 500° C and $4\pi M_s$ of about 70 emu/g. Beyond 15 w/o Cu both $4\pi M_s$ and T_c are considerably reduced.

REFERENCES

1. E.A. Nesbitt, J. Appl. Phys. 40, 1259 (1969).

2. T. Katayama and T. Shibata, Japan J. Appl. Phys. 12, 762 (1973).

3. K. Narita and H. Yamamoto, IEEE Trans. Magn. MAG-14, 785 (1978).

4. J.W. Walkiewicz and M.M. Wong, IEEE Trans. Magn. MAG-15, 1757 (1979).

5. A.J. Perry, J. Less-Common Metals 51, 153 (1977).

6. T.B. Rhinehamer, D.E. Etter, J.E. Selle and P.A. Tucker, Trans. Met. Soc. AIME 230, 1193 (1964).

7. K.H.J. Buschow and A.S. Van der Goot, J. Less-Common Metals 20, 309 (1970).

8. F. Lihl, Tech. Rep. AFML-TR-69-245, Wright-Patterson AFB, Ohio (October, 1969).

9. E.M.T. Velu, E.C. Subbarao, N.R. Bonda, D.K. Goel, K.P. Gupta, A.K. Majumdar, T.A. Padmavathi Sankar and J. Subramanyam, J. Appl. Phys. 51, 3322 (1980).

10. H. Nagel, H.P. Klein and A. Menth, J. Appl. Phys. 47, 3312 (1976).

11. B. Labulle and C. Petipas, J. Less-Common Metals 66, 183 (1979).

12. I. Pop, E. Rus, M. Coldea and O. Pop, J. Phys. Chem. Solids 40, 683 (1979).

13. M. Coldea and I. Pop, Phil. Mag. 28, 881 (1973).

7. PERMANENT MAGNET PROPERTIES OF 1:5 TYPE MM-Co ALLOYS

7.1 Introduction

Previous work on the development of mischmetal cobalt permanent magnets and the aims of the present work are given below.

7.1.1 Previous Work on $MMCo_5$ Magnets

The first successful results on the permanent magnet properties of sintered MM-Co magnets were reported by Fellows et.al.[1] Subsequently Nagel[2-3] and Narita[4-5] have also reported the properties achieved for $MMCo_5$ magnets. The materials used, the processes followed and the properties developed for $MMCo_5$ by them are summarised in Table 7.1. It could be seen from the table that the composition of MM used and the processes adopted for the fabrication of magnets are different in each case. Also the alloy composition used by Narita and Fellows et.al. is close to MM_5Co_{19} stoichiometry which on sintering results in a predominantly $MMCo_5$ phase magnet. The former used liquid phase sintering whereas the latter followed solid phases sintering on alloys of single composition without low melting sintering additive. The B_r and $(BH)_{max}$ values were not reported by Narita. He proposes that the large scale shift in composition should have occurred during sintering due to the loss of RE.

TABLE 7.1 MATERIALS USED, PROCESSES FOLLOWED AND PROPERTIES DEVELOPED FOR $MMCo_5$ MAGNETS

Material	Composition	Process	Properties	Reference
Cerium mischmetal and Co (RE distribution in MM and the purity of Co are not given)	64.5 w/o Co, 35.5 w/o MM (base); 27.0 w/o Co, 73.0 w/o MM (sinter additive). Aimed composition of the mixture of the powders 1 and 2 is 59.8 w/o Co and 40.2 w/o MM	Arc melted, attrition milled in petroleum ether, aligned in a pulse field of 50 KOe, axially pressed to 21 kbar in a holding field of 7 KOe and finally isostatically pressed to 7 kbar in the absence of field, sintered between 990 and 1110° C for 1 hr	ρ : 8.0–8.2 g/cc ${}_iH_c$: 4–6 KOe B_r : 4–7 KG $(BH)_{max}$: 3–8.8 MGOe	Fellows et al., 1972 (1)
Natural mischmetal (53 w/o Ce, 30 w/o La, 13 w/o Nd and 4 w/o Pr) and cobalt (99.9% pure)	Alloys on RE rich side of 1:5 stoichiometry were used. Actual composition studied is not given	Induction melted, jet milled with nitrogen, aligned in 50 KOe field, isostatically pressed at 6000 atm. Sintered at 1040° C and heat treated. Oxide content of the sintered magnet was $\sim$ 0.5 w/o	ρ : 94–97% of the theoretical density (8.3 g/cc) ${}_iH_c$: 9 KOe B_r : 8.1 KG $(BH)_{max}$: 14 MGO	Nagel et al., 1975, 1976 (2–3)
Mischmetal (49.5 % Ce, 20.2% La, 18.8% Nd, 5.0% Pr, 1.9% Sm, 3.9% Fe, 0.03% Mg and the balance impurities unidentified) and cobalt (99.5% Co, 0.15% Ni and 0.14% Fe), all in w/o	$MMCo_x$ alloys $3.6 \leq x \leq 4.8$ were used	Arc melted, ball milled in acetone, aligned in 10 KOe, pressed further in the absence of field, sintered between 960 and 1030° C with no sinter additives	ρ : 7.5 g/cc ${}_iH_c$: 8.3 KOe	Narita et al. 1978 (4–5)

7.1.2 Aims of the Present Work

Using commercial grade Indian mischmetal and cobalt (compositions are same as given under Section 3.1.1) work was undertaken (i) to develop the process: comminution, compaction and sintering procedures to fabricate MM-Co magnets (ii) to correlate the properties of the sintered magnets to their structure and (iii) to identify the problem - areas in the development of MM-Co permanent magnets.

7.2 Experimental

The experimental procedure for the magnet processing are described in detail in Chapter 3 under Section 3.3 and the steps involved are illustrated in Figure 3.3 together with the materials and the equipments used. The compositions of the alloys studied are given in Table 7.2.

7.3 Results

The permanent magnet properties of MM-Co alloys were studied under three different conditions: (1) Resin bonded sample, (2) powder compacts and (3) sintered pellets. In the case of sintered pellets, the properties obtained were monitored by studying their structure by X-ray diffraction.

7.3.1 Resin Bonded MM-Co Magnets

Prior to compaction and sintering it was necessary to select an appropriate composition and milling time that

TABLE 7.2 COMPOSITION OF MM-Co ALLOYS USED FOR MAGNET FABRICATION

Alloy formula	Composition (w/o, nominal)		
	MM	Co	Fe*
$MMCo_{3.5}$	40.9	56.5	2.6
$MMCo_{3.8}$	38.8	58.7	2.5
$MMCo_{4.0}$	37.5	60.1	2.4
$MMCo_{4.2}$	36.5	61.2	2.3
$MMCo_{4.4}$	35.4	62.4	2.2
$MMCo_{4.6}$	34.4	63.4	2.2
$MMCo_{4.8}$	33.3	64.6	2.1
$MMCo_{5.0}$	32.5	65.4	2.1
$MM^{*}\ Co_{3.8}$	31.4 MM 8.1 Sm	58.5	2.0
$MM^{*}\ Co_{4.0}$	30.3 MM 7.7 Sm	60.1	1.9

Fe^{*}, The impurity Fe in natural mischmetal is substracted (6 w/o assumed) and is shown separately.

MM^{*}, The mischmetal contains 20 w/o Sm added intentionally.

give powders with maximum coercivity. For this purpose $MMCo_x$ alloys with X lying between $MMCo_{3.5}$ and $MMCo_5$ were milled in 1 gm quantity in a plastic container upto 20 hours. The powder was mixed with an epoxy resin in a definite ratio, aligned in a magnetic field and set in air. The ${}_iH_c$ and $4\pi M_s$ of these resin bonded magnets were measured and the results are shown in Figure 7.1. A maximum ${}_iH_c$ of 3100 Oe

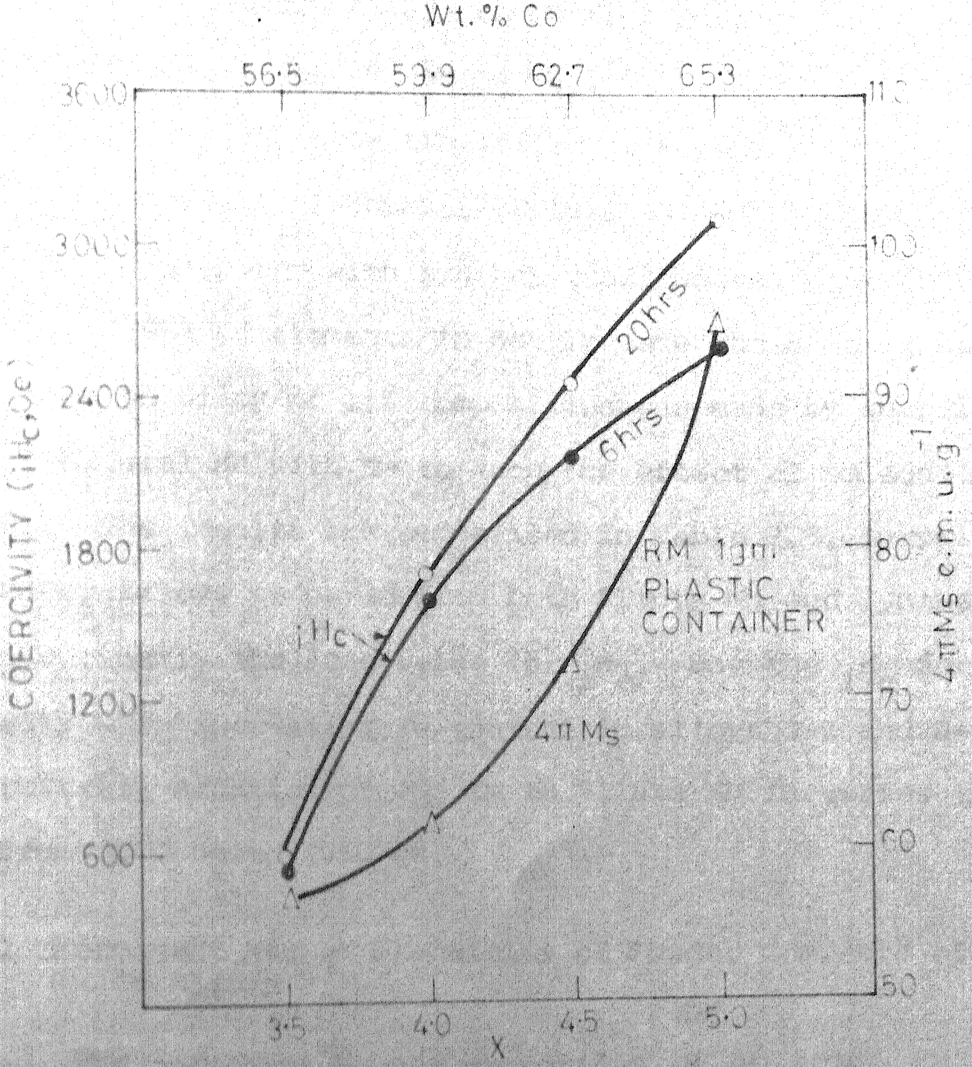

FIG. 7·1 $4\pi M_s$ and $_iH_c$ for MMCo$_X$ alloys

$3{\cdot}5 \leq X \leq 5{\cdot}0$

could be obtained for 20 hours milled $MMCo_5$ alloy and it has a $4\pi M_s$ of 95 emu/g. Alloys on MM rich side of $MMCo_5$ all have lower values for ${}_iH_c$ and $4\pi M_s$.

In order to know the effect of Fe and other impurities present in natural mischmetal (Flints MM) on the ${}_iH_c$, $MMCo_5$ alloys were prepared with synthetic mischmetal containing pure ($\geqslant$ 99.9%) RE elements in nearly same ratio as in natural MM. Also an alloy of 1:5 composition was made by substituting 20% of natural MM with Sm to know the effect of Sm addition on ${}_iH_c$. The results are summarised in Table 7.3. Surprisingly the $MMCo_5$ alloys prepared from both Flints MM and Synthetic MM show exactly the same value for ${}_iH_c$. But the ${}_iH_c$ decreases markedly with increasing Fe content in alloys S-1 and S-2. An arbitrary addition of 20% Sm to Flints MM increases the ${}_iH_c$ from 3200 Oe to 4950 Oe.

7.3.2 Permanent Magnet Properties of Powder Compacts of MM-Co Alloys

The permanent magnet properties, M_r/M_s, ${}_iH_c$, ${}_bH_c$ and $(BH)_{max}$ of field pressed powder compacts were measured for $MM\,Co_x$, $4.2 \leqslant X \leqslant 4.8$, alloys in order to select the best composition giving maximum value for $(BH)_{max}$. Five grams of the alloys were milled for 3 to 9 hours as described under Section 3. to make 2 or 3 pellets each weighing about 2 gms. The properties measured for these green pellets are shown in Figure 7.2. The green density of the pellets were between 4.7 and 5.0 g/cc. The $(BH)_{max}$ is highest for 6 hours milled

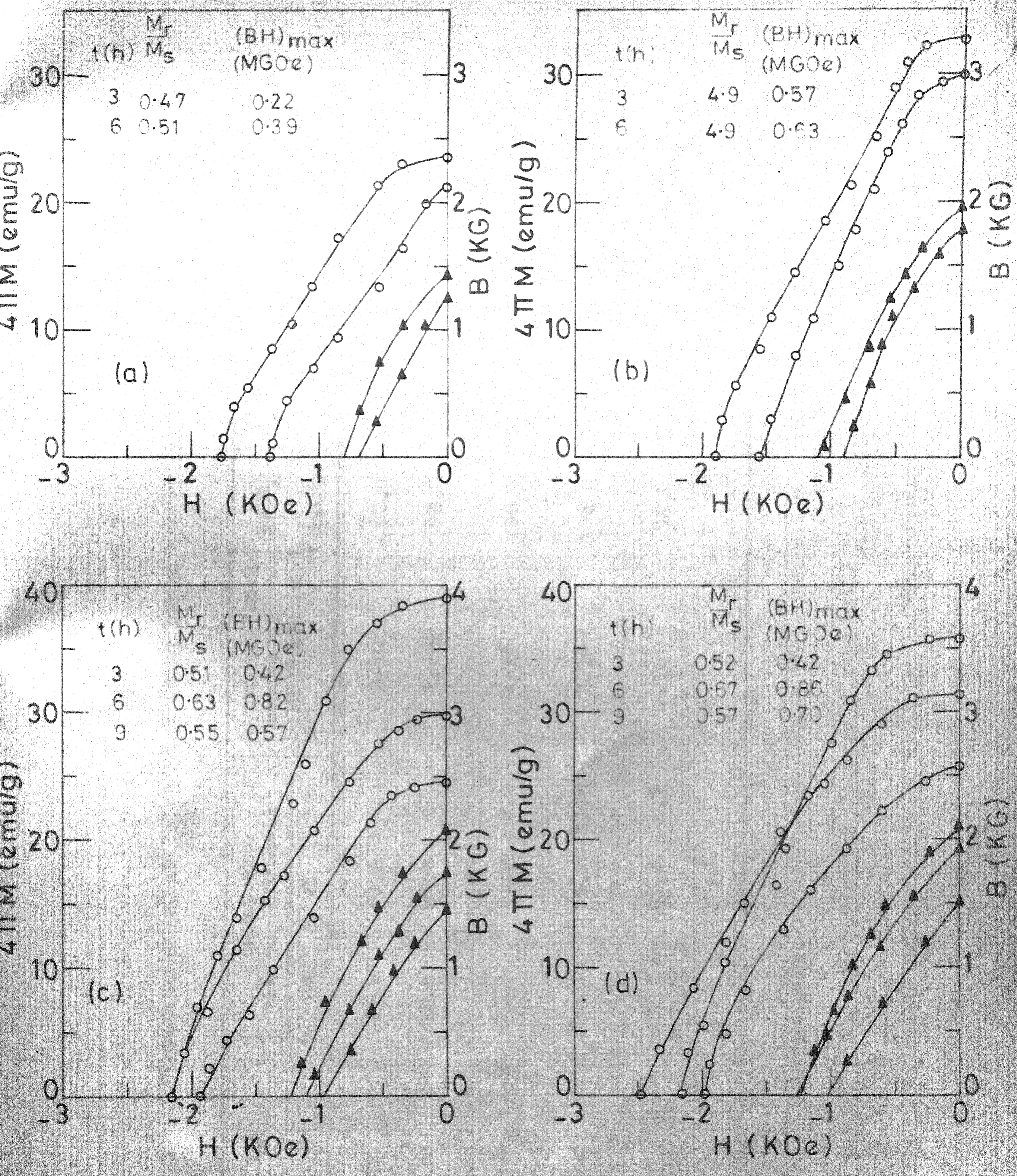

FIG.7·2 INTRINSIC AND INDUCTION DEMAGNETISATION CURVES FOR (a) MMCo$_{4.2}$ (b) MMCo$_{4.4}$ (c) MMCo$_{4.6}$ AND (d) MMCo$_{4.8}$ POWDER COMPACTS

TABLE 7.3 COMPARATIVE STUDY OF ${}_iH_c$ OF DIFFERENT RESIN BONDED $MMCo_5$ MAGNETS

Alloy	Composition (w/o, nominal)			Microstructure (amount of 5:19 phase in %)	$4\pi M_s$ (emu/g)	M_r/M_s	${}_iH_c$ (Oe)	Variable
	MM	Co	Fe					
$MMCo_5$ (F)	32.8	65.1	2.1	2-10	95.0	0.80	3200	Flints MM
MM^*Co_5 (S)	32.1	67.9	0	trace	98.0	0.81	3200	Synthetic MM with no Fe
$MM^*(Co,Fe)_5$ (S-1)	32.3	63.8	3.9	2-10	96.1	0.80	2450	Synthetic MM with 3.9% Fe
$MM^*(Co,Fe)_5$ (S-2)1	32.3	55.9	11.8	2-10	104.0	0.65	1300	Synthetic MM with 11.8% Fe
$MM_{0.8}Sm_{0.2}Co_5$	27.7 MM 6.8 Sm	65.4	1.7	~10	98.0	0.86	4950	Modified MM 20% Sm added to natural MM

MM^* : Synthetic MM.

powder compacts for each composition. Milling for greater than 6 hours increases ${}_iH_c$ for $MMCo_{4.8}$ but it lowers the B_r. Since the six hours milled powder compacts of $MMCo_{4.8}$ alloy show highest value for M_r/M_s (0.67) and $(BH)_{max}$ (0.86 MGOe), the powdere compacts of this composition were first tried for sintering studies.

7.3.3 Permanent Magnet Properties of Sintered MM-Co Magnets and Their Structure

A systematic sintering study on MM-Co alloy powder compacts was carried out varying the composition, sintering temperature and time. The pulse magnetic field applied during pressing and the compacting pressure were maintained constant at 13 KOe and 14 Tons/cm^2 respectively, for all the pellets used in the sintering studies. The density, M_r/M_s and ${}_iH_c$ of the powder compact and its sintered pellets were measured. The structure of the sintered pellets was analysed by X-ray diffraction.

7.3.3.1 $MMCo_{4.8}$ Sintered Pellets

The powder compacts of $MMCo_{4.8}$ prepared from 3 h, 6 h and 9 h milled powders were sintered at 1000°C for 15 mins. and their properties are shown in Table 7.4a to 7.4c. The three hours milled powder compact (Table 7.4a) has an ${}_iH_c$ of 1890 Oe, M_r/M_s of 0.52 and a density of 4.9 g/cc. After sintering at 1000°C for 15 mins. the ${}_iH_c$ decreases to 560 Oe, the M_r/M_s drops to 0.13 and the density increases to 6.1 g/cc. Subsequent sintering at higher temperature (1060°C)

TABLE 7.4a PERMANENT MAGNET PROPERTIES OF 3 h MILLED POWDER COMPACTS AND SINTERED PELLETS OF $MMCo_{4.8}$

Treatment	M_r/M_s	${}_iH_c$ (Oe)	Density, g/cc
1. Powder compact	0.52	1890	4.9
2. 1000° C/15 min.	0.13	560	6.1
3. 1000° C/15 min. + 1060° C/15 min.	0.09	520	7.0
4. 1000° C/15 min. + 1060° C/30 min.	0.08	520	8.0
5. 1000° C/15 min. + 1060° C/ 30 min. + 900° C/1 h	0.06	430	8.0

TABLE 7.4b PERMANENT MAGNET PROPERTIES OF 6 h MILLED POWDER COMPACTS AND SINTERED PELLETS OF $MMCo_{4.8}$

Treatment	M_r/M_s	${}_iH_c$ (Oe)	Density, g/cc
1. Powder compact	0.67	2060	4.8
2. 1000° C/15 min.	0.06	520	6.2
3. 1000° C/15 min. + 1060° C/15 min.	0.07	520	7.0
4. 1000° C/15 min. + 1060° C/30 min.	0.06	470	–
5. 1000° C/15 min. + 1060° C/ 30 min. + 900° C/1 h	0.04	410	–

TABLE 7.4c PERMANENT MAGNET PROPERTIES OF 9 h MILLED POWDER COMPACTS AND SINTERED PELLETS OF $MMCo_{4.8}$

Treatment	M_r/M_s	$_iH_c$ (Oe)	Density, g/cc
1. Powder compact	0.57	2400	5.0
2. 1000° C/15 min.	0.06	520	6.6
3. 1000° C/30 min.	0.05	520	6.7
4. 1000° C/30 min. + 1060° C/15 min.	0.05	520	7.0
5. 1000° C/30 min. + 1060° C/ 30 min. + 900° C/1 h	0.03	340	7.6

for longer time (30 m) increases the density to 8.0 g/cc but the M_r/M_s and $_iH_c$ are further reduced to 0.06 and 430 Oe respectively. The same trend is observed for the 6 h and 9 h milled powder compacts. The X-ray pattern of sintered pellet of 9 h milled powder compact is shown in Figure 7.3a. Surprisingly the expected $MMCo_5$ phase is hardly detectable. The observed lines could be accounted for by β-Co and MM_2O_3 phases.

7.3.3.2 $MMCo_{4.2}$ Sintered Magnets

The permanent magnet properties of sintered pellets of $MMCo_{4.2}$ composition are shown in Table 7.5 together with the values obtained for their powder compacts. The sintering was done at 1060° C for 15 m. Both the M_r/M_s ratio and $_iH_c$ decrease on sintering. The X-ray pattern of sintered pellet of 6 h milled powder compact is shown in Figure 7.3b. The

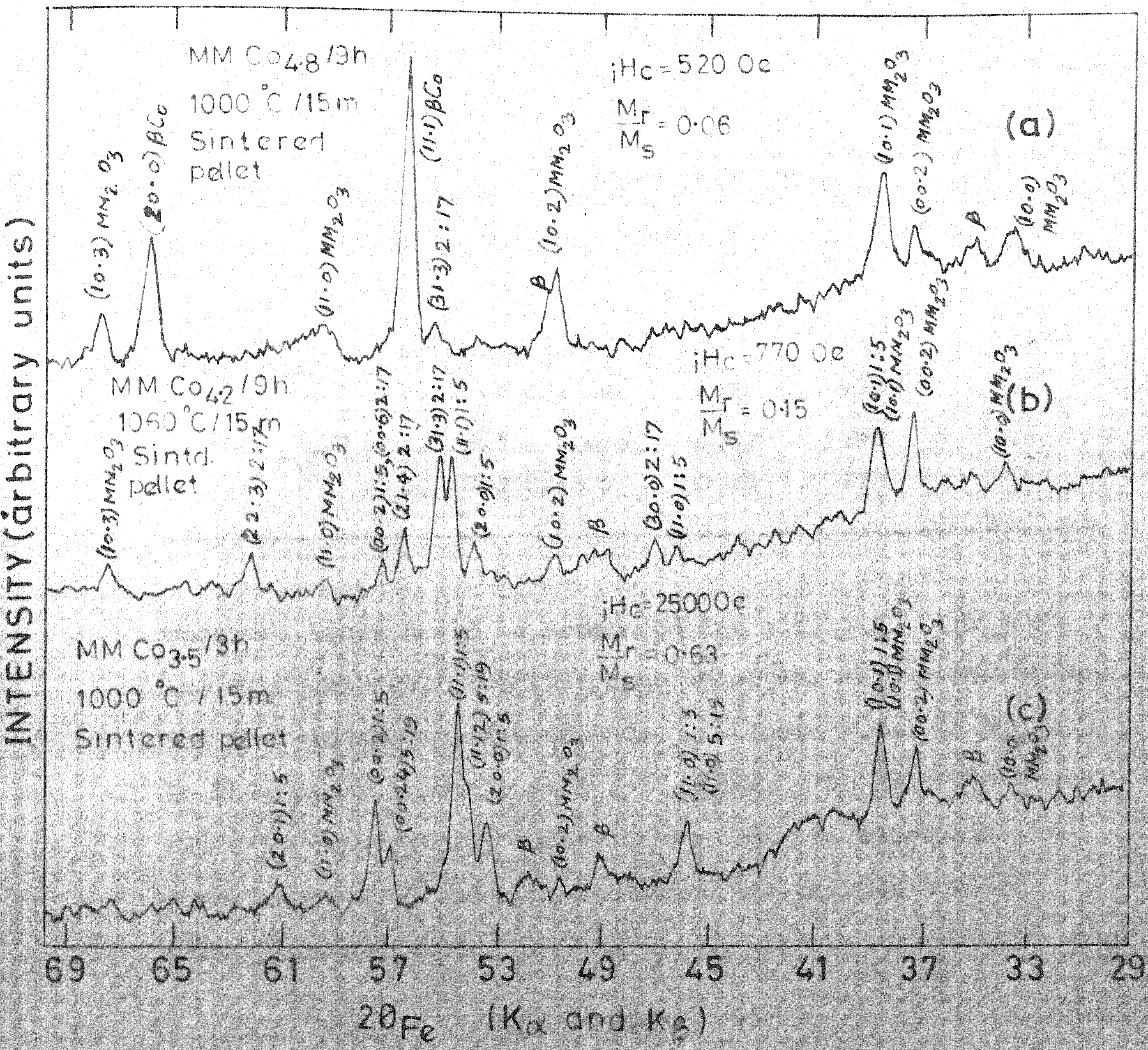

FIG.7·3 X-RAY DIFFRACTION PATTERNS OF SINTERED PELLETS OF (a) $MMCo_{4.8}$ (b) $MMCo_{4.2}$ AND (c) $MMCo_{3.5}$ ALLOYS

TABLE 7.5 PERMANENT MAGNET PROPERTIES OF POWDER COMPACTS AND SINTERED PELLETS OF $MMCo_{4.2}$

Sample	Treatment	M_r/M_s	$_iH_c$ (Oe)	Density, g/cc
1. $MMCo_{4.2}$/3 h	a. Powder compact	0.47	1380	-
	b. 1060° C/15 m	0.22	900	-
2. $MMCo_{4.2}$/6 h	a. Powder compact	0.51	1720	4.9
	b. 1060° C/15 m	0.23	950	7.7
3. $MMCo_{4.2}$/9 h	a. Powder compact	0.52	1890	4.8
	b. 1060° C/15 m	0.15	770	7.4

observed lines could be accounted for viz. 2:17, 1:5, β-Co and MM_2O_3 phases. The 1:5 phase which was hardly detectable for the sintered pellet of $MMCo_{4.8}$ (Figure 7.3a) is present in this alloy together with 2:17 phase. The amount of β-Co phase is considerably reduced. In order to eliminate the presence of 2:17 and β-Co sintering was carried out for $MMCo_{3.5}$ composition.

7.3.3.3 $MMCo_{3.5}$ Sintered Magnets

The M_r/M_s and $_iH_c$ of sintered pellets of 3 h milled powder compacts of $MMCo_{3.5}$ are shown in Table 7.6. Both the M_r/M_s and $_iH_c$ increase for the sintered pellets. The increase in $_iH_c$ is more than twice the value obtained for its powder compact. These values could be increased further by pulse magnetising the pellets at 60 KOe field.

TABLE 7.6 PERMANENT MAGNET PROPERTIES OF POWDER COMPACTS AND SINTERED PELLETS OF $MMCo_{3.5}$

Sample	Treatment	M_r/M_s	${}_iH_c$ (Oe)	Density, g/cc
$MMCo_{3.5}$/3 h	a. Powder compact	0.40	860	-
	b. 1000° C/15 m magnetised at 11 KOe	0.58	2100	7.6
	c. Pulse magnetised at 60 KOe	0.63	2500	7.6
	d. 1000° C/30 m magnetised at 11 KOe	0.58	2100	7.7

The X-ray pattern of this pellet is shown in Figure 7.3c. The observed lines could be accounted for 1:5, 5:19 and MM_2O_3 phases. The 2:17 and β-Co phases are hardly detectable. Though 1:5 is the predominant phase in the sintered pellet, still considerable amount of 5:19 is present. To reduce the amount of 5:19 phase, $MMCo_{3.8}$ composition was tried for sintering.

7.3.3.4 $MMCo_{3.8}$ Sintered Magnets

The magnet properties for the powder compacts and the sintered pellets of $MMCo_{3.8}$ are shown in Table 7.7. Sintering was carried out at three different temperatures 1000° C, 1030° C and 1060° C for 15 m. The 3 h milled powder compact shows M_r/M_s of 0.35 and ${}_iH_c$ of 1250 Oe. The increase

TABLE 7.7 PERMANENT MAGNET PROPERTIES OF POWDER COMPACTS AND SINTERED PELLETS OF $MMCo_{3.8}$

Sample	Treatment	M_r/M_s	$_iH_c$ (Oe)
$MMCo_{3.8}$/3 h	a. Powder compact	0.35	1250
	b. 1000° C/15 m, magnetised at 11 KOe	0.69	4080
	c. 1000° C/15 m, magnetised at 60 KOe	0.78	4900
$MMCo_{3.8}$/5 h	Powder compact	0.35	1030
	Magnetised at 11 KOe:		
	a. 1000° C/15 m	0.66	3310
	b. 1030° C/15 m	0.61	2710
	c. 1060° C/15 m	0.43	1460
	Magnetised at 60 KOe:		
	a. 1000° C/15 m	0.64	4130
	b. 1030° C/15 m	0.70	3400
	c. 1060° C/15 m	0.53	1800

to 0.78 and 4900 Oe respectively for a sintered pellet magnetised at 60 KOe sintering at temperatures higher than 1000° C for 5 h milled powder compacts leads to lower values only. The X-ray diffraction pattern of 1000° C/15 m sintered pellet is shown in Figure 7.4 together with the X-ray pattern of the as-cast $MMCo_{3.8}$ alloy. The 5:19, which is the predominant phase in the as-cast alloy, is not detectable in the sintered pellet. Also the MM_2O_3 peaks not present in the as-cast alloy pattern appears prominently in the X-ray

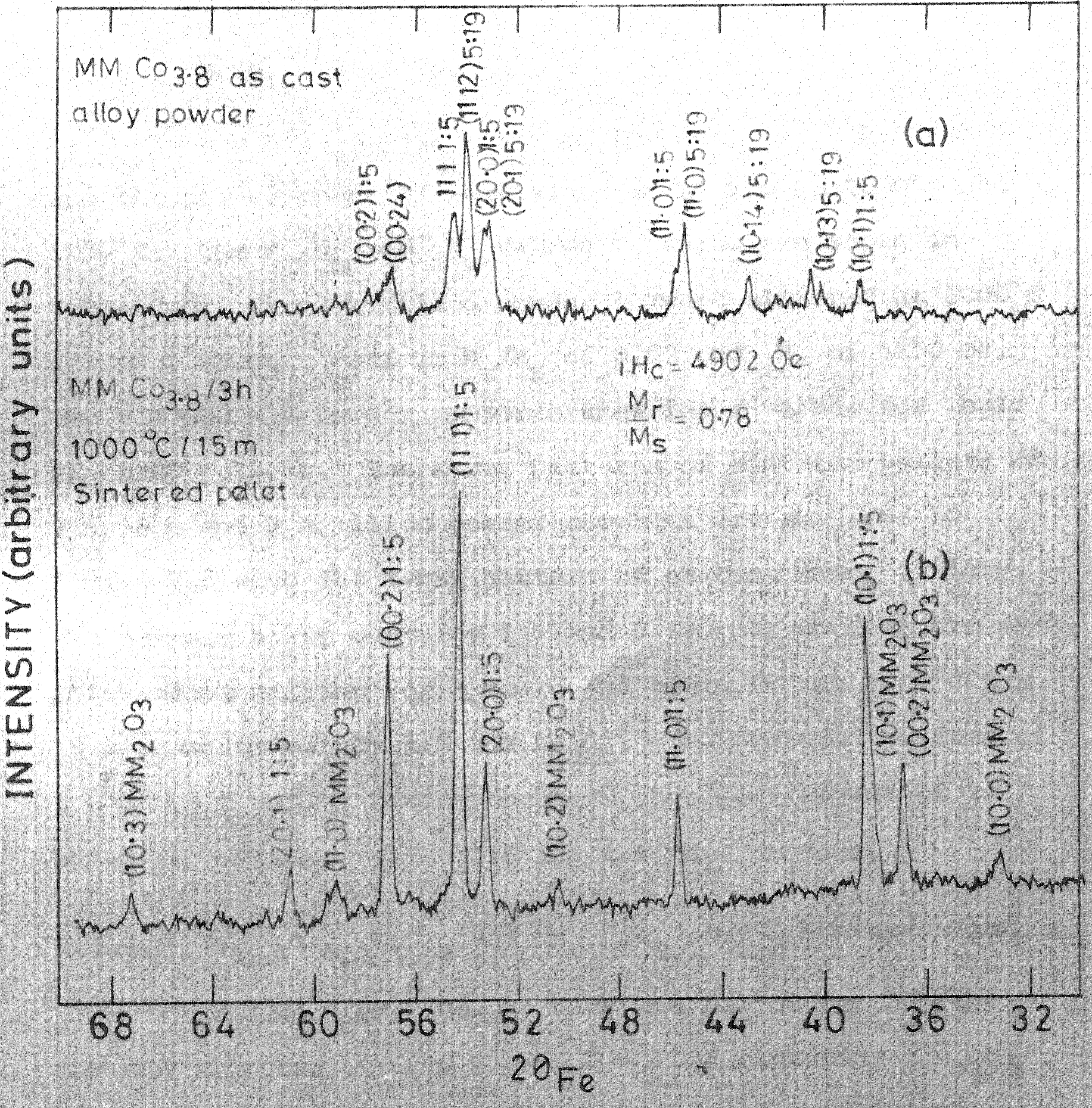

FIG. 7·4 X-RAY DIFFRACTION PATTERNS OF AS CAST AND SINTERED PELLETS OF MM Co$_{3·8}$ ALLOY pattern of the sintered pellets suggesting that the oxidation should have occurred during milling or sintering operation.

7.3.3.5 $MMCo_{4.0}$ Sintered Magnets

The $MMCo_{4.0}$ alloy was milled for 3 h, 6 h and 9 h and the powder compacts were sintered at 970° C, 1000° C and 1030° C. The M_r/M_s and ${}_iH_c$ values measured are shown in Table 7.8. The 3 h milled powder compact sintered at 1000° C for 15 m shows a maximum M_r/M_s of 0.83 and ${}_iH_c$ of 5250 Oe. The 6 h and 9 h powder compacts show lower values for their sintered pellets. The X-ray patterns of sintered pellets of 3 h, 6 h and 9 h milled powder compacts are compared in Figure 7.5 with the X-ray pattern of as-cast $MMCo_{4.0}$ alloy. The as-cast alloy contains 1:5 and 5:19 only whereas the same alloy after milling for 3 hours and sintering at 1000° C for 15 m contains mainly 1:5 and MM_2O_3. The sintered pellets of 6 h and 9 h milled powder compacts show some amount of 2:17 phase in addition to the 1:5 and the MM_2O_3 phases.

7.3.3.6 $MM_{0.8}Sm_{0.2}Co_{3.8}$ and $MM_{0.8}Sm_{0.2}Co_{4.0}$ Sintered Magnets

The $MM_{0.8}Sm_{0.2}Co_{3.8}$ alloy was milled for 3 h and 6 h and sintered at 1000° C for 15 m. On sintering the ${}_iH_c$ increased to more than three times their value for powder compacts and the M_r/M_s ratio also increased appreciably (Table 7.9). The as sintered pellet of 6 h milled powder compact showed an ${}_iH_c$ of 11000 Oe. This increased to $\gg$ 11000 Oe on pulse magnetising at 60 KOe. As the peak magnetic field

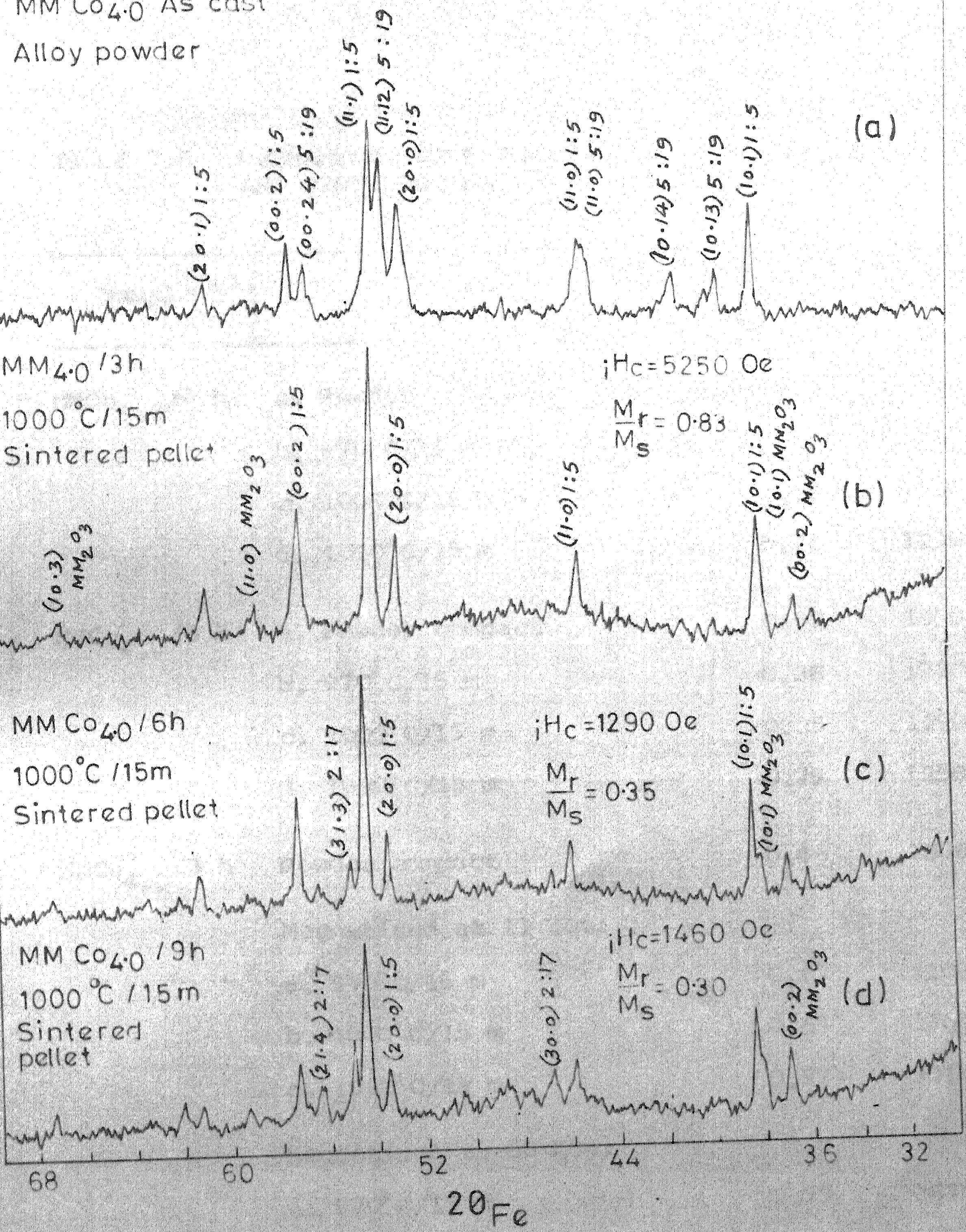

5 X-RAY DIFFRACTION PATTERNS OF (a) AS CAST MMCo$_{4·0}$ ALLOY AND SINTERED PELLETS OF (b) 3h (c) 6h AND (d) 9h MILLED POWDER COMPACTS OF MM Co$_{4·0}$ ALLOY

TABLE 7.8 PERMANENT MAGNET PROPERTIES OF POWDER COMPACTS AND SINTERED PELLETS OF $MMCo_{4.0}$

Sample	Treatment	M_r/M_s	$_iH_c$ (Oe)
$MMCo_{4.0}$/9 h	a. Powder compact	0.46	2060
	b. 970° C/15 m	0.28	1460
	c. 1000° C/15 m	0.30	1460
	d. 1030° C/15 m	0.26	1290
$MMCo_{4.0}$/6 h	a. Powder compact	0.50	1850
	b. 970° C/15 m	0.38	1720
	c. 1000° C/15 m	0.35	1290
	d. 1030° C/15 m	0.29	1250
$MMCo_{4.0}$/3 h	Powder compact	0.46	1806
	Magnetised at 11 KOe:		
	a. 970° C/15 m	0.67	3100
	b. 1000° C/15 m	0.67	3960
	c. 1030° C/15 m	0.57	3010
	Magnetised at 60 KOe:		
	a. 970° C/15 m	0.77	3870
	b. 1000° C/15 m	0.83	5250
	c. 1030° C/15 m	0.76	4210

TABLE 7.9 PERMANENT MAGNET PROPERTIES OF POWDER COMPACTS AND SINTERED PELLETS OF $MM_{0.8}Sm_{0.2}Co_{3.8}$ AND $MM_{0.8}Sm_{0.2}Co_{4.0}$

Sample	Treatment	M_r/M_s	${}_iH_c$ (Oe)
$MM_{0.8}Sm_{0.2}Co_{3.8}$/3 h	a. Powder compact	0.67	2840
	b. 1100° C/15 m, magnetised at 11 KOe	0.82	7570
	c. 1000° C/15 m, magnetised at 60 KOe	0.90	9720
$MM_{0.8}Sm_{0.2}Co_{3.8}$/6 h	a. Powder compact	0.66	3270
	b. 1000° C/15 m, magnetised at 11 KOe	0.81	11000
	c. 1000° C/15 m, magnetised at 60 KOe	0.92	>11000
$MM_{0.8}Sm_{0.2}Co_{4.0}$/3 h	a. Powder compact	0.59	3530
	b. 1000° C/15 m, magnetised at 11 KOe	0.48	3354

available for characterising the magnets in the present study was only 11 KOe, the magnitude of its coercivity could not be measured. The M_r/M_s ratio increased from 0.81 to 0.92 after pulse magnetising. The X-ray pattern shown in Figure 7.6a indicates the presence of 1:5 phase only together with considerable amount of MM_2O_3.

The $MM_{0.8}Sm_{0.2}Co_{4.0}$ alloy milled for 3 h and sintered at 1000° C for 15 m has lower values for M_r/M_s and ${}_iH_c$ than its powder compacts (Table 7.9). The study of its

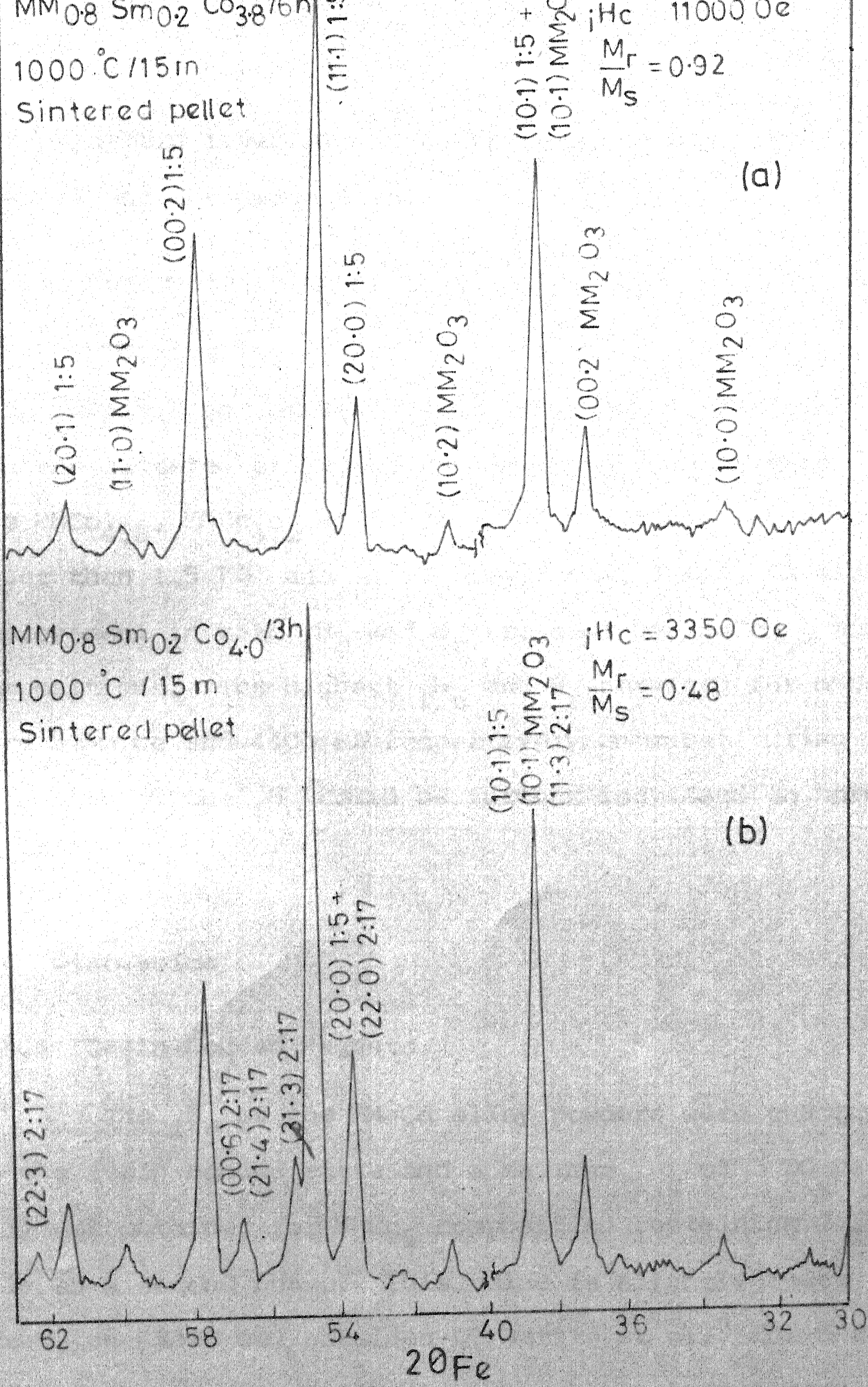

G.7·5 X-RAY DIFFRACTION PATTERNS OF SINTERED PELLETS OF (a) $MM_{0\cdot 8}\,Sm_{0\cdot 2}\,Co_{3\cdot 8}$ AND (b) $MM_{0\cdot 8}\,Sm_{0\cdot 2}\,Co_{4\cdot 0}$ COMPOSITIONS

X-ray pattern revealed the coexistence of the 2:17 phase with the 1:5 and the oxide phases (Figure 7.6b).

7.3.4 Demagnetisation Plots of MM-Co Sintered Magnets

The intrinsic demagnetisation curves of MM-Co alloys with composition between $MMCo_{3.5}$ and $MMCo_{5.0}$, all milled for 3 h and sintered at 1000° C for 15 m are shown in Figure 7.7. The $MMCo_{4.8}$, $MMCo_{4.2}$ and $MMCo_{3.5}$ sintered samples show a B_r lower than 1.5 KG and an ${}_iH_c$ lower than 3 KOe. A marked improvement in both ${}_iH_c$ and B_r are seen for $MMCo_{3.8}$ and $MMCo_{4.0}$ compositions. The highest ${}_iH_c$ and B_r obtained for $MMCo_{4.0}$ were 5250 Oe and 4400 KG respectively. On substituting 20% Sm to Flints MM the ${}_iH_c$ could be further increased to more than 11000 Oe.

7.4 Discussion

7.4.1 Resin Bonded Magnets

The ${}_iH_c$ of the MM-Co alloy powders were characterised in the resin bonded state and a maximum ${}_iH_c$ of 3200 Oe (Table 7.3) was obtained for $MMCo_5$ composition containing 2-10% 5:19 as a second phase. This value is slightly lower than the value (3600 Oe) obtained by Narita et al.[4] for $MMCo_5$. The Fe present as impurity in natural mischmetal does not seem to have a deleterious effect on ${}_iH_c$ as the $MMCo_5$ alloys prepared from the Flints mischmetal and Synthetic mischmetal show same value for ${}_iH_c$. However a small drop in $4\pi M_s$ is

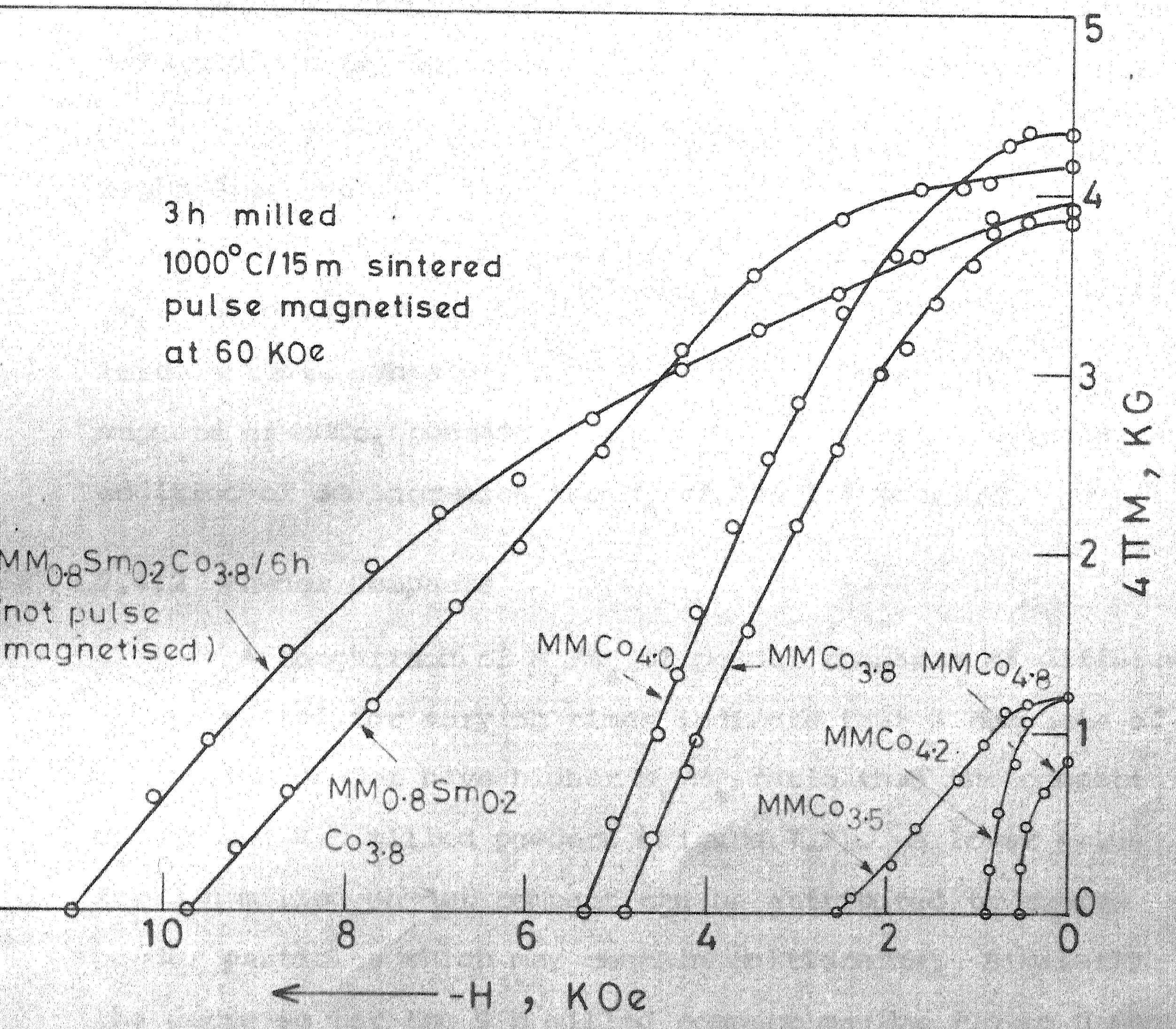

IG·7·7 INTRINSIC DEMAGNETISATION PLOTS OF SINTERED
. MAGNETS OF MMCo$_X$ ALLOYS $3\cdot5 \leq X \leq 4\cdot8$

seen for the $MMCo_5$ alloy (Table 7.3) whereas an increase is expected due to the presence of Fe. But MM contains other non-magnetic elements like Mg, Ca etc. upto 1.4 w/o which might decrease the magnetisation. At high concentration of Fe ($\gg$2 w/o) the Fe seems to have a deleterious effect on ${}_iH_c$. An addition of 20% Sm to MM increases the ${}_iH_c$ to a large extent. This was also observed by Nagel[2] for sintered magnets of $MMCo_5$ containing Sm. This increase occurs as the addition of Sm increases the H_A of the 1:5 phase.[2]

7.4.2 Powder Compacts

A comparison of M_r/M_s of powder compacts of different alloys milled for varying times indicate that a compacts of 6 h milled powder have higher M_r/M_s ratio than the compact of 3 h and 9 h milled powders (Figure 7.2). A lower value for 3 h milled powder compact can be attributed to coarse powder particles which may contain multigrains. Similarly the decrease for the 9 h milled compact may be due to damage or oxidation of the powder as a result of prolonged milling. The $MMCo_{4.8}$ alloy milled for 6 h shows the highest M_r/M_s of 0.67. This value is still much less than the expected value (0.8-0.9). The powders in this study were pressed axially in 13 KOe field (of 100-200 millisecond pulse width) in a non-magnetic die where the punch tips were also of non-magnetic material. Application of a continuous magnetic field perpendicular to the pressing direction have been reported to yield good alignment.[7]

7.4.3 Sintered MM-Co Magnets

7.4.3.1 The Occurrence of Oxide in MM-Co Sintered Magnets

An oxide of the stoichiometry MM_2O_3 could be detected in all the sintered pellets. The $MMCo_{4.8}$ alloy after sintering at 1000° C for 15 m has β-Co and MM_2O_3 with a trace of 2:17. The presence of oxide in sintered Sm-Co[8] and MM-Co[3] magnets have been reported to an extent upto 0.5 w/o. Ishigaki et al.[8] have made an exclusive study on the oxidation phenomena of $SmCo_5$ during sintering and they report that the ${}_iH_c$ of the sintered $SmCo_5$ increases with oxygen content upto 5000 ppm and then decreases at higher concentration. In samples containing 8000 ppm oxygen they could detect Sm_2Co_{17}, Sm_2O_3, CoO and hexagonal Co (α). But in the MM-Co sintered pellets the Co phase existed in f.c.c. form (β) and the oxide had the La_2O_3 type hexagonal structure. The lattice parameters and the X-ray diffraction data of MM_2O_3 and β-Co found in $MMCo_{4.8}$ sample (Figure 7.3a) are given in Tables 7.10 and 7.11.

7.4.3.2 Compositional Shift in MM-Co Sintered Magnets

The maximum ${}_iH_c$ obtained for different compositions of sintered MM-Co alloy is plotted in Figure 7.8 as a function of composition. It is seen that the ${}_iH_c$ reaches a maximum of 5250 Oe for $MMCo_{4.0}$ and it falls on either side of this composition. A curve of similar shape has been reported for $SmCo_5$ sintered magnets.[9] But in that case the maximum ${}_iH_c$ is observed at $SmCo_{4.9}$ (16.9 a/c Sm). Narita[4] in his study

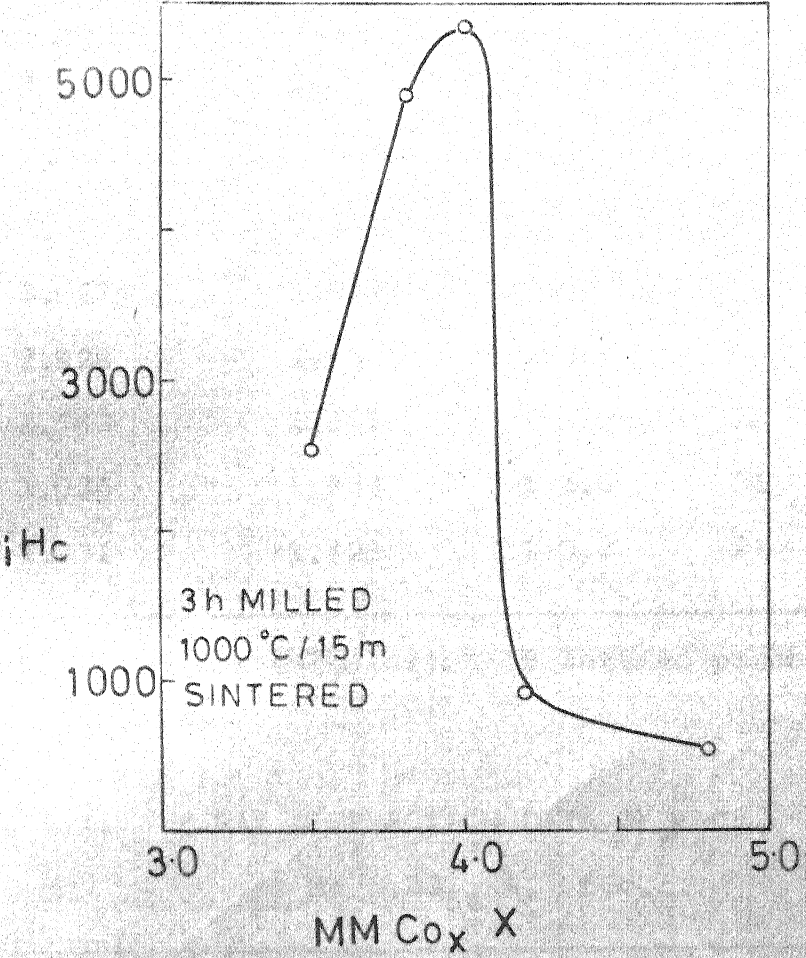

FIG. 7·8 INTRINSIC COERCIVITY VS COMPOSITION FOR SINTERED MMCo$_x$ ALLOYS $3.8 \leqslant x \leqslant 4.8$

TABLE 7.10 X-RAY DIFFRACTION DATA OF MM_2O_3

a: 3.86_{71} Å; b: 6.05_{40} Å; La_2O_3 type hexagonal structure

d_{ob} Å	d_{cal} Å	(h k.l)	% I_{ob}	2θ Fe (observed)
3.349*	3.349	1 0.0	28	33.6
3.027*	3.027	0 0.2	31	37.3
2.928	2.930	1 0.1	100	38.6
2.243	2.245	1 0.2	28	51.1
1.936	1.933	1 1.0	31	60.1
1.731	1.728	1 0.3	21	68.1

* Lines taken for calculation of lattice parameters.

TABLE 7.11 X-RAY DIFFRACTION DATA OF β-Co

a: 3.53_{56} Å, f.c.c.

d_{ob} Å	d_{cal} Å	(h k l)	% I_{ob}	2θ Fe (observed)
2.042	2.041	1 1 1	100	56.6
1.768*	1.768	2 0 0	52	66.4
1.250	1.250	2 2 0	32	101.5
1.066	1.066	3 1 1	36	130.5

* Line taken for calculation of lattice parameter.

of sintered MM-Co magnets found a similar shift in composition and reported that $MMCo_{3.8}$ after sintering turned out to be single phase $MMCo_5$ with a maximum ${}_iH_c$ of 8.3 KOe. The composition of MM used by Narita is very close to the composition of the Indian mischmetal but the former contains 1.9 w/o Sm and 3.9 w/o Fe whereas the Indian mischmetal contains about 6 w/o Fe and no Sm.[10] This shift in phase composition can occur either due to the loss of RE by evaporation during sintering or by selective oxidation of RE. If it is due to evaporation then there should be a weight loss in the sintered pellets and no oxide should be present. But the sintered pellets of MM-Co alloys in this study show negligible weight loss (0.1 w/o) and contain considerable amount of oxide.

The oxidation can occur in one of comminution and sintering operations or in both. In order to determine this the powder compact and its sintered pellets were analysed for their chemical composition. The analysis carried out for $MMCo_{4.2}$ alloy is shown in Table 7.12.

The following points could be noted from the chemical analysis. (1) The total weight of the elements analysed is always less than 100%. In the case of as-cast alloy the observed deficit of 1% could be attributed to the impurities present in MM that were not analysed but the deficit of 4 to 5 w/o for the powder compacts and the sintered pellets could be accounted for only due to oxidation for which X-ray evidence is there for the sintered pellets. Since the powder

TABLE 7.12 CHEMICAL COMPOSITION OF AS-CAST, POWDER COMPACT AND SINTERED PELLETS OF $MMCo_{4.2}$

Sample	Composition (w/o)			Total
	Co	RE	Fe	
As-cast	62.6	34.2	2.2	99.0
Powder compact				
3 h	59.1	34.2	3.0	96.3
6 h	58.0	33.8	3.1	94.9
9 h	58.4	33.6	3.6	95.6
Sintered, 1000° C/15 m				
3 h	59.2	34.4	3.1	96.7
6 h	58.5	34.1	3.3	95.9
9 h	58.4	33.6	3.6	95.6

compacts contain particles of few micron size the X-ray peaks were highly diffused and very weak. Hence the presence of oxide could not be confirmed unambiguously in the powder compacts. But the chemical analysis could be used as an indirect proof for it. (2) The compositions of the powder compacts and the sintered pellets are nearly the same suggesting that the factor causing the compositional shift (oxidation) occurs only during comminution and not during sintering. (3) The Fe content of the powder compact is about 1.5 w/o higher than that present in the corresponding as-cast alloy, the amount being higher for the 9 h milled powder than for the 3 h milled powder. This is expected to come from the wear of the stainless steel rods used as the grinding media. (4) Both for Co and RE the powder compacts show lower value than the as-cast alloy. This is only an apparent decrease and not a real one because the weight of the powder taken for chemical analysis includes the weight of oxygen also which actually goes into water during dissolution in the acid ($RE_2O_3 + 6HNO_3 \quad 2RE(NO_3)_3 + 3H_2O$). Thus the reference weight taken in the beginning should not be used as such for computing the percent composition of the elements. If we assume a 25-30% oxidation of RE to RE_2O_3 and 5-10% oxidation of Co to CoO and make a mass balance analysis, then this difference in chemical composition between the as-cast and the powder samples could be explained.

7.4.3.3 Structure and Properties of Sintered MM-Co Magnets

Maximum values for the coercivity was observed in those sintered pellets which contained 1:5 phase only. The presence of small amount of 5:19 does not seem to have adverse effect on ${}_iH_c$. But the presence of MM_2Co_{17} which has easy plane anisotropy,[11] needs to be totally avoided to obtain improved ${}_iH_c$. A maximum ${}_iH_c$ of 5250 Oe was obtained for the $MMCo_{4.0}$ composition which contained $MMCo_5$ and MM_2O_3 only after sintering. Narita[4] obtained a maximum value of 8.3 KOe for $MMCo_{3.8}$ which after sintering at 1030°C for 30 m contained 1:5 only as determined by thermomagnetic analysis. Owing to the presence of considerable amount of oxide, the 4π M_s of the sintered pellet was 65 emu/g only whereas a value of 95 emu/g is expected for $MMCo_5$.[12] Consequently the maximum B_r obtained for the oxide containing $MMCo_5$ was 4.5 KG only. Nagel et al.[3] report that a post sintering heat treatment is essential to improve the $_iH_c$ but in the present study no heat treatment was tried as the sintered pellets contained a large amount of oxide. The minimisation of the oxide content and a suitable post sintering heat treatment should certainly improve the $_iH_c$ and B_r from the present values.

7.4.4 Problem Areas in the Preparation of Sintered MM-Co Magnets

Two main obstacles, oxidation and limitation of magnetic field (of 11 KOe only for characterisation of $_iH_c$) were found out in this study. The oxidation seems to occur in the pre-sintering stage and mostly during the comminution. The method of powder preparation is to be perfected or to be modified altogether to minimise the oxidation. For $MMCo_5$ magnets containing a small amount of Sm, a magnetic field greater than 11 KOe is essential to measure the $_iH_c$.

7.5 Conclusions

A maximum $_iH_c$ of 3200 Oe was obtained for $MMCo_5$ powders. On sintering at 1000° C a large scale shift (5 to 6 w/o) in composition was observed as a result of oxidation. $MMCo_{4.0}$ alloy on sintering at 1000° C for 15 m contained only 1:5

phase together with MM_2O_3 and showed an ${}_iH_c$ of 5250 Oe and a B_r of 4.5 KG. A 20% substitution of Sm for the natural mischmetal increased the value of ${}_iH_c$ to greater than 11 KOe. The oxidation seems to occur during the pre-sintering stage, mostly during the period of powder preparation.

REFERENCES

1. C.J. Fellows and R.E. Johnson, Cobalt 56, 141 (1972).

2. H. Nagel and A. Menth, Goldschmidt Informiert 4/75, Nr. 35, 41 (1975).

3. H. Nagel, H.P. Klein and A. Menth, J. Appl. Phys. 47, 3312 (1976).

4. K. Narita, IEEE Trans. Magn. MAG-14, 785 (1978).

5. K. Narita and H. Yamamoto, Proc. of the 4th International Workshop on RE-Co Permanent Magnets and Their Application, May 1978, Japan Paper No. VIII.1.

6. A.E. Paladino, N.J. Dione, P.F. Weihrauch and E.C. Wettstein, Goldschmidt Informiert 4/75, Nr. 35, 63 (1978).

7. H. Umebayashi and Y. Fujimura, Japan Journal of Appl. Phys. 10, 1585 (1971).

8. N. Ishigaki and A. Higuchi, Proc. of the II International Symposium on Magnetic Anisotropy and Coercivity in Rare Earth Transition Metal Alloys,p54, July 1978, CA, U.S.A.

9. D.L. Martin and M.G. Benz, AIP Conf. Proc. 5, 2, 970 (1972).

10. T.A. Padmavathi Sankar, H.O. Gupta, E.C. Subbarao, K.P. Gupta, N.R. Bonda, D.K. Goel, S.N. Kaul, A.K. Majumdar, R.C. Mittal, G. Sarkar, M.V. Satyanarayana, K.S. Prasad, J. Subramanyam and E.M.T. Velu, Bull. Mater. Sci. 2 (3), 167 (1980).

11. K.J. Strnat and A.E. Ray, Goldschmidt Informiert 4/75, Nr. 35, 47 (1975).

12. E.M.T. Velu, E.C. Subbarao, N.R. Bonda, K.P. Gupta, S. Laha, A.K. Majumdar, T.A. Padmavathi Sankar and S. Pandian, IEEE Trans. Magn. MAG-16, 997 (1980).

8. CONCLUSIONS AND SUGGESTIONS FOR FUTURE WORK

Phase relationships in MM-Co-Fe system between 2:7 and 2:17 stoichiometries with Fe content upto 15 a/o were investigated and a 900°C isothermal section of the MM-Co-Fe phase diagram was obtained. The MM-Co-Fe phases between the 2:7 and 1:5 stoichiometries are structurally closely related and show very similar X-ray patterns. Hence extensive thermomagnetic study was carried out in addition to X-ray diffraction and metallography in order to confirm their identities. The sequence of occurrence of phases in the binary MM-Co system was found to be essentially similar to that observed in a binary Ce-Co system. $MMCo_3$, MM_2Co_7, MM_5Co_{19}, $MMCo_5$, MM_2Co_{17} and β-Co were found to exist in the MM-Co system between 73 and 92 a/o Co. The 5:19 phase was found to extend upto about 10 a/o Fe into the MM-Co-Fe ternary system whereas the 2:7, 1:5 and 2:17 phases extend to greater than 10 a/o Fe along their respective stoichiometric (MM/Co) lines. A new phase with a T_c of 340°C was found to coexist with 1:5 and 5:19 phases with a number of alloys between the 5:19 and 1:5 stoichiometric lines. The MM_2Co_7, MM_5Co_{19}, $MMCo_5$ and MM_2Co_{17} were obtained in single-phase form and their standard X-ray diffraction data and crystal lattice parameters were obtained. A homogeneity region for 1:5 phase containing 3 a/o Fe was investigated and it was found to have a narrow homogeneity region at 900°C extending over 1.5 a/o Co. Phase stability of 1:5 alloy containing different amount of Fe was studied at 700°C in view of their technological importance in the sintering process of these magnets. The $MMCo_5$ phase was found to undergo an eutectoid type reaction and the increasing amount of Fe substitution ($>$5 a/o) for Co in the 1:5 phase was found to accelerate the decomposition rate at 700°C.

In order to evaluate the suitability of the MM-Co-Fe phases for permanent magnets, the saturation magnetisation ($4\pi M_s$) and Curie temperature (T_c) were characterised for the 2:7, 5:19, 1:5 and 2:17 phases in the MM-Co-Fe system. The $MMCo_5$ and MM_2Co_{17} phases were found to have attractive properties for both $4\pi M_s$ and T_c. The $MMCo_5$ phase has a $4\pi M_s$ of 95 emu/g and the MM_2Co_{17} has a $4\pi M_s$ of 114 emu/g. Both the 2:7 and 5:19 phases have $4\pi M_s$ less than 45 emu/g. The T_c of the $MMCo_3$, MM_2Co_7, MM_5Co_{19}, $MMCo_5$ and MM_2Co_{17} phases were found to be $<$20°C, 67°C, 280°C, 540°C and $>$700°C respectively. The T_c of 2:7, 5:19 and 1:5 phases were found to increase with increasing substitution of Fe for Co. From the point of view of $4\pi M_s$ and T_c both the $MMCo_5$ and MM_2Co_{17} seem to be attractive for permanent magnet production.

The addition of Cu to MM-Co alloys was made to know to what extent Cu can be substituted in the $MMCo_5$ phase with tolerable magnetic properties suitable for permanent magnet production. The study revealed that stable 1:5 phase could be obtained in $MM(Co_{1-x}Cu_x)_5$ alloys replacing Co with Cu upto 100%. The a and c of the hexagonal 1:5 phase were found to increase linearly with increasing Cu substitution. Both the $4\pi M_s$ and T_c of the 1:5 phase were found to decrease steadily with the addition of Cu. It was found that Cu could be substituted upto 15 w/o with a T_c not less than 500°C and a $4\pi M_s$ of about 70 emu/g. Beyond 15 w/o Cu, both $4\pi M_s$ and T_c were considerably reduced.

MM-Co alloys on the MM rich side of $MMCo_5$ were processed to produce permanent magnets. A selected process parameters: alloy composition, milling time, sintering temperature and sintering time were investigated systematically. The optimum milling time was determined by studying the ${}_iH_c$ of the powder produced rather than its average particle size. A maximum ${}_iH_c$ of 3200 Oe was obtained for the $MMCo_5$ powders. The powder compacts of $MMCo_x$ alloys were sintered between 960 and 1030°C. Sintering at temperatures $\geqslant$1000°C was found necessary to obtain high density ($\geqslant$90% of the theoretical density) for these alloys. The structure of the sintered pellets was studied closely by metallography and X-ray diffraction. On sintering at 1000°C, a large scale shift in composition (5-6 w/o) was observed. $MMCo_{4.0}$ alloy after sintering at 1000°C for 15 minutes contained only 1:5 phase together with MM_2O_3. It showed an ${}_iH_c$ of 5250 Oe and a B_r of 4.5 KG. A 20% substitution of Sm in Indian mischmetal increased the ${}_iH_c$ to greater than 11 KOe. Chemical analysis and X-ray diffraction study revealed the presence of considerable amount of MM_2O_3 in the sintered pellets. The large scale shift in composition is attributed to oxidation and it seems to occur during the pre-sintering stage, mostly during the period of powder production.

In the MM-Co-Fe system the occurrence of different phases, their identities and the phase boundaries among them in alloys upto 10 a/o Fe are well established in the present study. These informations should be sufficiently helpful in the successful fabrication of MM-Co-Fe permanent magnets. However, in order to complete the isothermal section the following things may be worthwhile to be pursued.

1. Alloys containing $>$15 a/o Fe and lying between 2:7 and 1:5 stoichiometric lines (MM/Co) need further investigation by TMA at T $>$600° C to draw the phase boundaries.
2. The origin of occurrence of X phase between the 5:19 and 1:5 stoichiometries need to be established whether it is due to any phase separation.
3. The homogeneity region of 1:5 phase was investigated for MM-Co-Fe alloys along one tie line(~3 a/o) Fe only. To draw the boundaries of the homogeneity region it is necessary to investigate it at different Fe concentration along the 1:5 stoichiometric line.

In the case of processing of MM-Co magnets of 1:5 type the following need to be pursued:

1. The oxygen content of the sintered magnet should be reduced to a level of a few 1000 ppm or less in order to increase both the B_r and ${}_iH_c$ of the magnets. The oxidation seems to occur mostly during the stage of powder production inspite of the use of sodium gettered toluene during milling. The powder may have to be dried in a better vacuum than used presently (500 μ).
2. A systematic post sintering heat treatment of the sintered pellets should be tried as it is expected to alter the shape of the demagnetisation curve with a consequent increase in B_r, ${}_iH_c$ and $(BH)_{max}$.

APPENDIX 1

SPECIFICATIONS OF RAW MATERIALS: MM, Co, Fe and Cu

Material	Source	Purity/Composition	At. wt.
Co	1. Semi Elements, Inc., N.Y., U.S.A.	99.9%	58.93
	2. Moldex Co., Bombay, India	99.3%	
Fe	Gallard, Schelsinger Mfg. Co., N.Y., U.S.A.	99.9%	55.85
Cu	Semi Elements, Inc., N.Y., U.S.A.	99.9%	63.54
MM	Mischmetal & Flints Pvt. Ltd., Allepy, Kerala, India	Commercial grade Composition: 52.0% Ce, 20.1% La, 15.7% Nd, 4.8% Pr, 6% Fe and 1.4% unidentified impurities	140.82

APPENDIX 2

COMPUTATIONS OF ALLOY COMPOSITIONS

A procedure followed to prepare an alloy of composition, for example $RECo_{4.8}Fe_{0.2}$ is given.

Assumption: (a) Total RE in MM = 92.6 w/o

(b) Fe in MM = 6 w/o

(c) Impurities in MM = 1.4 w/o

(d) Effective gm. at. wt. of total RE in MM = 140.82 gms.

92.6 gms of RE $\equiv$ 100 gms. of MM

$\therefore$ 140.82 gms of RE $\equiv \frac{100}{92} \times 140.82 = 152.07$ gms of MM

Fe in 152.07 gms of MM = 0.06 x 152.07 = 9.12 gms

$$RECo_{4.8}Fe_{0.2} \equiv MM(Co_{4.8}Fe_xFe_{0.2-x})$$

where $x = 9.12/55.85 = 0.033$

Therefore materials to be weighed:

(a) 152.07 gms of MM

(b) 4.8 x 58.93 gms of Co

(c) (0.2 - 0.033) x 55.85 gms of Fe

w/o ratios of MM:Co:Fe to be weighed = 34.2:63.7:2.1.